Finite Element and Analytical Solutions for the Optimal Design of Laminated Composites

Talmon Reiss

Submitted in fulfilment of the academic requirements for the Degree of Doctor of Philosophy in the Department of Mechanical Engineering at the University of Natal.

Durban, South Africa
June 1996

Abstract

The present study involves the analysis and design optimisation of composite structures using analytical and numerical methods. Five different problems are considered.

The first problem considers the design of laminated plates subject to non-uniform temperature distributions. The plates are optimised for maximum buckling temperature using the fibre angle as the optimising variable. The method of solution involves the finite element method based on Mindlin theory for thin laminated plates and shells, and numerical optimisation. A computational approach is developed which involves successive stages of solution for temperature distribution, buckling temperature and optimal fibre angle. Three different temperature loadings are considered and various combinations of simply supported and clamped boundary conditions are studied. The effect of plate aspect ratio on the optimal fibre angle and the maximum buckling temperature is investigated. The influence of bending–twisting coupling on the optimum design is studied by considering plates with increasing number of layers.

The second problem concerns the optimal design of composite pressure vessels. Finite element solutions are presented for the design of hemispherically and flat capped symmetrically laminated pressure vessels subjected to external pressure. The effect of vessel length, radius and wall thickness, as well as bending–twisting coupling and hybridisation on the optimal ply angle and buckling pressure are numerically studied. Comparisons of the optimal fibre angles and maximum buckling pressures for various vessel geometries are made with those for hybrid pressure vessels.

In the third problem, the multiobjective design of a symmetrically laminated shell is obtained with the objectives defined as the maximisation of the axial and torsional buckling loads. The ply angle is taken as the optimising variable and the performance index is formulated as the weighted sum of individual objectives in order to obtain Pareto optimal solutions of the design problem. Single objective design results are obtained and compared with the multiobjective design. The effect of weighting factors on the optimal design is investigated. Results are given illustrating the dependence of the optimal fibre angle and performance index on the cylinder length, radius and wall thickness.

In the fourth problem, the optimal layup with least weight or cost for a symmetrically laminated plate subject to a buckling load is determined using a hybrid composite construction. A hybrid construction provides further tailoring capabilities and can meet the weight, cost and strength constraints while a non–hybrid construction may fail to satisfy the design requirements. The objective of the optimisation is to minimise either the weight or cost of the plate using the ply angles, layer thicknesses and material combinations as design variables. As the optimisation problem contains a large number of continuous (ply angles and thicknesses) and discrete (ma-

terial combinations) design variables, a sequential solution procedure is devised in which the optimal variables are computed in different stages. The proposed design method is illustrated using graphite, kevlar and glass epoxy combinations and the efficiency of the hybrid designs over the non-hybrid ones are computed.

Finally, the minimum deflection and weight designs of laminated composite plates are given in the fifth and last problem. The finite element method is used in conjunction with optimisation routines in order to obtain the optimal designs, as was the procedure in the first problem. Various boundary conditions are considered and results are given for varying aspect ratios and for different loading types.

Declaration

I declare that this dissertation is my own unaided work except where due acknowledgement is made to others. This dissertation is being submitted for the Degree of Doctor of Philosophy to the University of Natal, Durban, and has not been submitted previously for any other degree or examination.

Talmon Reiss June 1996

Acknowledgements

I wish to thank my supervisor Professor Sarp Adali and Mark Walker for their guidance and help.

Contents

List of Tables

List of Figures

Chapter 1

Introduction

Structures made of composite materials have found extensive applications due to the high strength and stiffness to weight ratios that these materials afford. Another advantage of these materials over conventional materials is the possibility of tailoring their properties to the specific requirements of a given application.

The process of optimising composite structural designs is of importance since the cost of advanced composite materials is significantly higher than that of conventional materials. The benefits which these materials offer must thus be maximised and better utilised. The optimisation may take the form of designing for a maximum strength, a minimum deflection, weight or cost for example. In order to achieve these aims, one or more geometric or material parameters are varied such that an optimum design is obtained, as a function of these parameters. The design variables may include the layer fibre angle, layer thickness or layup configuration for example.

This thesis is made up of various different problems which have a number of elements in common. All the structures considered are laminated composites with symmetric layups. Apart from one of the problems, which considers bending loads, all the other problems deal with buckling loads. All the studies involve the optimal design of the structures considered, either for maximum strength or minimum weight. In each case, continuous fibre angles are considered, and form one of the optimising variables.

The design problems considered in the thesis demonstrate how different approaches may be employed in the optimisation of composite structures. Numerical or analytical solutions may be used depending on the nature of the problem. The

optimisation may be for one or several variables, or a a sequential design procedure may be formulated.

In order to obtain solutions for the optimal design problems investigated in this study, two approaches were considered. The finite element method was employed for those problems for which closed form solutions do not exist. Alternatively, analytical solutions were obtained using symbolic computation for the problems where closed form solutions are available. The analysis of laminated structures manufactured from different materials is a demanding area of computational solid mechanics and one well suited to the use of symbolic computation. Symbolic computation systems are able to mathematically manipulate expressions in symbolic forms and may be used to derive analytical results or formulae for numerical computations.

In recent years the use of composite materials in high temperature environments has grown markedly, which has resulted in increased research in thermal loading problems of laminated structures. An important subject in this field is thermal buckling. The first problem in this study considers the optimal thermal buckling design of laminated plates with non-uniform temperature distributions and combinations of simply supported and clamped boundary conditions. The effect of aspect ratio on the optimal buckling temperature and optimal fibre angle is investigated. First the uniform temperature distributions are considered. With symmetric angle-ply laminates, the number of layers is shown to have an effect on the critical temperature due to bending–twisting coupling. However this effect decreases as the number of layers increases.

Little work has been done on the optimal design of composite pressure vessels, especially those for which closed form solutions are not available. The second problem of this study thus adopts a numerical method to determine the optimal buckling design of flat and hemispherically capped thin walled, laminated pressure vessels. The finite element method, in conjunction with an optimisation routine, is used to determine optimal fibre angles for vessels of various geometries, thicknesses and boundary conditions. The effect of hybridisation on the optimal design is also considered.

There are many situations where structures are subjected to multiple loading

conditions throughout their life. In order to ensure an optimal design of these structures, the different loading conditions must be taken onto account. Single objective designs would not accurately predict the behaviour of the structure and in these instances a multiobjective design approach is necessary. When composite structures are subjected to multiple buckling loading conditions such as axial compressive and torsional loadings, a multiobjective design approach can be formulated in order to ensure an optimally designed structure. The third problem of this study considers such a case. The buckling strength of laminated shells under multiple loading conditions is optimised with respect to the layer fibre angle and the effect of the structure geometry on the optimal design is investigated. Closed form solutions are generated using the symbolic computation package MATHEMATICA.

An effective way to reduce the cost of composite structures is via hybridisation. A laminated structure may fulfil the design requirement yet be substantially cheaper than a homogeneous structure owing to the use of cheaper materials as filler layers. The optimal layup with least weight or cost for a symmetrically laminated hybrid plate is determined by admitting hybrid constructions into the design space. The design space consists of three continuous variables, namely the layer fibre angle, the layer thickness of a reference material and the relative thickness of the layers of the different materials. There is also one discrete variable in the design space ie. the material combination. The plates are optimised for minimum weight or cost subject to a minimum buckling load constraint. For this purpose an optimisation procedure is devised such that at every stage of the solution the optimal value of one of the continuous design variables is determined. This value carries off to the next stage and several candidate designs with different material combinations are generated. The optimal design is chosen from among these candidate designs.

It is observed that in many cases a non–hybrid design fails to satisfy the design constraints and in all cases hybrid constructions perform better than the non–hybrid ones. Numerical results on the efficiency of the designs indicate more than 45% weight or cost improvement in many cases. As in the third problem, symbolic computation is used to obtain the optimal design.

Closed form solutions for laminated structures under transverse loading are generally unobtainable when boundary conditions other than simply supported or clamped are considered and a numerical method must be employed.

The final design problem of the study considers the optimal design of laminated plates for minimum deflection and minimum weight. In the first part of this design problem, the ply angle is taken as the optimising variable for the minimum deflection design and the minimum weight is then obtained using a failure criterion with the optimising variable then becoming the plate thickness. Results are presented for different loadings both symmetrical and unsymmetrical, and various combinations of clamped, simply supported and free boundary conditions are considered. The effect of aspect ratio on the minimum deflection and weight, and optimal ply angle, is investigated. In the second part of this design problem, only the minimum weight is taken as the design objective, and the fibre orientation and the laminate thickness are determined to achieve a minimum weight design. Comparative results are given to assess the effect of design priority on the deflection and weight.

Chapter 2

Literature Survey

2.1 Finite Element Method

2.1.1 Theoretical Formulation of FEM

Continuum Problems

In the *continuum* or Eulerian approach to nature, all processes are characterized by field quantities that are defined at every point in space. The independent variables in continuum problems are the coordinates of space and time. Continuum problems are concerned with fields of temperature, stress, mass concentration, displacement, electromagnetic and acoustic potentials, etc. These problems arise from the phenomena in nature that are approximately characterized by partial differential equations and their boundary conditions.

Continuum problems of mathematical physics are often referred to as boundary value problems because their solution is sought in some domain defined by a given boundary, on which certain conditions called *boundary conditions* are specified. The boundary is said to be closed if conditions affecting the solution of the problem are specified everywhere on the boundary and open if part of the boundary extends to infinity and no boundary conditions are specified on the part at infinity [1].

Problem Statement

Consider some domain D bounded by the surface Σ [2]. Let ϕ be a scalar function defined in the interior of D such that the behaviour of ϕ in D is given by

$$L(\phi) - f = 0 \tag{2.1}$$

where f is a known scalar function of the independent variables and L is a linear or nonlinear differential operator. It is assumed that the physical parameters in the differential operator are known constants or functions. In n dimensions, second-order differential operators can usually be reduced, by a suitable transformation, to the form

$$L(\ ) = \sum_{i=1}^{n} A_i \frac{\partial^2(\ )}{\partial x_i^2} + \sum_{i=1}^{n} B_i \frac{\partial(\ )}{\partial x_i} + (\ )C + D \tag{2.2}$$

where coefficients A_i, B_i and C and the term D may be functions. The operator as given in equation (2.1) is linear if A_i, B_i, C and D are functions only of the independent variables (x_1, x_2, x_3,..., x_n), and quasilinear if A_i, B_i, C and D are functions of x_i; and the dependent parameter, as well as first derivatives of the dependent parameter. An operator is linear only if

$$L(f + g) = L(f) + L(g) \tag{2.3}$$

The general definition of the operator $L(\ )$ in equation (2.1) precludes a discussion of appropriate boundary conditions. However, without boundary conditions, equation (2.1) does not describe a specific problem.

Some Methods for Solving Continuum Problems

From equation (2.1), it is seen that the general problem is to find the unknown function ϕ that satisfies equation (2.1) and the associated boundary conditions specified on Σ.

There are many alternative approaches to the solution of linear and nonlinear boundary value problems and they range from completely analytical to completely numerical. These can be listed as follows:

1. *Direct integration (exact solutions).*

a. Separation of variables.

b. Similarity solutions.

c. Fourier and Laplace transformations.

2. *Approximate solutions.*

a. Perturbation.

b. Power series.

c. Probability schemes.

d. Method of weighted residuals (MWR).

e. Finite difference techniques.

f. Ritz method.

g. Finite element method.

The Variational Approach

Often continuum problems have the different, but equivalent, differential and variational formulations. In the differential equation formulation, the problem is to integrate a differential equation or a system of differential equations subject to given boundary conditions. In the *classical variational formulation*, the problem is to find the unknown function or functions that extremize or make stationary a functional such as $I(\phi)$ or system of functionals subject to the same boundary conditions. The two problem formulations are equivalent because the functions which satisfy the differential equations and their boundary conditions also *extremize* or make *stationary* the functionals. The classical variational formulation of a continuum problem often has advantages over the differential equation formulation from the viewpoint of obtaining an approximate solution.

Firstly, the functional, which may actually represent some physical quantity in the problem, contains derivatives of order lower than that of the differential operator and an approximate solution can be sought in a larger class of functions.

Secondly, the problem may possess reciprocal variational formulations, that is, one functional must be minimized and another one of a different form must be maximized.

Third, the variational formulation allows us to treat very complicated boundary conditions as *natural boundary conditions.*

Fourth, from a mathematical viewpoint the variational formulation is helpful because it can sometimes be used to prove the existence of a solution by using calculus of variations.

This approach is especially convenient when it is applicable; but before it can be used, a variational statement for the continuum problem must be formulated, which means that the problem must be posed in a variational form.

Historically, variational methods are among the oldest means of obtaining solutions to problems in physics and engineering. One general method for obtaining approximate solutions to problems expressed in variational form is known as the Ritz method. This method is basically a forerunner of the finite element procedure. In fact, the finite element method is a special case of the Ritz method when the

interpolation functions satisfy certain continuity requirements.

The Ritz Method

The Ritz method consists of assuming the form of the unknown solution in terms of known functions (trial functions) with unknown adjustable parameters. (The trial functions are also called coordinate functions). The procedure is to substitute the trial functions into the functional and thereby express the functional in terms of the adjustable parameters. The functional is then differentiated with respect to each parameter and the resulting equation is set equal to zero. If there are n unknown parameters, there will be n simultaneous equations to be solved for these parameters. The accuracy of the approximate solution depends on the choice of trial functions. The trial functions are defined over the whole solution domain and they satisfy at least some and usually all of the boundary conditions. If the exact solution is contained in the family of trial solutions, the Ritz procedure gives the exact solution. Generally, the approximation improves as the size of the family of trial functions and the number of adjustable parameters increase. The process of including more and more trial functions leads to a series of approximate solutions which converges to the true solution. Often a family of trial functions is constructed from polynomials of successively increasing degree, but in certain cases other kinds of functions may also offer advantages [3].

Relation of FEM to the Ritz Method

The finite element method and the Ritz method are essentially equivalent. Each method uses a set of trial functions as the starting point for obtaining an approximate solution; both methods take linear combinations of these trial functions and both models seek the combination of the trial functions that makes a given functional stationary. The major difference between the methods is that the assumed trial functions in the finite element method are not defined over the whole solution domain and they have to satisfy no boundary conditions but only certain continuity conditions. Because the Ritz method uses functions defined over the whole domain, it can be used only for domains of relatively simple geometric shape. In the finite element method the same geometric limitations exist, but only for the elements. Due to the fact that elements with simple shapes can be assembled to represent quite complex geometries, the finite element is far more versatile and flexible than

the Ritz method.

Generalising the definition of an element

The mathematical interpretation of the finite element requires the generalisation of the definition of an element which is in less physical terms. The elements are interconnected only at imaginary node points at the boundaries or surfaces of the elements. For the solid mechanics problems, in general, elements do not deform or change shape. They are defined as regions of space where a displacement field exists. The nodes of an element are located in space where the displacement and possibility of its derivatives are known or sought. The mathematical interpretation of a finite element mesh is that it is a spatial subdivision rather than a material subdivision [4].

Once the element mesh for the solution domain has been decided, the behaviour of the unknown field variable over each element is approximated by continuous functions expressed in terms of the nodal values of its derivatives up to a certain degree. The functions defined over each finite element are called *interpolation functions, shape functions*, or field variable models. The collection of the interpolation functions for the whole solution domain provides a piecewise approximation to the field variable.

Element Equations from the Variational Principle

The finite element solution to the problem involves determining the nodal values of ϕ so as to make the functional $I(\phi)$ stationary [2]. To make $I(\phi)$ stationary with respect to the nodal values of ϕ, it is required that

$$\partial I(\phi) = \sum_{i=1}^{n} \frac{\partial I}{\partial \phi_i} \delta\phi_i = 0 \tag{2.4}$$

where n is the total number of discrete values of ϕ assigned to the solution domain. Since the $\delta\phi_i$'s are independent, equation (2.4) can be satisfied only if

$$\frac{\partial I}{\partial \phi_i} = 0, i = 1, 2, ..., n \tag{2.5}$$

The functional $I(\phi)$ may be written as a sum of individual functionals defined for all elements of the assemblage, that is,

$$I(\phi) = \sum_{e=1}^{M} I^{(e)}(\phi^{(e)}) \tag{2.6}$$

where M is the total number of elements and the superscript (e) denotes an element. From equation (2.6), it follows that

$$\delta I = \sum_{e=1}^{M} \delta I^{(e)} = 0 \tag{2.7}$$

where the variation of $I^{(e)}$ is taken only with respect to the nodal values associated with the element (e). Equation (2.7) implies that

$$\{\frac{\partial I^{(e)}}{\partial \phi}\} = \frac{\partial I}{\partial \phi_j} = 0,\ j = 1, 2, ..., r \tag{2.8}$$

where r is the number of nodes assigned to element (e). Equation (2.8) comprises a system of r equations that characterize the behavior of element (e). Equation (2.8) for element (e) can always be written as [2]

$$\{\frac{\partial I^{(e)}}{\partial \phi}\} = [K]^{(e)}\{\phi\}^{(e)} - \{F\}^{(e)} = \{0\} \tag{2.9}$$

where $[K]^{(e)}$ is a square matrix of constant *stiffness* coefficients, $\{\phi\}^{(e)}$ is the column vector of nodal values and $\{F\}$ is the vector of resultant nodal actions. Symbolically, the complete set of equations can be written as

$$\frac{\partial I}{\partial \phi_i} = \sum_{e=1}^{M} \frac{\partial I^{(e)}}{\partial \phi_i} = 0,\ i, 1, 2, ..., n \tag{2.10}$$

or

$$\{\frac{\partial I}{\partial \phi}\} = \{0\} \tag{2.11}$$

The problem is solved when the set of n equations (2.10) is solved simultaneously for the n nodal values of ϕ. If there are q nodes in the solution domain where ϕ is specified by boundary conditions, there will be $n - q$ equations to be solved for the $n - q$ unknowns.

Requirements for Interpolation Functions Approximate solutions converge to the correct solution where an increasing number of elements are used, that is, when the element mesh is refined. Mathematical proofs of convergence assume that the process of mesh refinement occurs in a regular fashion, defined by three conditions [5].

1. the elements must be made smaller in such a way that every point of the solution domain can always be within an element, regardless of how small the element may be;

2. all previous meshes must be contained in the refined meshes;

3. the form of interpolation functions must remain unchanged during the process of mesh refinement.

These first two conditions are shown in Figure 2.1.

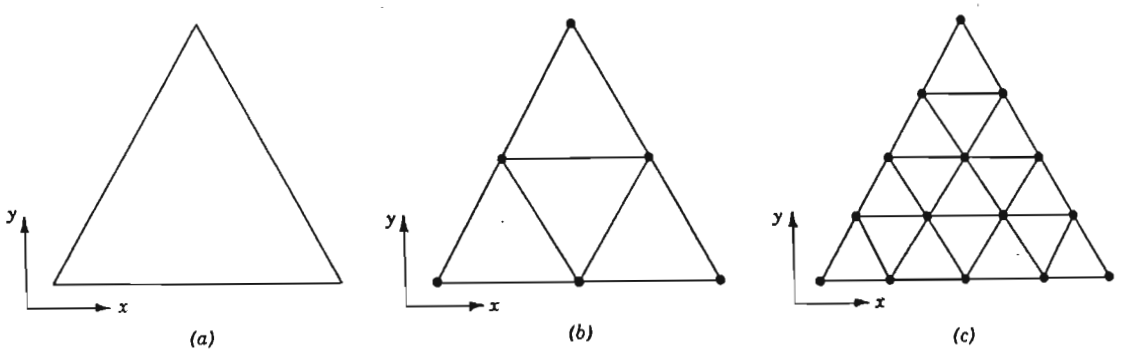

Figure 2.1. An example of successive mesh refinements. a). Original solution domain b). Discretization with four triangular elements c). Discretization with sixteen triangular elements.

To guarantee monotonic convergence in the sense just described and to make the assembly of the individual equations meaningful, it is required that the interpolation functions $N^{(e)}$ in the expressions

$$\phi^{(e)} \left[N^{(e)}\right] \{\phi\}^{(e)}, \; e = 1, 2, ..., M \tag{2.12}$$

be chosen so as to satisfy the following general requirements:

1. At element interfaces (boundaries) the field variable ϕ and any of its partial derivatives up to one order less than the highest order derivative appearing in $I(\phi)$ must be continuous.

2. All uniform states of ϕ and its partial derivatives up to one order less than the highest order derivative appearing in $I(\phi)$ should have representation in $\phi^{(e)}$ when, in the limit, the element size shrinks to zero.

These requirements were given by Felippa and Clough [5] and justified by Oliveira [6]. The first one is known as the *compatibility* requirement, and the second as the

completeness requirement. Elements whose interpolation functions satisfy the first requirement are called *compatible* elements, those satisfying the second requirement, *complete* elements.

In addition to satisfying these requirements, it is also required that the field variable representation within an element and hence the polynomial expansion for the element remain unchanged under a linear transformation from one Cartesian coordinate system to another. Polynomials that exhibit this invariance property are said to posses *geometric isotropy.*

Domain Discretization

The first task in a finite element solution consists of discretizing the continuum by dividing it into a series of elements. The type of element that should be used depends on the problem being considered. Often only one type of element is used to represent the continuum, unless the circumstances dictate otherwise. It is easy to imagine the problem for which several different types of elements would be necessary. An example from solid mechanics would be an elastic body supported by pin connected bars. In this case the elastic body would be represented by three dimensional solid elements such as *bricks,* and the bars would be approximated by one dimensional elements. The most popular and versatile elements, because of the ease with which they can be assembled to fit complex geometries, are triangular elements in two dimensions.

A uniform element mesh is easy to construct, but it may not always provide a good representation of the continuum. More elements should be used in regions where the boundary is irregular than in regions where it is smooth. More elements are also needed in the vicinity of concentrated loads.

The ratio of elements smallest dimension to its largest dimension should be near unity. Long narrow elements should be avoided because they lead to a solution with direction bias that may lead to inaccurate results.

When solving a particular type of problem for the first time, it is good practice to obtain several solutions with different numbers of element. By comparing the results, it is possible to see whether enough elements are being used in the solution. This is known as convergence testing.

Derivation of Finite Element Equations using the Method of Weighted Residuals

The method of weighted residuals is a technique for obtaining approximate solutions to linear and non-linear partial differential equations. The method offers another means of formulating the finite element equations.

Applying the method of weighted residuals involves basically two steps. The first is to assume the general functional behavior of the dependent field variable to approximately satisfy the given differential equation and boundary conditions. Substitution of this approximation into the original differential equation and boundary conditions then results in some error called a *residual.* This residual is required to vanish in some average sense over the entire solution domain.

The second step is to solve the equations resulting from the first step and specialize the general function form to a particular function, which then becomes the approximate solution sought.

A typical example given below is to find an approximate functional representation for a field variable ϕ governed by the differential equation

$$\mathrm{L}(\phi) - f = 0 \tag{2.13}$$

in the domain D bounded by the surface Σ. The function f is a known function of the independent variables and it is assumed that sufficient boundary conditions are prescribed on Σ.

First the unknown exact solution ϕ is approximated by $\tilde{\phi}$ where either the functional behavior of $\tilde{\phi}$ is completely specified in terms of unknown parameters, or the functional dependence on all but one of the independent variables is specified while the functional dependence on the remaining independent variables is left unspecified. Thus the dependent variable is approximated by

$$\phi \approx \tilde{\phi} = \sum_{i=1}^{m} N_i C_i \tag{2.14}$$

where N_i are the assumed functions and the C_i are either the unknown parameters or unknown functions of one of the independent variables. The upper limit on the summation, m, is the number of unknowns, C_i. The m functions N_i are usually chosen to satisfy the global boundary conditions.

When $\tilde{\phi}$ is substituted in equation (2.13), viz.

$$\mathrm{L}(\tilde{\phi}) - f = R \tag{2.15}$$

where R is the residual or error that results from approximating ϕ by $\tilde{\phi}$. The method of weighted residuals seeks to determine the m unknowns C_i in such a way that error R over the entire solution domain is small. This is accomplished by forming a weighted average of the error and specifying that the weighted average vanishes over the solution domain. Hence m linearly independent weighting functions W_i are chosen and the weighted average is computed as

$$\int_D [\mathrm{L}(\tilde{\phi}) - f] W_i dD = \int_D R W_i dD = 0, \; i = 1, 2, ..., m \tag{2.16}$$

In this case $R = 0$.

The form of the error distribution principle expressed in equations (2.16) depends on the choice of the weighting functions. Once the weighting functions are specified, equations (2.16) represent a set of m equations, other algebraic or ordinary differential equations to be solved for the coefficients of C_i. The second step is to solve equations (2.16) for C_i and hence obtain an approximate representation of the unknown field variable ϕ via equations (2.14).

There is a variety of weighted residual techniques available because of the broad choice of weighting functions or error distribution functions that can be used. The error distribution principle most often used to derive finite element equation is known as the *Galerkin criterion.* According to the *Bubnow-Galerkin* method, the weighting functions are chosen to be the same as the approximating functions used to represent ϕ, that is $W_i = N_i$ for $i = 1, 2, ..., m$. Thus Galerkin's method requires that

$$\int_D [\mathrm{L}(\phi^{(e)}) - f^{(e)}] N_i^{(e)} dD^{(e)} = 0, \; i = 1, 2, ..., r \tag{2.17}$$

where the superscript (e) restricts the range to one element, $\phi^{(e)} = \left\lfloor N^{(e)} \right\rfloor \{\phi\}^{(e)}$, $f^{(e)}$ is a forcing function defined over the element (e) and r is a number of unknown parameters assigned to the elements.

Elements and Interpolation Functions

A standard definition and notation to express the degree of continuity of a field variable at element interfaces are given next. If the field variable is continuous at element interfaces it is said that there is C^0 continuity. If the field variable is continuous for the first derivatives there is C^1 continuity; if second derivatives are also continuous there is C^2 continuity and so on.

The functions appearing under the integrals in the element equations contain derivatives up to $(r+1)th$ order. Following requirements must be satisfied to have assurance of convergence as element size decreases.

Compatibility requirements: At element interfaces there must be C^r continuity.

Completeness requirements: Within an element there must be C^{r+1} continuity.

These requirements hold whether the element equations were derived using the variational method, the Galerkin method or some other method.

Basic Element Shapes

The continuum or solution domain of arbitrary shape can be accurately modeled by an assemblage of simple shapes. Most finite elements are geometrically simple.

For one-dimensional problems with only one independent variable, the elements are line segments (Figure 2.2).

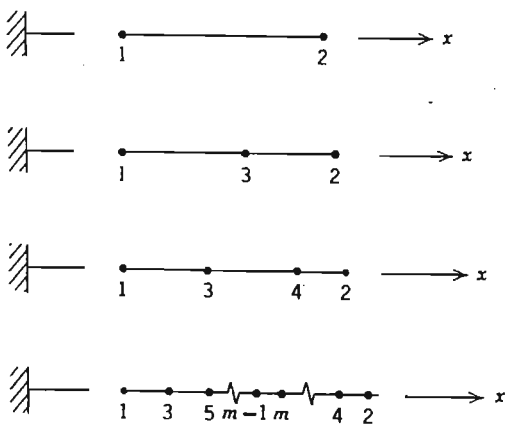

Figure 2.2. A family of one-dimensional line elements.

Common two-dimensional element shapes are shown in Figure 2.3.

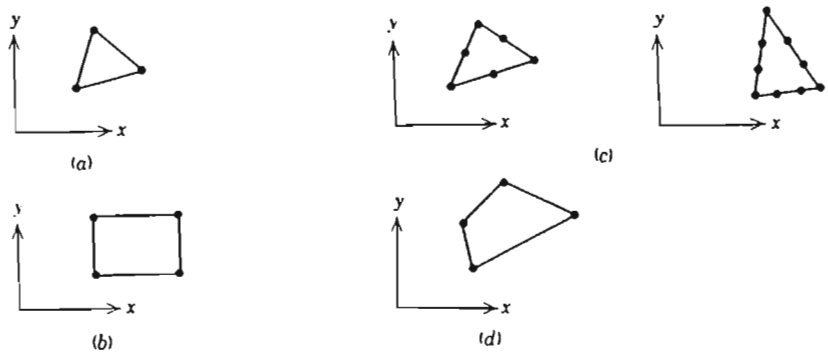

Figure 2.3. Examples of two dimensional elements a). Three node triangle b). Rectangle c). Triangles with six and ten nodes d). General quadrilateral.

The number of nodes assigned to a particular element depends on the type of nodal variables, the type of interpolation function and the degree of continuity required. For some one-dimensional problems the finite element method is the most rational approach, foe example, frame analysis in solid mechanics and flow network analysis in fluid mechanics. In elasticity problems where spars are used as stiffeners, one-dimensional elements can represent the spars while being connected to other two- or three-dimensional elements that represent the rest of the elastic solid.

The three-node flat triangular element (Figure 2.3a) is the simplest two-dimensional element and it enjoys the distinction of being the first and most often used basic finite element. The reason is that an assemblage of triangles can always represent a two-dimensional domain of any shape. A simple but less useful two-dimensional element is the four node rectangle (2.4b) whose sides are parallel to the global co-ordinate system.

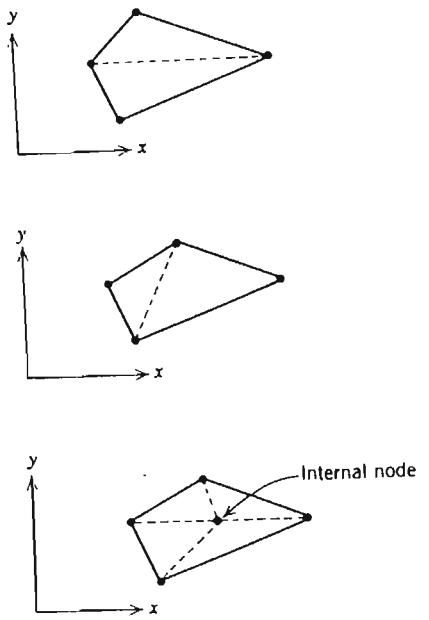

Figure 2.4. The quadrilateral element formed by combining triangles.

This type of element is easy to construct automatically by computer because of its regular shape, but is not well suited for approximating curved boundaries. In addition to the simplest triangle and the rectangle, other common two-dimensional elements are six-node triangle (Figure 2.3c), and the general quadrilateral (Figure 2.3d). Quadrilateral elements may be formed directly or they may be developed by combining two or four basic triangle elements as shown in Figure 2.4. Other types of elements that are actually three-dimensional but described by only one or two independent variables are axisymmetric or ring-type elements (Figure 2.5). These elements are useful when treating problems that possess axial symmetry in

cylindrical coordinates.

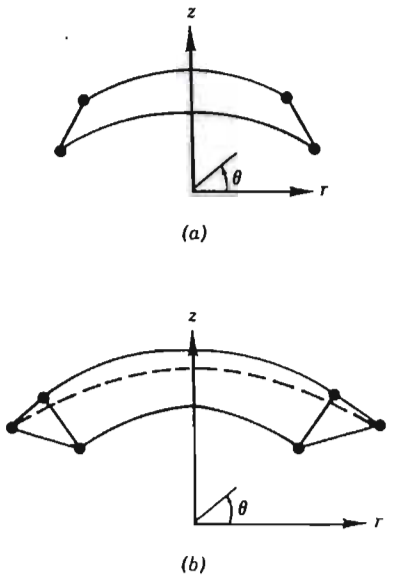

Figure 2.5. Examples of axisymmetric elements.

The four-node tetrahedron element in three-dimensions (Figure 2.6a) is the simplest and the most useful element in three-dimensional problems.

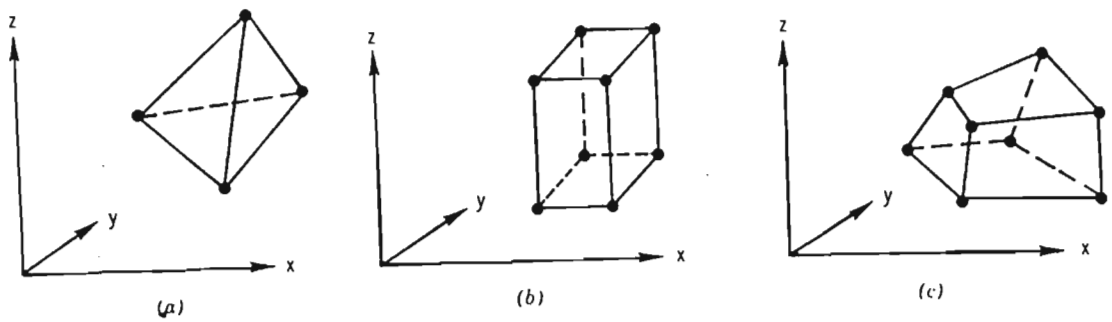

Figure 2.6. Three dimensional elements a). Tetrahedron b). Right prism c). General hexahedron.

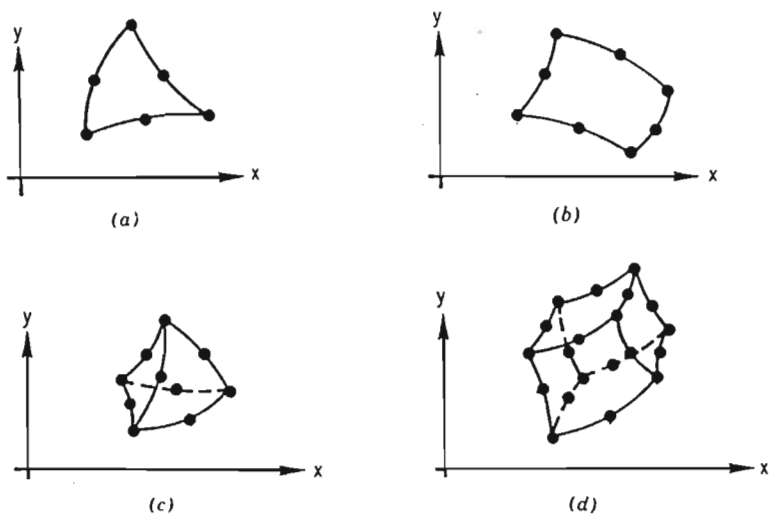

Figure 2.7. Common isoparametric elements a). Triangle b). Quadrilateral c). Tetrahedron d). Hexahedron.

Another simple three-dimensional element is the right hand prism shown in Figure 2.6b. A general hexahedron (Figure 2.6c) may be constructed from five tetrahedra. Elements which are constructed with curved boundaries are known as isoparametric elements. These elements, some examples of which are shown in Figure 2.7 are most useful when it is desirable to approximate curved boundaries with only a

few elements. They have especially been useful in the solution of three-dimensional problems, where it is necessary to reduce the computations by using fewer elements.

Basic Element Shape Functions

Interpolation Functions - Polynomials

Although it is conceivable that many types of functions could serve as interpolation functions, only polynomials have received widespread use. They can be integrated or differentiated without difficulty.

One independent variable

In one dimension a general complete nth-order polynomial may be written as

$$P_n(x) = \sum_{i=0}^{T_n^{(1)}} \alpha_i x^i \tag{2.18}$$

where the number of terms in the polynomial is $T_n^{(1)} = n + 1$. For $n = 1$, $T_1^{(1)} = 2$ and $P_1(x) = \alpha_o + \alpha_1 x$; for $n = 2$, $T_2^{(1)} = 3$ and $P_2(x) = \alpha_o + \alpha_1 x + \alpha_2 x^2$; and so on.

Two independent variables

In two dimensions a complete nth-order polynomial may be written as

$$P_n(x,y) = \sum_{k=0}^{T_n^{(2)}} \alpha_k x^i y^j, \; i + j \leq n \tag{2.19}$$

where the number of terms in the polynomial is $T_n^{(2)} = (n+1)(n+2)/2$. For $n = 1$, $T_1^{(2)} = 3$ and $P_1(x,y) = \alpha_1 + \alpha_2 x + \alpha_3 y$; for $n = 2$, $T_2^{(2)} = 6$ and $P_2(x,y) = \alpha_1 + \alpha_2 x + \alpha_3 y + \alpha_4 xy + \alpha_5 x^2 + \alpha_6 y^2$; and so on.

Three independent variables

In three dimensions a complete nth-order polynomial may be written as

$$P_n(x,y,z) = \sum_{l=0}^{T_n^{(3)}} \alpha_l x^i y^j z^k, \; i + j + k \leq n \tag{2.20}$$

where the number of terms in the polynomial is

$$T_n^{(3)} = \frac{(n+1)(n+2)(n+3)}{6} \tag{2.21}$$

For $n = 1$, $T_1^{(3)} = 4$ and $P_1(x,y,z) = \alpha_1 + \alpha_2 x + \alpha_3 y + \alpha_4 z$; for $n = 2$, $T_2^{(3)} = 10$ and $P_2(x,y,z) = \alpha_1 + \alpha_2 x + \alpha_3 y + \alpha_4 z + \alpha_5 xy + \alpha_6 xz + \alpha_7 yz + \alpha_8 x^2 + \alpha_9 y^2 + \alpha_{10} z^2$; and so on.

Two-Dimensional Problems

Elements for C^0 problems

The number of elements capable of satisfying C^0 continuity is infinite since nodes and degrees of freedom may be added to the elements to form ever increasing higher-order elements. In general, as the complexity of the elements is increased by adding more nodes and more degrees of freedom and using higher-order polynomials, the number of elements and total number of degrees of freedom needed to achieve a given accuracy in a given problem are less than would be required if simpler elements were used [7]. None the less, this does not suggest that higher-order elements always be used in preference to lower order elements.

There is no general guideline for choosing the optimum element for a given problem, because the type of element that yields good accuracy with low computing time is problem dependent. For C^0 problems, elements that require polynomials of order greater than three are rarely used, since little additional accuracy is gained for the extra effort expended. If a complicated boundary is to be modeled, it is more advantageous to use a large number of simple elements than a few complex elements.

Triangular elements

A portion of the family of higher-order elements may be obtained by assigning additional external and interior nodes to triangles. Each element in this series has a sufficient number of nodes to specify a complete polynomial of the order necessary to give C^0 continuity. The compatibility, completeness and geometric isotropy requirements are satisfied.

For the three-node triangular element, the linear variation of ϕ is written as

$$\phi(x,y) = \alpha_1 + \alpha_2 x + \alpha_3 y = [1\ x\ y]\{\alpha\} = [P]\{\alpha\} \tag{2.22}$$

and by evaluating this expression at each node, we obtain

$$\{\phi\} = [G]\{\alpha\} \tag{2.23}$$

According to the procedure of deriving interpolation functions, this can be written as

$$\begin{aligned} \phi &= [P][G]^{-1}\{\alpha\} = [N]\{\phi\} \\ [N] &= [P][G]^{-1} \end{aligned} \tag{2.24}$$

where the elements of $[N]$, $N_i = L_i$ are the area coordinates for the triangle.

Rectangular elements

Interpolation functions for rectangular elements with sides parallel to the global axes are easily developed using Lagrangian interpolation concepts. After the local coordinates are defined the function may be written as

$$\phi(\xi,\eta) = N_1(\xi,\eta)\phi_1 + N_2(\xi,\eta)\phi_2 + N_3(\xi,\eta)\phi_3 + N_4(\xi,\eta)\phi_4 \tag{2.25}$$

where

$$\begin{aligned} N_1(\xi,\eta) &= L_1(\xi)L_1(\eta), \\ N_2(\xi,\eta) &= L_2(\xi)L_2(\eta), \\ &\textit{etc.} \end{aligned} \tag{2.26}$$

and the L_i are the Lagrange polynomials. Interpolation functions formed as products in this way satisfy the requirements of possessing unit value at the node for which they are defined and zero at the other nodes.

Elements for C^1 Problems

Constructing two-dimensional elements that can be used for problems requiring continuity of the field variable ϕ as well as its normal derivative $\frac{\partial\phi}{\partial n}$ along element boundaries is far more complicated than constructing elements for C^0 continuity alone. The field variable ϕ and $\frac{\partial\phi}{\partial n}$ are uniquely specified along the element boundaries by the degrees of freedom assigned to the nodes along a particular boundary. According to Felippa and Clough [5], the difficulties arise from the following principles:

1. The interpolation functions must contain at least some cubic terms, because the three nodal values ϕ, $\frac{\partial\phi}{\partial x}$ and $\frac{\partial\phi}{\partial y}$ must be specified at each corner of the element.

2. For non rectangular elements C^1 continuity requires the specification of at least the six nodal values, ϕ, $\frac{\partial\phi}{\partial x}$, $\frac{\partial\phi}{\partial y}$, $\frac{\partial^2\phi}{\partial x^2}$, $\frac{\partial^2\phi}{\partial y^2}$ and $\frac{\partial^2\phi}{\partial x\partial y}$. at the corner nodes. For a rectangular element with sides parallel to the global axes it is necessary to specify at the corner nodes only ϕ, $\frac{\partial\phi}{\partial x}$, $\frac{\partial\phi}{\partial y}$ and $\frac{\partial^2\phi}{\partial x\partial y}$.

Three Dimensional Elements

Elements for C^o problems

Constructing three-dimensional elements to give C^0 continuity at element interfaces follows immediately from a natural extension of the corresponding elements in

two dimensions. Instead of requiring continuity of the field variable along the edge of the element, continuity is required on the faces of the elements.

Hexahedral elements

The concept of Lagrange and Hermite interpolation for two-dimensional elements extend also to hexahedral elements in three dimension. Interpolation functions for this family of elements may be written as the product of the Lagrange polynomials in all of the orthogonal coordinate directions ξ, η, ζ, (origin at the centroid of the element). Hence for node k

$$N_k(\xi, \eta, \zeta) = L_k(\xi), L_k(\eta), L_k(\zeta) \tag{2.27}$$

where it is understood that each function L_k is properly formed to account for number of subdivisions (nodes) in the particular coordinate direction. Zienkiewicz *et al* [8] generated the series of such elements. The interpolation functions for these serendipity elements are incomplete polynomials and are derived by inspection.

Linear element

Equation 8-node linear element is written as

$$N_i = \frac{1}{8}(1 + \xi\xi_i)(1 + \eta\eta_i)(1 + \xi\xi_i) \tag{2.28}$$

Higher-order elements of this family are seldom considered because interior nodes must be introduced to continue the construction of the interpolation functions.

Triangular prisms

Modeling complex-shape, three-dimensional solution domains with hexahedral elements can cause some difficulties because these *brick*-shaped elements may not fit the boundary. Rather than using a large number of small *bricks*, it is advantageous to mix hexahedra and triangular prisms to obtain a good fit. Lagrange hexahedra

or serendipity hexahedra are shown in Figure 2.8.

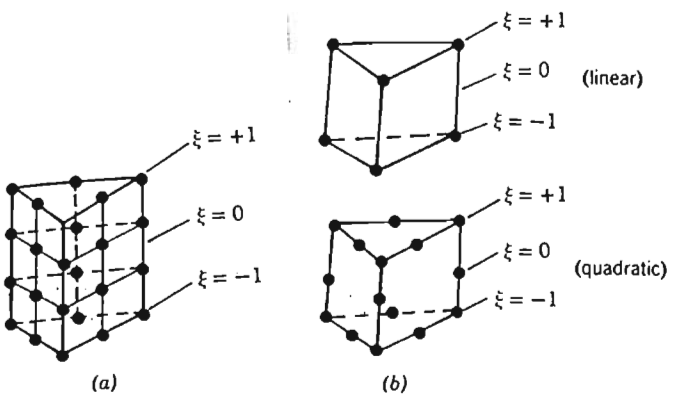

Figure 2.8. Families of triangular prism elements.

For the quadratic prism of the serendipity type (Figure 2.8b);
Corner nodes:

$$N_i = \frac{1}{2}L_i(2L_i - 1)(1 + \xi) - \frac{1}{2}L_i(1 - \xi^2) \tag{2.29}$$

Midsides of triangles

$$N_i = 2L_iL_j(1 + \xi) \tag{2.30}$$

Midsides of rectangles

$$N_i = L_i(1 + \xi)^2 \tag{2.31}$$

2.1.2 Elasticity Problems

An Introduction to Elasticity Problems

Model	Variational principle	Inside each element	Along Interelement boundary	Unknown in final equations
Compatible	Minimum potential energy	Continuous displacements	Displacement compatibility	Nodal displacements
Equilibrium	Minimum complementary energy	Continuous and equilibrating stresses	Equilibrium boundary tractions	Stress parameters Generalized nodal displacements
Hybrid 1	Modified complementary energy	Continuous and equilibrating stresses	Assumed compatible displacements	Nodal displacements
Hybrid 2	Modified potential energy	Continuous displacements	Assumed equilibrating boundary tractions	Displacement parameters and boundary forces
Hybrid 3	Modified potential energy	Continuous displacements	Assumed boundary tractions for each element and assumed boundary displacements	Nodal displacements
Mixed (Plate-bending problems)	Reissner's principle	Continuous stresses and displacements	Combinations of boundary displacements and tractions	Combination of boundary displacements and tractions

Table 2.1. Classification of finite element methods in elasticity.

Most applications of the finite element method to solid mechanics problems use a variational principle to derive the necessary element properties or equations.The three most commonly used variational principles are the principle of minimum potential energy, the principle of complementary energy and Reissner's principle. When the potential energy principle is used, the form of the displacement field within each element must be assumed. This is sometimes called the *displacement method* or the *compatibility method* in the finite element analysis. When the complementary energy method is used, the form of the stress field is assumed and this is called the *force method* or *equilibrium method.* Pian and Tong [9] tabulated (Table 2.1) these and other variational bases of the finite element method in solid mechanics. For particular problems, one principle may be more suitable than another, but for a large class of problems the displacement method is the simplest to apply and the

most widely used.

General Formulation for Two-dimensional Problems

The variational principle

The potential energy of a two-dimensional elastic body acted upon by surface and body forces and in equilibrium can be written as:

$$\begin{aligned}\Pi(u,v) = \tfrac{1}{2}\int\int_A [\left\lfloor\tilde{\delta}\right\rfloor [B]^T[C]\{\delta\} - 2\left\lfloor\tilde{\delta}\right\rfloor [B]^T[C]\{\epsilon_0^*\}]t dA \\ - \int\int_A \lfloor F^*\rfloor \lfloor\delta\rfloor t dA - \int_{C_1}[T^*]\{\delta\}dS\end{aligned} \tag{2.32}$$

where $t = t(x,y)$ is the thickness of the body,

$\{\delta\} = \begin{Bmatrix} u(x,y) \\ v(x,y) \end{Bmatrix}$ is the column matrix of the components of the displacement field measured from some datum,

$[B] = \begin{bmatrix} \partial/\partial x & 0 \\ 0 & \partial/\partial y \\ \partial/\partial x & \partial/\partial y \end{bmatrix}$ is the matrix relating strains and displacements,

$[C]$ is the material stiffness which takes different forms according to the problem considered,

$\{\epsilon_0^*\}$ is the column vector of initial strains which may be due to nonuniform temperature distributions, shrink fits etc.

$\lfloor F^*\rfloor = \lfloor X^*, Y^*\rfloor$ are the body force components due to gravity, centrifugal action, and the like,

$\lfloor T^*\rfloor = \left\lfloor T_x^*, T_y^*\right\rfloor$ are the boundary traction components acting on portion C_1 of the boundary; these are defined per unit length for a unit thickness.

The asterisk superscript denotes known quantities. At equilibrium the displacement field (u,v) in the body is such that the total system potential energy assumes a minimum value.

After using a suitable variational principle, general finite element equations for the elastic continuum may be developed. First the continuum will be subdivided into elements of some shape, then the form of displacement function is assumed over each element. For the general formulation, it is not needed to specify the type of element nor the particular displacement function. Firstly the equations for the general case can be developed. Subsequently they are specialised for particular cases.

Requirements for the Displacement Interpolation Functions

It is assumed that the area A (Figure 2.9) is divided into M discrete elements.

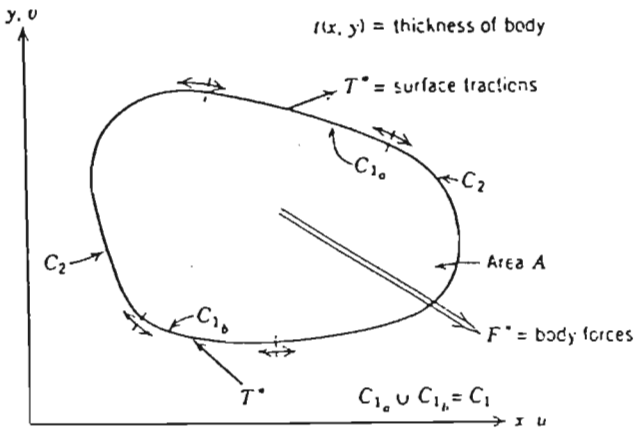

Figure 2.9. Arbitrary two-dimensional elastic body experiencing surface tractions and body forces.

The potential energy of the elements is the sum of the potential energies of all elements provided that the interpolation functions expressing the variation of the displacement within each element satisfy the compatibility and completeness requirements. In other words to write

$$\Pi(u,v) = \sum_{e=1}^{M} \Pi^{(e)}(u,v) \tag{2.33}$$

and to be assured of convergence as element mesh size decreases, the interpolation must satisfy the compatibility and completeness requirements.For plane stress and plane strain as well as three-dimensional elasticity problems polynomial interpolations satisfy the compatibility and completeness requirements when the polynomials contain at least a constant and linear terms.

To express $\Pi^{(e)}(u,v)$, which is the potential energy function for one element, in terms of discrete values of displacement components, it is assumed that within each element having r nodes, the displacement field is approximately related to its nodal

values by r interpolating functions $N_i(x,y)$. Thus the distributed displacement field can be expressed as

$$\{\tilde{\delta}\}^{(e)} = \left\{ \begin{array}{c} u(x,y) \\ v(x,y) \end{array} \right\}^{(e)} = \left\{ \begin{array}{c} \sum_{i=1}^{r} N_i(x,y)u_i \\ \sum_{i=1}^{r} N_i(x,y)v_i \end{array} \right\} = \left\{ \begin{array}{c} \lfloor N \rfloor \{u\} \\ \lfloor N \rfloor \{v\} \end{array} \right\} (e) = [N]\{\delta\}^{(e)} \tag{2.34}$$

where $\{\delta\}^{(e)}$ denotes the element nodal displacements.

Element Stiffness Equations Since the displacement field for the element has been expressed in terms of known interpolation functions and unknown displacements, the potential energy functional will be similarly expressed. Thus for element (e), the discretised functional is

$$\Pi^{(e)}(\{\delta\}^{(e)}) = \Pi^{(e)}(u_1, u_2, ..., u_r, v_1, v_2, ..., v_r) \tag{2.35}$$

or more explicitly

$$\begin{array}{c} \Pi^{(e)}(\{\delta\}^{(e)}) = \frac{1}{2} \int\int_{A^{(e)}} [\lfloor \delta \rfloor^{(e)} [B]^{T^{(e)}} [C]^{(e)} [B]^{(e)} \{\delta\}^{(e)} \\ -2 \lfloor \delta \rfloor^{(e)} [B]^{T^{(e)}} [C]^{(e)} \{\epsilon_0^*\}^{(e)}] t^{(e)} dA^{(e)} \\ - \int\int_{A^{(e)}} \lfloor F^* \rfloor^{(e)} \{\delta\}^{(e)} t^{(e)} dA^{(e)} \\ - \int_{C_1^{(e)}} \lfloor T^* \rfloor^{(e)} \{\delta\}^{(e)} dS^{(e)} \end{array} \tag{2.36}$$

At equilibrium, the potential energy of the system assumes a minimum value when the first variation of the functional vanishes, that is

$$\delta\Pi(u,v) = \sum_{e=1}^{M} \delta\Pi^{(e)}(u,v) = 0 \tag{2.37}$$

where

$$\delta\Pi(u,v) = \sum_{i=1}^{r} \frac{\delta\Pi^{(e)}}{\delta u_i} \delta u_i + \sum_{i=1}^{r} \frac{\delta\Pi^{(e)}}{\delta v_i} \delta v_i = 0 \tag{2.38}$$

But the δu_i and the δv_i are independent variations and equation (2.38) is satisfied only if

$$\frac{\delta\Pi^{(e)}}{\delta u_i} = \frac{\delta\Pi^{(e)}}{\delta v_i} = 0, \; i = 1, 2, ..., r \tag{2.39}$$

for every element (e) of the system. Equations (2.39) express the conditions used to find the element equations. Then, considering node q, and using equation (2.36), we have at node q

$$\begin{array}{c} \left\{ \frac{\delta\Pi^{(e)}}{\delta u_q} \quad \frac{\delta\Pi^{(e)}}{\delta u_v} \right\}^T = \{0\} = \int\int_{A^{(e)}} [B]_q^{T^{(e)}} [C]^{(e)} [B]_p^{(e)} \{\delta\}^q t^{(e)} dA^{(e)} \\ - \int\int_{A^{(e)}} [B]_q^{T^{(e)}} [C]^{(e)} \{\epsilon_0^*\}_q^{(e)} t^{(e)} dA^{(e)} \\ - \int\int_{A^{(e)}} N_q \{F^*\}_q^{(e)} t^{(e)} dA^{(e)} - \int_{C_i^{(e)}} N_q \{T^*\}_q^{(e)} dS_q^{(e)} \end{array} \tag{2.40}$$

where

$$\{\delta\}^q = \begin{Bmatrix} u_q \\ v_q \end{Bmatrix} \tag{2.41}$$

is the column vector of the two displacement components at node q.

$$[B]_q^{(e)} = \begin{bmatrix} \delta N_q/\delta x & 0 \\ 0 & \delta N_q/\delta y \\ \delta N_q \delta y & \delta N_q/\delta x \end{bmatrix} \quad q = 1, 2, ..., r \tag{2.42}$$

The definition of $[B]_q^{(e)}$ in equation (2.42), for a two-dimensional elastic follows from the definitions of the three nonzero strain components ε_x, ε_y, and γ_{xy}. Since the traction vector $\{T^*\}$ is a boundary effect, the last term of equation (2.40) applies only if element (e) lies on the boundary where traction is specified.

Equation (2.40) is the force-displacement relation for node q. In matrix notation it can be written as

$$[k]^{qp}\{\delta\}^q = \{F_0\}^q + \{F_B\}^q + \{F_T\}^q = \{F\}^q \tag{2.43}$$

where

$$[k]^{qp} = \int\int_{A^{(e)}} [B]_q^{T^{(e)}} [C]^{(e)} \{\epsilon_0^*\}_q^{(e)} t^{(e)} dA^{(e)} \tag{2.44}$$

is the initial force vector at node q,

$$\{F_B\}^q = \int\int_{A^{(e)}} N_q(x,y) \{F^*\}_q^{(e)} t^{(e)} dA^{(e)} \tag{2.45}$$

is the nodal body force vector and

$$\{F_T\}^q = \int\int_{C_1^{(e)}} N_q(x,y) \{T^*\}_q^{(e)} dS_q^{(e)} \tag{2.46}$$

is the nodal force vector due to surface loading (present only for boundary elements).

$$\{F\}^q = \textit{resultant external load vector at node } q \tag{2.47}$$

Equation (2.42) expresses the stiffness submatrices associated with a typical node, but since each element has r nodes, the complete stiffness for the element is a $2r \times 2r$ matrix of the form

$$[K]^{(e)} = \begin{bmatrix} [k]^{11} & [k]^{12} & \dots & [k]^{1r} \\ [k]^{21} & [k]^{22} & \dots & [k]^{2r} \\ \vdots & \vdots & \vdots & \vdots \\ [k]^{q1} & [k]^{q2} & \dots & [k]^{qr} \\ \vdots & \vdots & \vdots & \vdots \\ [k]^{r1} & [k]^{r2} & \dots & [k]^{rr} \end{bmatrix} \tag{2.48}$$

The arrangement of terms in the element stiffness matrix implies that the column matrix of discrete nodal displacements for the elements has the form

$$\{\delta\}^{(e)} = \begin{Bmatrix} \{\delta\}^1 \\ \{\delta\}^2 \\ \vdots \\ \{\delta\}^r \end{Bmatrix} = \begin{Bmatrix} u_1 \\ v_1 \\ u_2 \\ v_2 \\ \vdots \\ u_r \\ v_r \end{Bmatrix} \tag{2.49}$$

thus the force-displacement equations for the element take the standard form

$$[K]^{(e)}\{\delta\}^{(e)} = \{F\}^{(e)} \tag{2.50}$$

where

$$\{F\}^{(e)} = \begin{Bmatrix} \{F\}^1 \\ \{F\}^2 \\ \vdots \\ \{F\}^q \\ \vdots \\ \{F\}^r \end{Bmatrix} \tag{2.51}$$

It is important to note that $\{\delta\}^{(e)}$, defined by equation (2.49), is the column vector of discrete nodal displacements for element (e), whereas $\{\tilde{\delta}\}^{(e)}$, defined by equation (2.34) is the column vector of the continuous displacement field within the element.

The System Equations

Equation (2.48) with its components given by equation (2.11) is the general form of the element stiffness matrix for two-dimensional elasticity problems. The *system* equations have the same form as the *element* equations except that they are expanded in dimension to include all nodes. Hence, when the discretised system has m nodes, the system equations become

$$(2m \times 2m)[K]\,(2m \times 1)\{\delta\} = (2m \times 1)\{F\} \tag{2.52}$$

where $\{\delta\}$ is a column vector of nodal displacement components for the entire system and $\{F\}$ is the column vector of the resultant nodal forces.

For the displacement formulation either force or displacement is known in every node of the system. If body forces and initial strains are absent, the vector $\{F\}$ has zero components except for the components corresponding to nodes where concentrated external forces or displacements are specified.

For steady-state problems, once the system equations are solved for the nodal displacements, the basic relations between stress and strain, and strain and displacement, may be defined to find the stress at any point in any of the elements. A general equation for the stress components, including stresses due to displacements and initial strains, can be written as

$$\{\sigma\}^{(e)} = [C]^{(e)}[B]^{(e)}\{\delta\}^{(e)} - [C]^{(e)}\{\epsilon_0^*\}^{(e)} \tag{2.53}$$

If any initial stresses are present, these must also be added.

2.1.3 Bending of Thin Plates: A C_1- Continuity Problem

In the classic theory of plates, certain approximations are introduced initially to simplify the problem to two dimensions. These assumptions concern the linear variation of strains and stresses on lines normal to the plane of the plate. So-called exact solutions of plate theory are only true if these assumptions are valid. This is so when the plates are thin and the deflections small. In the following, the starting point will be based on the classical plate theory assumptions.

The state of deformation of a plate can be described by one quantity. This is the lateral displacement w of the *midplane* of the plate. Continuity conditions between elements have to be imposed not only on this quantity, but also its derivative, in order to ensure that the plate remains continuous, and does not 'kink'. If kinking occurs, the second derivative or curvature becomes infinite and certain infinite terms occur in the energy expression. At each node, therefore, three conditions of and continuity will usually be imposed.

Determination of suitable interpolation functions is thus a more complex task. It is, however, possible to find interpolation functions which, while preserving continuity of w, may violate its slope continuity between elements, although not at the node where such continuity is imposed. If such chosen functions satisfy the *constant strain* criterion, and in addition pass the patch test, then convergence will still be found. These are termed *non-conforming* interpolation functions.

The simplest type of element shape is thus the rectangle. The problem of thin plates, where the potential energy function contains *second derivatives* of unknown

functions, is characteristic of a large class of physical problems associated with *fourth order differential equations.*

Displacement Formulation of the Plate Problem

The displacement of a plate, under the usual thin plate theory is uniquely specified once the deflection, w, is known at all points.

In general

$$w = Na^{(e)} \tag{2.54}$$

in which the interpolation functions are dependant on Cartesian coordinates x, y, and $a^{(e)}$ list the element (nodal) parameters.

By defining the strain and stress carefully, the product of the two will correspond to the internal work requirements. Thus, the *strain* is defined as

$$\varepsilon = \left\{ \begin{array}{c} -\frac{\partial^2 w}{\partial x^2} \\ -\frac{\partial^2 w}{\partial y^2} \\ 2\frac{\partial^2 w}{\partial xy} \end{array} \right\} \tag{2.55}$$

The corresponding *stresses* are the bending and twisting moments per unit lengths in the x and y directions:

$$\sigma = \left\{ \begin{array}{c} M_x \\ M_y \\ M_{xy} \end{array} \right\} \tag{2.56}$$

Since the true strains and stresses vary linearly across the plate thickness, these can be found from such expressions as:

$$\sigma = \frac{12M_x}{t^3} z, \text{ etc} \tag{2.57}$$

where z is measured from the plate midplane, and t is the thickness of the plate. As the strains are defined by second derivatives, the continuity criterion requires that the interpolation functions be such that both w and its slope normal to the interface between elements be continuous.

The criterion of constant strain requires that any constant arbitrary value of

second derivative should be reproducible within the element.

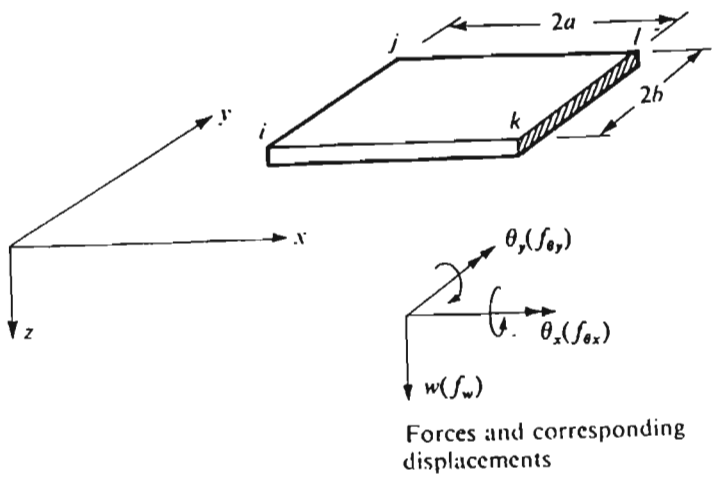

Figure 2.10. A rectangular plate element.

To ensure at least an approximate satisfaction of slope continuity, three displacement components are considered as nodal parameters: the first the actual displacement w_n in the z direction, the second a rotation about the x axis $(\theta_x)_n$, and the third about the y axis $(\theta_y)_n$. Figure 2.10 shows these rotations with their positive directions determined by the right-hand screw rule.

It is obvious that the slopes of w and the rotation are identical (except for the sign), and thus

$$a_i = \left\{ \begin{array}{c} w_i \\ \theta_{xi} \\ \theta_{yi} \end{array} \right\} = \left\{ \begin{array}{c} w_i \\ -\left(\frac{\partial w}{\partial y}\right)_i \\ \left(\frac{\partial w}{\partial x}\right)_i \end{array} \right\} \tag{2.58}$$

The nodal 'forces' corresponding to theses displacements can be interpreted as a direct force and two couples

$$f_i = \left\{ \begin{array}{c} f_{wi} \\ f_{\theta xi} \\ f_{\theta yi} \end{array} \right\} \tag{2.59}$$

as shown in Figure 2.10. It follows immediately that

$$B_i = \begin{Bmatrix} -\frac{\partial^2}{\partial x^2} N_i \\ -\frac{\partial^2}{\partial y^2} N_i \\ 2\frac{\partial^2}{\partial xy} N_i \end{Bmatrix} \tag{2.60}$$

The elasticity matrix D is given by

$$\sigma \equiv M = D(\varepsilon - \varepsilon_0) + \sigma_0 \tag{2.61}$$

For an *isotropic* plate

$$D = \frac{Et^3}{12(1-\nu^2)} \begin{bmatrix} 1 & \nu & 0 \\ \nu & 1 & 0 \\ 0 & 0 & (1-\nu)/2 \end{bmatrix} \tag{2.62}$$

and for an *orthotropic* slab with principal directions of orthotropy coinciding with the x and y axes, four constants are needed to define the behavior:

$$D = \begin{bmatrix} D_x & D_1 & 0 \\ D_1 & D_y & 0 \\ 0 & 0 & D_{xy} \end{bmatrix} \tag{2.63}$$

Clearly, for a most complete case of anisotropy, six constants at most will need to define D since the matrix has to be symmetric.

Rectangular Elements with Corner Nodes

Interpolation functions

Consider a rectangular element of a plate $ijkl$ coinciding with the $x - y$ plane as shown in Figure 2.10. At each node, displacements a_n are introduced [10]. These have three components: the first a displacement in the z direction, w_n, the second a rotation about the x axis $(\theta_x)_n$, the third a rotation about the y axis $(\theta_y)_n$.

The nodal displacements are defined by equation (2.58) while the element displacement will, as usual, be given by the listing of the nodal displacements:

$$a^{(e)} = \begin{Bmatrix} a_i \\ a_j \\ a_l \\ a_k \end{Bmatrix} \tag{2.64}$$

A polynomial expression is conveniently used to define interpolation functions in terms of the twelve parameters. Certain terms must be omitted for a complete fourth order polynomial. Expressing

$$\begin{aligned} w = \alpha_1 + \alpha_2 x + \alpha_3 y + \alpha_4 x^2 + \alpha_5 xy + \alpha_6 y^2 + \\ \alpha_7 x^3 + \alpha_8 x^2 y + \alpha_9 x y^2 + \alpha_{10} y^3 + \alpha_{11} x^3 y + \alpha_{12} x y^3 \end{aligned} \tag{2.65}$$

has some advantages. In particular, along any $x = const$ or $y = const$ line, the displacement w will vary as a cubic. The element boundaries or interfaces are composed of such lines. As a cubic is uniquely defined by four constants, the two end values of slopes displacements at the ends of the boundaries will therefore define the displacements along this boundary uniquely. As such end values are common to adjacent elements, continuity of w will be imposed all along any interface. This function can be shown to be *non-conforming.*

The constants α_1 to α_{12} can be evaluated. For instance

$$\begin{aligned} w_i &= \alpha_1 + \alpha_2 x_i + \alpha_3 y_i + ... \\ (-\tfrac{\partial w}{\partial y})_i &= \theta_{x_i} = \ -\alpha_3 + ... \\ (\tfrac{\partial w}{\partial x})_i &= \theta_{y_i} = \ -\alpha_3 + ... \\ & etc. \end{aligned} \tag{2.66}$$

In matrix form

$$a^{(e)} = C\alpha \tag{2.67}$$

where C is a 12×12 matrix depending on the nodal coordinates and α is a vector of the twelve unknown constants. Thus

$$\alpha = C^{-1} a^{(e)} \tag{2.68}$$

It is now possible to write the expression for the displacement in the standard form as

$$u \equiv w = N a^{(e)} = P C^{-1} a^{(e)} \tag{2.69}$$

where

$$P = (1, x, y, x^2, xy, y^2, x^3, x^2 y, xy^2, y^3, x^3 y, xy^3) \tag{2.70}$$

For any node, in terms of normalised coordinates

$$\begin{aligned} N_i = \tfrac{1}{2}[\zeta_0 + 1](\eta_0 + 1)(2 + \xi_0 + \eta_0 - \xi^2 - \eta^2), \\ a\xi_i(\xi_0 + 1)^2(\xi_0 - 1)(\eta_0 + 1), \\ b\eta_i(\xi_0 + 1)(\eta_0 + 1)^2(\xi_0 - 1)] \end{aligned} \tag{2.71}$$

with

$$\begin{aligned} \xi &= (x - x_c)/a \\ \xi &= (y - y_c)/b \\ \xi_0 &= \xi.\xi_i \\ \eta_0 &= \eta.\eta_i \end{aligned} \tag{2.72}$$

The form of B is obtained directly from equations (2.65) or (2.69) using equation (2.60). Thus

$$\varepsilon = \begin{Bmatrix} -2\alpha_4 & -6\alpha_7 x & -2\alpha_8 y & -6\alpha_{11} xy & \\ -2\alpha_6 & -2\alpha_9 x & -6\alpha_{10} y & -6\alpha_{12} y & \\ 2\alpha_5 & 4\alpha_8 x & 4\alpha_9 y & 6\alpha_{11} x^2 & 6\alpha_{12} y^2 \end{Bmatrix} \tag{2.73}$$

and

$$\varepsilon = Q\alpha = QC^{-1}a^{(e)} \tag{2.74}$$

and thus

$$B = QC^{-1} \tag{2.75}$$

in which

$$Q = \begin{bmatrix} 0 & 0 & 0 & -2 & 0 & 0 & -6x & -2y & 0 & 0 & -6xy & 0 \\ 0 & 0 & 0 & 0 & 0 & -2 & 0 & 0 & -2x & -6y & 0 & -6xy \\ 0 & 0 & 0 & 0 & 2 & 0 & 0 & 4x & 4y & 0 & 6x^2 & 6y^2 \end{bmatrix} \tag{2.76}$$

Note that the displacement function chosen permits a state of constant strain (curvature) to exist. This satisfies one of the criteria of convergence.

Stiffness and Load Matrices The stiffness matrix relating the nodal *forces* (given by a lateral force and two moments at each node) to the corresponding nodal displacement is

$$K^{(e)} = \int\int_{v^{(e)}} B^T D B dx dy \tag{2.77}$$

Substituting equation (2.75) and taking t as constant within the element,

$$K^{(e)} = C^{-1T}(\int\int Q^T D Q dx dy) C^{-1} \tag{2.78}$$

An explicit expression for the stiffness matrix K has been evaluated for the case of an orthotropic material and the result is given in Table 2.2.

Stiffness matrix

$$[k] = \frac{1}{60ab}[L]\{D_x[K_1] + D_y[K_2] + D_1[K_3] + D_{xy}[K_4]\}[L]$$

with

$$\begin{Bmatrix} F_i \\ F_j \\ F_k \\ F_l \end{Bmatrix} = [k] \begin{Bmatrix} \delta_i \\ \delta_j \\ \delta_k \\ \delta_l \end{Bmatrix}$$

$K_1 = p^{-2}$

$$\begin{bmatrix}
60 & & & & & & & & & & & \\
0 & 0 & & & & & & & & & & \\
30 & 0 & 20 & & & & & & & & & \\
30 & 0 & 15 & 60 & & & & & & & & \\
0 & 0 & 0 & 0 & 0 & & & & & & & \\
15 & 0 & 10 & 30 & 0 & 20 & & & & & & \\
-60 & 0 & -30 & -30 & 0 & -15 & 60 & & & & & \\
0 & 0 & 0 & 0 & 0 & 0 & 0 & 0 & & & & \\
30 & 0 & 10 & 15 & 0 & 5 & -30 & 0 & 20 & & & \\
-30 & 0 & -15 & -60 & 0 & -30 & 30 & 0 & -15 & 60 & & \\
0 & 0 & 0 & 0 & 0 & 0 & 0 & 0 & 0 & 0 & 0 & \\
15 & 0 & 5 & 30 & 0 & 10 & -15 & 0 & 10 & -30 & 0 & 20
\end{bmatrix}$$

$p^{-2} = \dfrac{b^2}{a^2}$

Symmetrical

$K_2 = p^2$

$$\begin{bmatrix}
60 & & & & & & & & & & & \\
-30 & 20 & & & & & & & & & & \\
0 & 0 & 0 & & & & & & & & & \\
-60 & 30 & 0 & 60 & & & & & & & & \\
-30 & 10 & 0 & 30 & 20 & & & & & & & \\
0 & 0 & 0 & 0 & 0 & 0 & & & & & & \\
30 & -15 & 0 & -30 & -15 & 0 & 60 & & & & & \\
-15 & 10 & 0 & 15 & 5 & 0 & -30 & 20 & & & & \\
0 & 0 & 0 & 0 & 0 & 0 & 0 & 0 & 0 & & & \\
-30 & 15 & 0 & 30 & 15 & 0 & -60 & 30 & 0 & 60 & & \\
-15 & 5 & 0 & 15 & 10 & 0 & -30 & 10 & 0 & 30 & 20 & \\
0 & 0 & 0 & 0 & 0 & 0 & 0 & 0 & 0 & 0 & 0 & 0
\end{bmatrix}$$

$p^2 = \dfrac{a^2}{b^2}$

Symmetrical

$K_3 =$

$$\begin{bmatrix}
30 & & & & & & & & & & & \\
-15 & 0 & & & & & & & & & & \\
15 & -15 & 0 & & & & & & & & & \\
-30 & 0 & -15 & 30 & & & & & & & & \\
0 & 0 & 0 & 15 & 0 & & & & & & & \\
-15 & 0 & 0 & 15 & 15 & 0 & & & & & & \\
-30 & 15 & 0 & 30 & 0 & 0 & 30 & & & & & \\
15 & 0 & 0 & 0 & 0 & 0 & -15 & 0 & & & & \\
0 & 0 & 0 & 0 & 0 & 0 & -15 & 15 & 0 & & & \\
30 & 0 & 0 & -30 & -15 & 0 & -30 & 0 & 15 & 30 & & \\
0 & 0 & 0 & -15 & 0 & 0 & 0 & 0 & 0 & 15 & 0 & \\
0 & 0 & 0 & 0 & 0 & 0 & 15 & 0 & 0 & -15 & -15 & 0
\end{bmatrix}$$

Symmetrical

$K_4 =$

$$\begin{bmatrix}
84 & & & & & & & & & & & \\
-6 & 8 & & & & & & & & & & \\
6 & 0 & 8 & & & & & & & & & \\
-84 & 6 & -6 & 84 & & & & & & & & \\
-6 & -2 & 0 & 6 & 8 & & & & & & & \\
-6 & 0 & -8 & 6 & 0 & 8 & & & & & & \\
-84 & 6 & -6 & 84 & 6 & 6 & 84 & & & & & \\
6 & -8 & 0 & -6 & 2 & 0 & -6 & 8 & & & & \\
6 & 0 & -2 & -6 & 0 & 2 & -6 & 0 & 8 & & & \\
84 & -6 & 6 & -84 & -6 & -6 & -84 & 6 & 6 & 84 & & \\
6 & 2 & 0 & -6 & -8 & 0 & -6 & -2 & 0 & 6 & 8 & \\
-6 & 0 & 2 & 6 & 0 & -2 & 6 & 0 & -8 & -6 & 0 & 8
\end{bmatrix}$$

$$L = \begin{bmatrix} l & 0 & 0 & 0 \\ 0 & l & 0 & 0 \\ 0 & 0 & l & 0 \\ 0 & 0 & 0 & l \end{bmatrix}, \quad \text{where} \quad \begin{bmatrix} 1 & 0 & 0 \\ 0 & 2b & 0 \\ 0 & 0 & 2a \end{bmatrix}$$

Table 2.2. Stiffness Matrix for a Rectangular Element.

The corresponding stress matrix for the internal moments of all the nodes is given in Table 2.3.

$6p^{-1}D_x$ $+6pD_1$	$-8aD_1$	$8bD_x$	$-6pD_1$	$-4aD_1$	0	$-6p^{-1}D_x$	0	$4bD_x$	0	0	0
$6pD_y$ $+6p^{-1}D_1$	$-8aD_y$	$8bD_1$	$-6pD_y$	$-4aD_y$	0	$-6p^{-1}D_1$	0	$4bD_1$	0	0	0
$-2D_{xy}$	$4bD_{xy}$	$-4aD_{xy}$	$2D_{xy}$	0	$4aD_{xy}$	$2D_{xy}$	$-4bD_{xy}$	0	$-2D_{xy}$	0	0
$-6pD_1$	$4aD_1$	0	$6p^{-1}D_x$ $+6pD_1$	$8aD_1$	$8bD_x$	0	0	0	$-6p^{-1}D_x$	0	$4bD_x$
$-6pD_y$	$4aD_y$	0	$6pD_y$ $+6p^{-1}D_1$	$8aD_y$	$8bD_1$	0	0	0	$-6p^{-1}D_1$	0	$4bD_1$
$-2D_{xy}$	0	$-4aD_{xy}$	$2D_{xy}$	$4bD_{xy}$	$4aD_{xy}$	$2D_{xy}$	0	0	$-2D_{xy}$	$-4bD_{xy}$	0
$-6p^{-1}D_x$	0	$-4bD_x$	0	0	0	$6p^{-1}D_x$ $+6pD_1$	$-8aD_1$	$-8bD_x$	$-6pD_1$	$-4aD_1$	0
$-6p^{-1}D_1$	0	$-4bD_1$	0	0	0	$6pD_y$ $+6p^{-1}D_1$	$-8aD_y$	$-8bD_1$	$-6pD_y$	$-4aD_y$	0
$-2D_{xy}$	$4bD_{xy}$	0	$2D_{xy}$	0	0	$2D_{xy}$	$-4bD_{xy}$	$-4aD_{xy}$	$-2D_y$	0	$4aD_{xy}$
0	0	0	$-6p^{-1}D_x$	0	$-4bD_x$	$-6pD_1$	$4aD_1$	0	$6p^{-1}D_x$ $+6pD_1$	$8aD_1$	$-8bD_x$
0	0	0	$-6p^{-1}D_1$	0	$-4bD_1$	$-6pD_y$	$4aD_y$	0	$6pD_y$ $+6p^{-1}D_1$	$8aD_y$	$-8bD_1$
$-2D_{xy}$	0	0	$2D_{xy}$	$4bD_{xy}$	0	$2D_{xy}$	0	$-4aD_{xy}$	$-2D_{xy}$	$-4bD_{xy}$	$4aD_{xy}$

Table 2.3. Rectangular Element of Figure 2.10 (Orthotropic Material).

If a distributed load q acts per unit area on an element in the direction of w then the contribution of these forces to each of the nodes is

$$f_i = -\int\int N^T q dx dy \tag{2.79}$$

or by equation (2.69)

$$f_i = -C^{-1T}\int\int P^T q dx dy \tag{2.80}$$

Quadrilateral and Parallelogram Elements

The rectangular element is not easily generalised into the quadrilateral shape. Transformation of coordinates can be performed, but generally results in the violation of

the constant curvature criterion. Thus such elements behave badly, but convergence may still occur providing the patch test is passed in the curvilinear coordinates.

Only for the case of the parallelogram is it possible to achieve constant curvature exclusively using functions of ξ and η. For a parallelogram the local coordinates (Figure 2.11) can be related to the global coordinates by an explicit expression

$$\begin{aligned} \xi &= (x - y\cot\alpha)/a \\ \eta &= \csc\alpha/b \end{aligned} \tag{2.81}$$

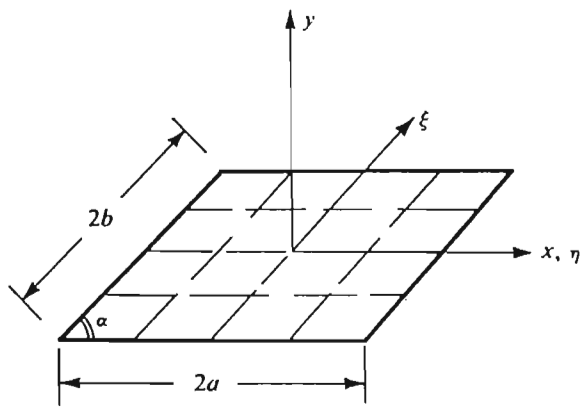

Figure 2.11. Parallelogram Element and Skew Coordinates.

2.2 Theory for Laminated Plates and Shells

2.2.1 Governing Equations for Laminated Plates: Thermal loading

Consider a symmetrically laminated rectangular plate of length a, width b and thickness H lying in the x, y, z plane and constructed of an arbitrary number K of or-

thotropic layers of equal thickness h_k and fibre orientation θ_k where $k = 1, 2, ..., K$.

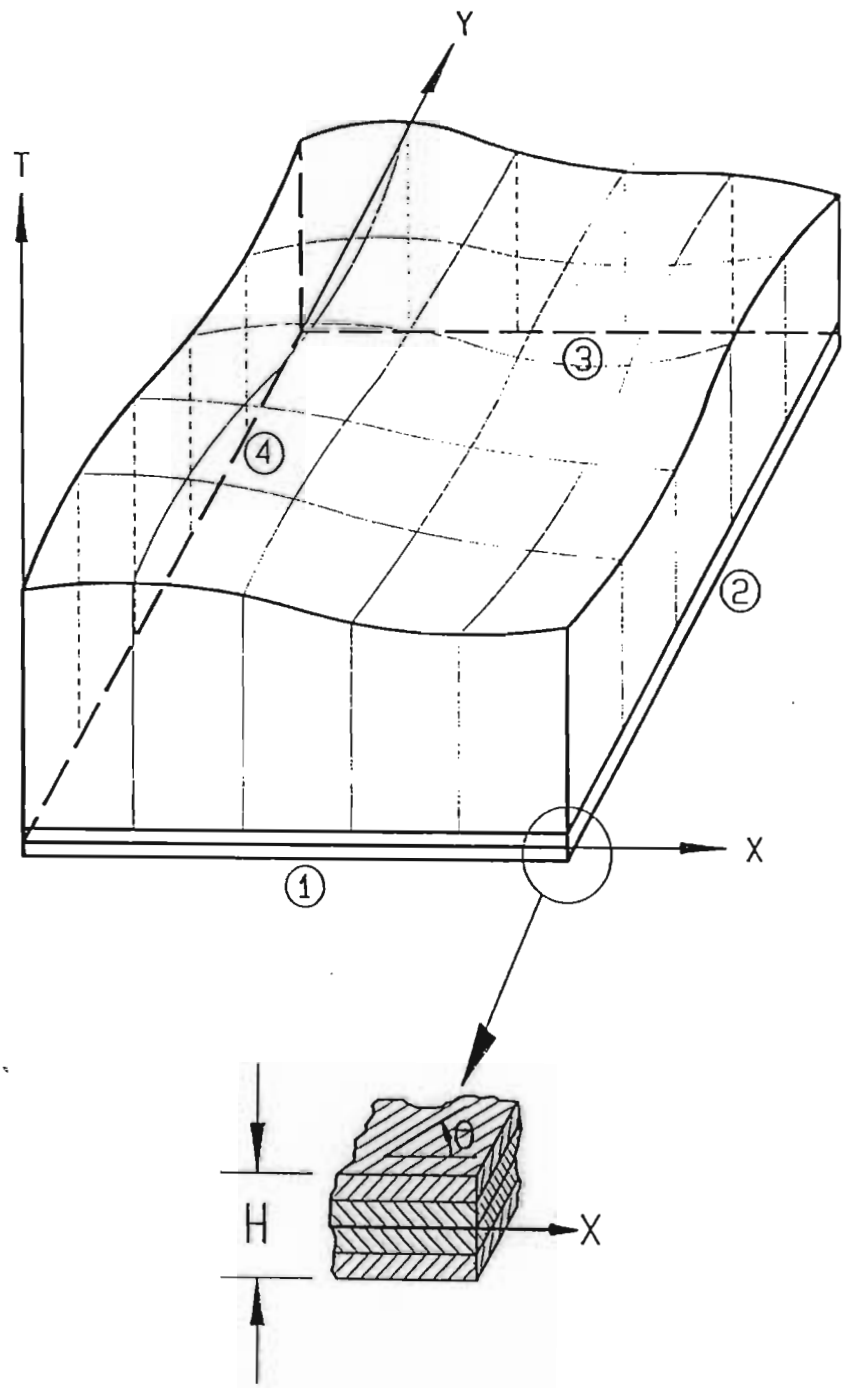

Figure 2.12. Geometry and temperature distribution of the plate.

The plate is subject to a thermal loading $T(x, y)$ which is constant in the thickness direction but variable in the x, y directions as shown in Figure 2.12, where the vertical axis indicates the temperature T at a point (x, y).

The force (N_x, N_y, N_{xy}) and moment (M_x, M_y, M_{xy}) resultants in a symmetric angle-ply laminate are related to the middle surface displacement components (u, v, w), thermal forces (N_x^T, N_y^T, N_{xy}^T) and thermal moments (M_x^T, M_y^T, M_{xy}^T) through the constitutive equations:

$$\begin{Bmatrix} N_x \\ N_y \\ N_{xy} \end{Bmatrix} = \begin{bmatrix} A_{11} & A_{12} & A_{16} \\ A_{12} & A_{22} & A_{26} \\ A_{16} & A_{26} & A_{66} \end{bmatrix} \begin{Bmatrix} u_{,x} \\ v_{,y} \\ u_{,y} + v_{,x} \end{Bmatrix} - \begin{Bmatrix} N_x^T \\ N_y^T \\ N_{xy}^T \end{Bmatrix} \tag{2.82}$$

$$\begin{Bmatrix} M_x \\ M_y \\ M_{xy} \end{Bmatrix} = \begin{bmatrix} D_{11} & D_{12} & D_{16} \\ D_{12} & D_{22} & D_{26} \\ D_{16} & D_{26} & D_{66} \end{bmatrix} \begin{Bmatrix} -w_{,xx} \\ -w_{,yy} \\ -2w_{,xy} \end{Bmatrix} - \begin{Bmatrix} M_x^T \\ M_y^T \\ M_{xy}^T \end{Bmatrix} \tag{2.83}$$

in which a comma denotes differentiation with respect to the subscript and where

$$A_{ij} = \sum_{k=1}^{K} \bar{Q}_{ij}^{(k)} (h_k - h_{k-1}) \tag{2.84}$$

and

$$D_{ij} = \frac{1}{3} \sum_{k=1}^{K} \bar{Q}_{ij}^{(k)} (h_k^3 - h_{k-1}^3) \tag{2.85}$$

are the extensional and bending stiffnesses, respectively, and $\bar{Q}_{ij}^{(k)}$ are components of the transformed reduced stiffness matrix for the $k-th$ layer.

The thermal forces and moments appearing in equations (2.82) and (2.83) are defined by

$$\begin{Bmatrix} N_x^T & M_x^T \\ N_y^T & M_y^T \\ N_{xy}^T & M_{xy}^T \end{Bmatrix} = \sum_{k=1}^{N} \int_{z_{k-1}}^{z_k} \begin{bmatrix} \bar{Q}_{11} & \bar{Q}_{12} & \bar{Q}_{16} \\ \bar{Q}_{12} & \bar{Q}_{22} & \bar{Q}_{26} \\ \bar{Q}_{16} & \bar{Q}_{26} & \bar{Q}_{66} \end{bmatrix}_k \begin{Bmatrix} \alpha_x \\ \alpha_y \\ 2\alpha_{xy} \end{Bmatrix} (1, z) T dz \tag{2.86}$$

where T is the temperature distribution and α_x, α_y and α_{xy} are the coefficients of thermal expansion. For a symmetric laminate exposed to a uniform temperature distribution, say $T = T_1$, the thermal moments M_x^T, M_y^T and M_{xy}^T vanish, while the thermal forces N_x^T, N_y^T and N_{xy}^T become functions of T_1 alone.

2.2.2 Governing Equations for Laminated Plates: Transverse loading

Consider a symmetrically laminated rectangular plate of length a, width b and thickness H under a transverse bending load $q(x,y)$. The plate is located in the x,y, z plane and constructed of an arbitrary number K of orthotropic layers of equal thickness h_k and fibre orientation θ_k where $k = 1,2,...,K$ (Figure 2.14).

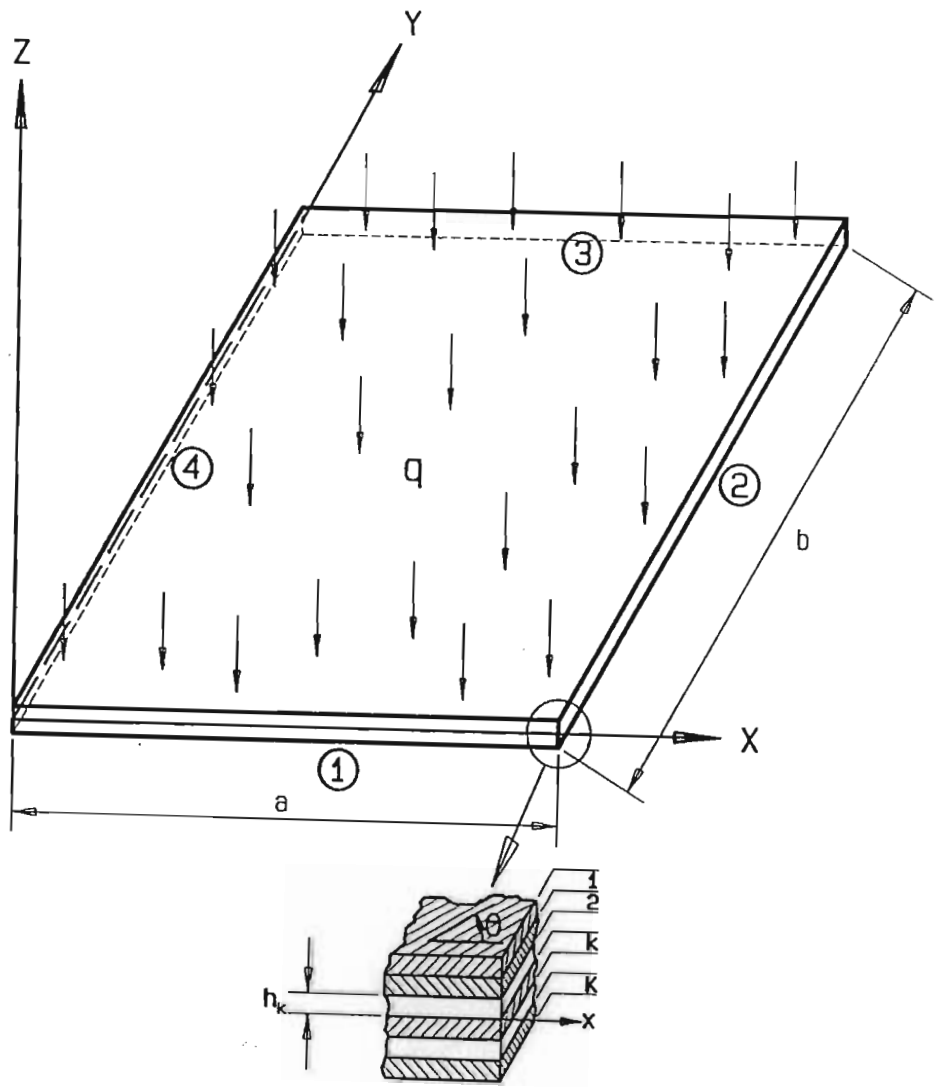

Figure 2.13. Geometry and loading of the plate.

The displacement of a point (x^0, y^0, z^0) on the reference surface is denoted by (u^0, v^0, w^0). The governing equation for the deflection w in the z direction under a transverse load q is given by [11]:

$$D_{11}w_{,xxxx} + 4D_{16}w_{,xxxy} + 2(D_{12} + 2D_{66})w_{,xxyy} + 4D_{26}w_{,xyyy} + D_{22}w_{,yyyy} = q \tag{2.87}$$

where variables after the comma denote differentiation with respect to that variable, and

$$D_{ij} = \int_{-h/2}^{h/2} \bar{Q}_{ij}^{(k)} z^2 \, dz \tag{2.88}$$

are the bending stiffnesses and $\bar{Q}_{ij}^{(k)}$ are components of the transformed reduced stiffness matrix for the $k-th$ layer.

2.2.3 Buckling Equation for Laminated Plates

Consider a laminated rectangular plate of length a, width b and height h lying in the Cartesian $x-y$ plane. The plate is constructed of orthotropic layers with fiber angles of θ_k, $k = 1, 2, ..., K$, where K denotes the total number of layers. The coordinate system x y z is located in the mid-plane, and the plate is subject to compressive forces N_{x0} in the x direction, and N_{y0} in the y direction with the load ratio defined as $\lambda = N_{y0}/N_{x0}$. The plate is symmetrically laminated with respect to the mid-plane and simply supported on all edges. It may be shown that the buckling load is given by [12]

$$N(m,n) = \frac{n^2\pi^2}{b^2(1 + \lambda\alpha_{mn}^2)}[D_{11}\alpha_{mn}^{-2} + 2(D_{12} + 2D_{66}) + D_{22}\alpha_{mn}^2] \tag{2.89}$$

where m and n represent the half wave numbers, $\alpha_{mn} = na/mb$ and D_{ij} are the bending stiffnesses.

2.2.4 Governing Equations for Cylindrical Shells

Consider a laminated circular cylindrical shell of length L, radius R, and total thickness H

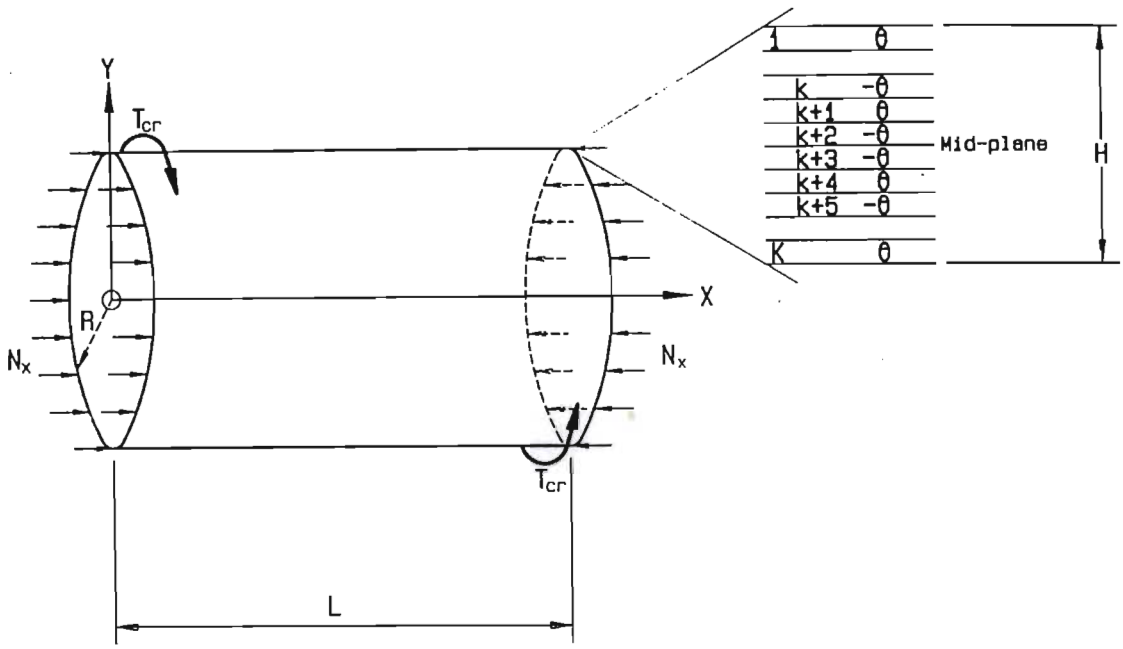

Figure 2.14. Geometry of Symmetrically Laminated Cylindrical Shell.

The shell has a symmetric layup consisting of K layers of equal thickness t. The structure is referenced in an orthogonal coordinate system (x, y, z), where x is the longitudinal, y the circumferential, and z the radial direction. The displacement components u, v and w are for the x, y and z directions respectively.

The fibre angle is defined as the angle between the fibre direction and the longitudinal (x) axis. The fibre orientations are symmetric with respect to the mid-plane of the shell and are given by $\theta_k = (-1)^{k+1}\theta$ for $k \leq K/2$ and $\theta_k = (-1)^k\theta$ for $k \geq K/2 + 1$, where $k = 1, ..., K$ with k being the layer number. The equilibrium equations for the mid-plane of this type of shell is [13]:

$$\begin{aligned} A_{11}\, u_{xx} + A_{12}(v_{,xy} + w_{,x}/R) + A_{66}(v_{,xy} + u_{,yy}) &= 0 \\ A_{66}(v_{,xx} + u_{,xy}) + A_{12}\, u_{,xy} + A_{22}(v_{,yy} + w_{,y}/R) &= 0 \\ D_{11}\, w_{,xxxx} + 2(D_{12} + 2D_{66})w_{,xxyy} + D_{22}\, w_{,yyyy} & \\ +[A_{12}\, u_{,x} + A_{22}(v_{,y} + w/R)]/R &= N_x w_{,xx} + 2N_{xy} w_{,xy} + N_y w_{,yy} \end{aligned} \tag{2.90}$$

where A_{ij} and D_{ij} are the extensional and bending stiffnesses respectively, and $\bar{Q}_{ij}^{(k)}$ are modulus components for the $k-th$ layer. Owing to the midsurface symmetry of the shell, the bending–extension coupling matrix B_{ij} does not appear in eqn. (2.90). For a simply supported shell under axial loading, the boundary conditions are given as follows:

$$w = 0,\ v = 0\ at\ x = 0,\ L \tag{2.91}$$

In this study, since only the axial load is considered,

$$N_y = 0\ and\ N_{xy} = 0 \tag{2.92}$$

Simply Supported Shells subject to Axial Buckling For laminated shells which are simply supported at $x = 0$ and $x = L$, the solution to the system of equations (2.90) which satisfies the boundary conditions (2.91) is obtained by taking the displacements in the form

$$\begin{aligned} u &= u_{mn}\cos(\lambda_m x)\sin(\lambda_n y) \\ v &= v_{mn}\sin(\lambda_m x)\sin(\lambda_n y) \\ w &= w_{mn}\sin(\lambda_m x)\sin(\lambda_n) \end{aligned} \tag{2.93}$$

where $\lambda_m = m\pi/L$, $\lambda_n = n/R$, and u_{mn}, v_{mn} and w_{mn} are the amplitudes of the displacement components, and $2m$ and n are numbers of half waves in the buckle pattern in the axial and circumferential direction respectively. The buckling load N_x corresponding to these wave numbers is obtained as an eigenvalue of the linear system of equations obtained by substituting (2.93) into (2.90). The following expression results from this [13]:

$$N_x(m,n,\theta) = \frac{1}{\lambda_m^2}\frac{\begin{vmatrix} C_{11} & C_{12} & C_{13} \\ C_{21} & C_{22} & C_{23} \\ C_{31} & C_{32} & C_{33} \end{vmatrix}}{\begin{vmatrix} C_{11} & C_{12} \\ C_{21} & C_{22} \end{vmatrix}} \tag{2.94}$$

where

$$\begin{aligned} C_{11} &= A_{11}\lambda_m^2 + A_{66}\lambda_n^2 \\ C_{22} &= A_{22}\lambda_n^2 + A_{66}\lambda_m^2 \\ C_{33} &= D_{11}\lambda_m^4 + 2(D_{12} + 2D_{66})\lambda_m^2\lambda_n^2 + D_{22}\lambda_n^4 + D_{22}/R^2 \\ C_{12} &= C_{21} = (A_{12} + A_{66})\lambda_m\lambda_n \\ C_{13} &= C_{31} = A_{12}\lambda_m/R \\ C_{23} &= C_{32} = A_{22}\lambda_n/R \end{aligned} \tag{2.95}$$

The critical buckling load $N_{cr}(\theta)$ is calculated by minimising (2.94) as a function of m and n:

$$N_{cr} = \min_{m,n} N_x(m, n; \theta) \tag{2.96}$$

Simply Supported Shells subject to Torsional Buckling Load For the same shell subject to a torsional load N_{xy}, the critical torsional buckling load $N_{xy}^*$is given as [13]:

$$N_{xy}^* = 21.75(D_{22})^{5/8}\left(\frac{A_{11}A_{22} - A_{12}^2}{A_{22}}\right)^{3/8}\frac{R^{5/4}}{L^{1/2}} \tag{2.97}$$

subject to

$$\left(\frac{D_{22}}{D_{11}}\right)^{5/6}\left(\frac{A_{11}A_{22} - A_{12}^2}{12A_{22}D_{11}}\right)^{1/2}\frac{L^2}{R} \geq 500 \tag{2.98}$$

Simply Supported Shells subject to External Buckling Pressure For this case, the only loading applied is the external pressure and the loading conditions are given by

$$N_x = qR/2, \; N_y = qR, \; N_{xy} = 0 \tag{2.99}$$

where q is the external pressure.

Equations (2.93) can be used as displacements to solve the eigenvalue problem (2.90), (2.91) and (2.99). Substituting (2.93) into (2.90) with the force resultants (2.99) gives the eigenvalue corresponding to the wave numbers m and n [13]:

$$q(m, n, \theta) = \frac{1}{R(\lambda_n^2 + \lambda_m^2/2)} \frac{\begin{vmatrix} C_{11} & C_{12} & C_{13} \\ C_{21} & C_{22} & C_{23} \\ C_{31} & C_{32} & C_{33} \end{vmatrix}}{\begin{vmatrix} C_{11} & C_{12} \\ C_{21} & C_{22} \end{vmatrix}} \tag{2.100}$$

where C_{ij} are as above (2.95).

2.3 Laminated Plates under Thermal Loading

In recent years the use of composite materials in high temperature environments has grown markedly, which has resulted in increased research both into the thermal properties of composites, as well as into the behaviour of laminated structures under thermal loads. Studies on the temperature properties of composites include those by Ishikawa *et al* [14], Schapery [15] and Cairns and Adams [16]. There are a number of studies concerning thermoelastic behaviour of laminates. Weinstein *et al* [17] established a finite element approach for the analysis of sandwich plates with different anisotropic facings. Reddy and Hsu [18] considered the effects of shear deformation and anisotropy on the thermal bending of composite plates. A closed form solution is also presented to validate their finite element results. A higher order thermoelastic theory was developed by Jonnalagadda *et al* [19] which considered the effects of transverse shear and transverse normal strain. The theory is compared with several published theories. Optimal thermoelastic design is considered by Tauchert and Adibhatla [20] using the Rayleigh-Ritz procedure and a quasi-Newton method for the optimisation.

An important subject in this field is the thermal buckling problem. This field has been studied by various researchers, and a survey paper of developments by Tauchert [21] reviews the recent work in this area.

Results given by Tauchert and Huang [22] indicated that buckling temperatures can be maximised by means of layup optimisation. In particular, for simply supported symmetric laminates with $a/b = 1$, the maximum buckling temperature occurs at $\theta_{opt} = 45^{\circ}$ for plates of more than three layers but at $\theta_{opt} \approx 25^{\circ}$ (or 65°) for single layered laminates.

Optimal design of antisymmetric laminates under thermal loads was given by Adali and Duffy [23] for the non-hybrid and hybrid cases. In the case of hybrid laminates, the optimisation is carried over the ply angles and the hybridisation parameter, and numerical results are given for simply supported laminates with graphite, boron and glass layers under a uniform temperature change. Multiobjective designs of antisymmetric laminates under thermal loads was given by Adali and Duffy [24] taking the buckling temperature and the maximum deflection as the design objectives, and ply angles and thicknesses as design variables.

Thangaratnam *et al* [25] studied the thermal buckling of composite laminated plates using the finite element method. First the uniform temperature distribu-

tions are considered. With symmetric cross-ply laminates, the number of layers is shown to have an effect on the critical temperature due to bending–twisting coupling ($D_{16} \neq 0$, $D_{26} \neq 0$). However this effect decreases as the number of layers increases. While only thermal force resultants N_x^T, N_y^T are produced in symmetric laminates, a thermal moment M_{xy}^T is also generated in antisymmetric angle ply laminates. While N_x^T and N_y^T do not change, M_{xy}^T decreases with total number of layers. This M_{xy}^T and the bending–twisting coupling cause the critical temperature to depend on the number of plies. However as the number of plies increases this effect becomes negligible. In addition, this paper shows that when the temperature varies linearly across the thickness, the buckling temperature is double that for the uniform temperature case.

Finite element solutions for the buckling behaviour of laminates subjected to a uniform temperature field were given by Chandrashekhara [26]. Transverse shear flexibility was accounted for in the analysis using the thermoelastic version of the first order shear deformable theory.

2.4 Multiobjective Design of Symmetrically Laminated Shells

Various researchers have considered the design of thin laminated cylindrical shells. Early studies include Sherrer [27] who presented a theoretical elastic solution for filament wound cylinders with any number of layers and for any loading conditions; and Reuter [28], who analyzed laminated alternate-ply cylindrical shells using classical laminated shell theory. Optimal design of these structures has been considered by several authors, using analytical or numerical methods. Hu [29] investigated the influence of shell length and thickness on the optimal layer fibre angle. Onoda [30], and Tripathy and Rao [31], using the finite element method, considered optimal layups for laminated shells under axial buckling loads. Further studies concerning buckling of circular shells include Yamaki [32] and Nshanian and Pappas [33].

Multiobjective design of composite structures includes that by Adali *et al* [34], Sun and Hansen [35] and Tennyson and Hansen [36], who studied the optimal design of laminated cylindrical shells under torsional, axial and external and internal pressure loadings. Kumar and Tauchert [37], Grandhi and Bharatram [38], and Rao *et al* [39] all considered multiobjective designs for various structures. Shape and

material optimisation was investigated by Saravanos and Chamis [40].

2.5 Optimal Design of Symmetrically Laminated Pressure Vessels

A fair number of studies dealing with laminated composite shells and vessels have been reported in the literature. Authors have considered various approaches for the purposes of designing these structures, including Reissner, Urazgil'dyaev, Eckold and Fukunaga *et al* [41], [42], [43], [44]. Karandikar *et al* [45] propose an approach using compromise Decision Support Problems in *designing for concept* of a pressure vessel made of composite materials. Some of these authors used finite element methods to model and analyse the structures. Such techniques allow effects like bending–twisting coupling to be incorporated in the problem formulation. The optimal distribution of fibres in reinforced pressure vessels for minimum strain energy was studied by Tauchert [46]. Adali *et al* [47] investigated the optimal design of laminated pressure vessels for maximum burst pressure and minimum weight, using fibre angle as the optimising variable.

2.6 Minimum Weight and Cost Design

Literature concerning minimum weight and cost design of various composite structures includes Huang and Alspaugh [48] who studied the optimal design of sandwich beams. Their optimisation software was based on the recursive quadratic programming algorithm. Another study to investigate sandwich beams was that of Paydar and Park [49] who treated the minimum weight design with a specially developed theory. Triantafillou *et al* [50] and Phillips and Gurdal [51] detailed the optimal design of hybrid box beams and composite panels, respectively. The latter used analysis routines in conjunction with an optimisation package to provide design schemes for geodesically stiffened minimum weight aircraft wing rib panels. Optimal weight design of shells is considered by Min and Charanteney [52], who investigated sandwich cylinders under combined loadings. A study by Ostwald [53] considered the combined loading cases of external pressure and axial compression in the optimisation of thin walled shells. The Bubnov-Galerkin method was used to solve the stability problem.

The optimal design of plates for minimum weight was considered by various researchers. Shin *et al* [54] designed minimum weight symmetric plates to operate in the postbuckling range. It was shown that by operating in the postbuckling range, a reduction in the plate weight can be achieved.

Studies dealing with the concept of hybridisation, whereby the distinctive properties of different materials are employed in the best way possible, include Adali and Duffy [55], which involved the minimum cost design of antisymmetric laminates subject to a frequency constraint. Other studies of hybrid laminates include Adali and Duffy ([56] to [58]) and Miki and Tonomura [59].

2.7 Minimum Deflection Design of Laminated Plates

The optimal design of laminated plates for minimum deflection has been investigated by several authors. Jiang and Chiang [60] considered symmetric, simply supported angle-ply laminates. Optimal fibre angles for a four-layered laminate under uniform pressure loading were determined using a numerical procedure. Johnson and Sims [61] studied the optimal design of symmetric simply supported plates for two types of loading conditions, uniformly distributed and point loading, applied at the centre of the plate. The plate deflection and optimal fibre angles is calculated using a one term Rayleigh-Ritz approximation. Cross–ply, simply supported square plates subjected to sinusoidally distributed loads were optimised by Rao and Singh [62]. The maximum deflection in this case occurred at the centre of the plate. Iyengar and Umeratiya [63] considered symmetrically laminated plates with a combination of simply supported and clamped boundary conditions. Maximum deflection, using the fibre angle as the optimising variable, was minimised for various hybrid laminates. A minimum thickness design for plates with discrete ply angles subject to strength and buckling constraints was considered by Kogiso *et al* [64]. A genetic algorithm search technique was used to achieve the optimal design.

A number of studies concerning the minimum weight design of laminated plates appear in the literature. Angle-ply laminates subjected to uncertain loads were considered by Adali *et al* [65] who used a convex modelling approach in their analysis. The optimal design of symmetrically laminated plates under transverse loads was given by Tauchert and Adibhatla [20] using the minimum strain energy criterion,

and by Quian *et al* [66] and by Kengtung [67] using the minimum structural compliance criterion. A maximum stiffness design for both symmetric and antisymmetric laminates was considered by Kam and Chang [68]. Adali *et al* [69] investigated the minimum weight and deflection design of thick laminates via symbolic computation.

Chapter 3

Optimal Design Problems

3.1 Optimal Design of Symmetrically Laminated Plates for Maximum Buckling Temperature

The objective of the first design problem is to maximise the buckling temperature T_b for a given plate thickness H by optimally determining the fibre orientations given by $\theta_k = (-1)^{k+1}\theta$ for $k \leq K/2$ and $\theta_k = (-1)^k\theta$ for $k \geq K/2+1$, where K is the total number of layers. Let the temperature distribution be given by $T(x,y) = T_b t(x,y)$ where $t(x,y)$ is the temperature distribution corresponding to a unit temperature input. The critical buckling temperature $T_{cr}(\theta)$ is given by

$$T_{cr}(\theta) = \min_{m,n}[T_{b,mn}(m,n;\theta)] \tag{3.1}$$

where $T_{b,mn}$ is the buckling temperature corresponding to the half-wave numbers m and n in the x and y directions, respectively. The design objective is to maximise $T_{cr}(\theta)$ with respect to θ, viz.

$$T_{\max} \triangleq \max_{\theta}[T_{cr}(\theta)], 0° \leq \theta \leq 90° \tag{3.2}$$

where $T_{cr}(\theta)$ is determined for a given θ from the finite element solution of the thermal buckling problem defined by

$$([K] + \lambda[K_G])\{u\} = 0 \tag{3.3}$$

where $[K]$ is the stiffness matrix, $[K_G]$ is the initial temperature matrix and u is the required displacement vector. The lowest eigenvalue of the homogeneous system

(3.3) yields the buckling temperature.

The present study [70] allows the temperatures to be described along the edges of the plate resulting in a temperature distribution across the plate which is a function of x and y. Before the buckling problem (3.3) can be solved, the temperature distribution has to be determined and this computation is again performed using the heat conduction module of a finite element program. This calculation yields the thermal stress field applicable to that loading condition and this solution is incorporated into the eigenvalue problem in order to compute the corresponding buckling temperature.

The optimisation procedure involves the stages of evaluating the buckling temperature $T_{cr}(\theta)$ for a given θ and improving the fibre orientation to maximise T_{cr}. Thus the computational solution consists of successive stages of analysis and optimisation until a convergence is obtained and the optimal angle θ_{opt} is determined within a specified accuracy. In the optimisation stage, the *Golden Section* method is employed.

The overall solution strategy involves three stages of computation and can be summarised as follows:

i) The solution of the temperature distribution problem for given temperatures along the edges by finite elements.

ii) The solution of the thermal buckling problem for a given θ_{opt} by finite elements.

iii) The solution of the optimisation problem to determine θ_{opt} corresponding to the maximum buckling temperature by *Golden Section* method.

This approach allows the solution of the design optimisation problem under a variety of boundary and temperature conditions along the edges.

3.2 Optimal Design of Laminated Cylindrical Pressure Vessels for Maximum External Pressure

Consider a symmetrically laminated cylindrical pressure vessel of length L, radius R, wall thickness H and total number of layers K. The vessel may be either hemispherically or flat capped as shown in Figure 3.2.1 and is subjected to external pressure $P_{ext} = P$.

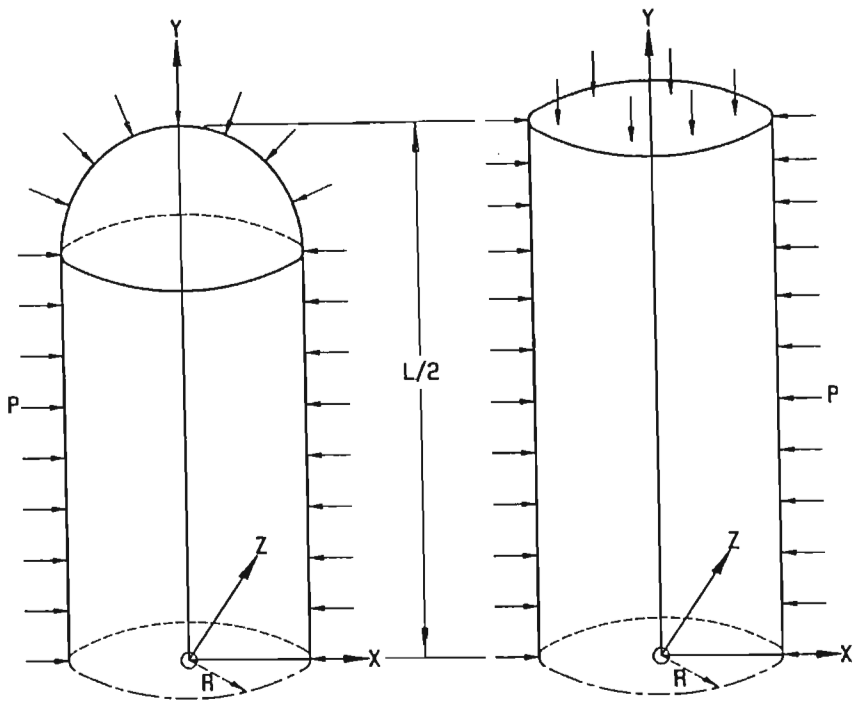

Figure 3.2.1. Diagram showing geometry and loading of a) hemispherically capped b) flat capped pressure vessel.

The objective of the second design problem is to maximise the buckling pressure $P = P(\theta)$ for a given thickness H by optimally determining the fibre orientations given by $\theta_k = (-1)^{k+1}\theta$ for $k \leq K/2$ and $\theta_k = (-1)^k\theta$ for $k \geq K/2 + 1$. This is written as [71], [72], [73]:

$$P_{\max} \triangleq \max_{\theta} [P(\theta)],\ 0° \leq \theta \leq 90° \tag{3.4}$$

where $P(\theta)$ is determined from the finite element solution of the eigenvalue problem of the same nature as that given by equation (3.3). The optimisation procedure involves the stages of evaluating the buckling pressure $P(\theta)$ for a given θ and improving the fibre orientation to maximise P. Thus, the computational solution consists of successive stages of analysis and optimisation until a convergence is obtained and the optimal angle θ_{opt} is determined within a specified accuracy. In the optimisation stage, the *Golden Section* method is employed.

3.3 Multiobjective Design of Laminated Cylindrical Shells for Maximum Torsional and Axial Loads

This problem, the third in the study, is concerned with the multiobjective optimisation of a laminated shell by determining the Pareto optimal value of the design variable θ. The concept of Pareto optimality was first introduced by Pareto [74], and is basically a maximisation of a weighted sum of the various objectives under consideration. Due to conflicting objectives, it is genarally impossible to optimise these objectives simultaneously and Pareto optimality provides a concept which is physically meaningful and easy to apply. At the beginning of a design process, it is impossible for the designer to specify the relative importance of each objective function in a chosen performance index, which is a weighted combination of all the objectives. These may be better determined after studying the response of the structure. Optimal trade–off curves, giving the points of optimal response, are useful in this process since they show the trade-offs involved in choosing a certain design. The reader is directed to Reference [75] for further study. The objectives of the design involve the maximisation of the buckling loads N^*_{xy} and N_{cr}. In general, these objectives conflict with each other necessitating a multiobjective formulation. With this situation in mind, the performance index $J(\alpha, \beta; \theta)$ of the design problem is specified as [76]:

$$J(\alpha, \beta; \theta) = \alpha N^*_{xy}(\theta)/N^*_0 + \beta N_{cr}(\theta)/N_0$$

where $\alpha, \beta \geq 0$, $\alpha + \beta > 0$ are the weighting factors, and the N^*_0 and N_0 denote the values of N^*_{xy} and N_{cr} at $\theta = 0^o$. Single objective designs correspond to $\alpha = 1$, $\beta = 0$ for maximum N^*_{xy} and $\alpha = 0$, $\beta = 1$ for maximum N_{cr}. For $\alpha, \beta > 0$, the fibre orientation θ maximising $J(\alpha, \beta; \theta)$ gives the Pareto optimal θ.

Thus the design objective can be stated as

$$J_{\max} \triangleq \max_{\theta}[J(\alpha,\beta;\theta)] = \max_{\theta}[\alpha N^*_{xy}(\theta)/N^*_0 + \beta N_{cr}(\theta)/N_0] \qquad (3.5)$$

subject to

$$0^\circ \leq \theta \leq 90^\circ$$

The optimisation procedure [77] involves the stages of evaluating the buckling loads $N^*_{xy}(\theta)$ and $N_{cr}(\theta)$ for a given θ and improving the fibre orientation to maximise

$J(\alpha, \beta; \theta)$ at a given set of weighting factors. Thus, the computational solution consists of successive stages of analysis and optimisation until a convergence is obtained and the Pareto optimal angle θ_{opt} is determined within a specified accuracy. In the optimisation stage, the *Golden Section Method* is employed.

3.4 Minimum Weight and Cost Design of Hybrid Laminated Plates

The objective of the fourth design problem involves minimising the weight and cost of a hybrid symmetrically laminated plate subject to biaxial buckling loads.

The plate is constructed of layers of different materials resulting in a hybrid laminate. Let I denote the total number of materials used in the construction, and t_i the thickness of an individual layer of the $i-th$ material. Then the total thickness of the $i-th$ material is $T_i = n_i k_i$ where n_i is the number of layers of the $i-th$ material. For each hybrid construction comprising a combination of different materials, the layer thickness of one of the materials is chosen as the reference thickness and is denoted by t_{ref}. The layer thicknesses t_i of the other materials are expressed in terms of t_{ref} by means of thickness parameters γ_i, viz

$$t_i = \gamma_i \, t_{ref} \quad i = 1, 2, \ldots, I-1 \tag{3.6}$$

The parameter γ_i indicates the ratio of layer thicknesses of the $i-th$ and reference materials. For $\gamma_i = 0$, the $i-th$ material drops out of the construction. The total thickness of the laminate is given by

$$H = \sum_{i=1}^{I} T_i = \sum_{i=1}^{I} n_i \, t_i = t_{ref}(\sum_{i=1}^{I-1} n_i \gamma_i + n_{ref}) \tag{3.7}$$

where n_{ref} is the number of layers of the reference material.

The weight W_i of the $i-th$ material is given by $W_i = ab\rho_i T_i$ where ρ_i is the density of the $i-th$ material. The total weight W_T of the laminate is given by

$$W_T = \sum_{i=1}^{I} W_i = ab \sum_{i=1}^{I} \rho_i \, T_i \tag{3.8}$$

Let P_i denote the cost per unit weight of the $i-th$ material. Then the cost of the $i-th$ material is $C_i = P_i \, W_i$ and the total material cost of the laminate is given by

$$C_T = \sum_{i=1}^{I} C_i = \sum_{i=1}^{I} P_i W_i \tag{3.9}$$

Optimal Design problem

A design problem can be formulated either as a minimum weight or a minimum cost problem. However, these problems are not dual because of the fact that although the cost function is a monotonic function of the thickness parameters γ_i, the weight function may or may not be a monotonic function of γ_i depending on the material combinations. Thus in the minimum cost problem, the weight constraint is always active, ie., it is a boundary point of the feasible region. However, in the minimum weight problem, the cost constraint may be a point in the design space away from the constraint boundary. Thus, the solutions of these problems may not produce dual results. This point will be further illustrated in the discussion of method of solution and the numerical results.

The design space involves four design parameters, namely, the fibre orientations θ_k, $k = 1, 2, \ldots, K/2$, thickness parameters γ_i, $i = 1, 2, \ldots, I-1$, the reference thicknesses t_{ref} and the materials $i = 1, \ldots, I$. The buckling load N_{cr} given by equation (2.89) depends on all these parameters explicitly. However, the weight and cost functions do not depend on θ_k explicitly. Their dependence on these variables is indirect and by virtue of the minimum buckling constraint given by

$$N \geq N_0 \tag{3.10}$$

where N_0 is a specified constant. Similarly the thickness ratios are constrained from above by imposing

$$\gamma_i \leq \gamma_0 \quad , \quad i = 1,\ 2, \ldots, I-1 \tag{3.11}$$

in order to limit the thickness ratios of different materials. The inequality constraints (3.10) and (3.11) apply to both problems.

Of the four design parameters, three are continuous variables, namely, θ_k, γ_i and t_{ref}. However, the material combination is a discrete variable. The dependence of weight and cost functions on theses parameters are shown by using the notation

$$W_T = W_T(\theta_k,\ \gamma_i,\ t_{ref};\ M) \tag{3.12}$$

$$C_T = C_T(\theta_k,\ \gamma_i,\ t_{ref};\ M) \tag{3.13}$$

where M denotes the material selection. Furthermore the dependence of W_T and C_T on θ_k is implicit and is due to the buckling constraint (3.10).

The formulations of the design problems are given next.

Problem 1. Minimum weight problem.

The objective is to minimise the weight of the laminate subject to the symmetry condition

$$\theta_k = \theta_{K+1-k} \quad k = 1, \ldots, K/2 \tag{3.14}$$

on the ply angles $0° \leq \theta_k \leq 90°$, and constraints on the buckling load N and the material cost C_T. The problem can be stated as

$$W_{min} = \min_S W_T(\theta_k,\ \gamma_i,\ t_{ref};\ M) \tag{3.15}$$

subject to the constraints (3.10), (3.11) and

$$C_T \leq C_0 \tag{3.16}$$

where C_0 is the specified maximum cost. In equation (3.15), S denotes the design space of the problem which involves the continuous parameters θ_k, γ_i, and t_{ref}, and the discrete parameter M indicating the material combination employed.

Problem 2: Minimum Cost Problem

The objective is to minimise the cost of the materials used in the construction of the laminate with ply angles satisfying the symmetry condition (3.14). The problem can be stated as

$$C_{min} = \min_S C_T(\theta_k,\ \gamma_i,\ t_{ref};\ M) \tag{3.17}$$

subject to the buckling constraint (3.10), (3.11) and

$$W_T \leq W_0 \tag{3.18}$$

where W_0 is the specified maximum weight.

3.5 Optimal Design of Symmetrically Laminated Plates for Minimum Deflection and Weight

The final problem in this study consists of two parts. The first (A) considers both the minimum deflection and minimum weight design of laminated plates, while the second (B) is concerned with only the minimum weight design.

3.5.1 A: Minimum deflection and weight design

The objective of the first design problem [78] is to minimise the maximum deflection $w_{max}(x, y)$ and then the weight W of the laminated plate. The minimum deflection is achieved by optimally determining the fibre orientations, given by $\theta_k = (-1)^{k+1}\theta$ for $k \leq K/2$ and $\theta_k = (-1)^k\theta$ for $k \geq K/2+1$. The first part of the design problem may thus be stated as:

$$w_{\min} \triangleq \min_{\theta} [w_{\max}(\theta)], \quad 0° \leq \theta \leq 90° \tag{3.19}$$

where

$$w_{\max}(\theta) = \max_{x,y} w(x, y; \theta) \tag{3.20}$$

The second part of problem A. involves minimising the laminate thickness H subject to a failure criterion. In this study, the Tsai-Wu failure criterion [79] is used which stipulates that the condition for non-failure for any particular ply is

$$\begin{aligned} F(\theta) = F_{11}\sigma_1^{(k)}\sigma_1^{(k)} + F_{22}\sigma_2^{(k)}\sigma_2^{(k)} + F_{66}\tau_{12}^{(k)}\tau_{12}^{(k)} \\ +2F_{12}\sigma_1^{(k)}\sigma_2^{(k)} + F_1\sigma_1^{(k)} + F_2\sigma_2^{(k)} \leq 1 \end{aligned} \tag{3.21}$$

where the strength parameters F_{11}, F_{22}, F_{66}, F_{12}, F_1 and F_2 are given by

$$F_{11} = 1/(X_t X_c)\ ;\ F_{22} = 1/(Y_t Y_c)\ ;\ F_{66} = 1/G^2$$

$$F_1 = 1/X_t - 1/X_c\ ;\ F_2 = 1/Y_t - 1/Y_c\ ; F_{12} = -\frac{1}{2}\sqrt{F_{11}F_{22}} \tag{3.22}$$

and X_t, X_c, Y_t, Y_c are the tensile and compressive strengths of the composite material in the fibre and transverse directions, and G is the in-plane shear strength.

The second part of problem A. may thus be stated as

$$W_{\min} = \min_{H} W(\theta_{opt}) \tag{3.23}$$

subject to constraint (3.21), which is evaluated for all plies.

The maximum deflection w_{max} is determined from the finite element solution of the standard expression given by

$$[K]\{\Delta\} - \{F\} = \{0\} \tag{3.24}$$

where K and F are the stiffness and force coefficients respectively, and the variable Δ denotes the nodal values of w,the transverse deflection, and its derivatives.

The first optimisation procedure involves the stages of determining the maximum deflection $w_{max}(x, y)$ for a given θ and improving the fibre orientation to minimise w_{max}. The second optimisation stage involves evaluating $F(\theta)$ using eqn. (3.21) for a given H and improving the laminate thickness to minimise the weight. This step may be described explicitly as

$$\min_{H} \; |F(\theta_{opt}) - 1| \tag{3.25}$$

in order to minimise thickness. Thus the computational solution consists of successive stages of analysis and optimisation until a convergence is obtained and the optimal angle θ_{opt} and then $H_{\min}$ is determined within a specified accuracy. In both optimisation stages, the *Golden Section* method is employed firstly to determine θ_{opt} and then H_{min}.

3.5.2 B: Minimum weight design

In the second part of the last design problem, the objective is to minimise the weight only. The problem can be stated as

$$W_{min} = \min_{\theta} W(H_{min}) \tag{3.26}$$

In this case the minimum thickness H_{min} of the plate is evaluated using eqn. (3.21) at each value of θ until θ_{opt} is obtained. As before, H_{min} for each value of θ, and θ_{opt} are determined using the *Golden Section* method. Finally the maximum deflection $w_{max}(x, y)$ corresponding to H_{min} and θ_{opt} is obtained to compare the results with those of the first design problem.

Chapter 4

Results and Discussion

4.1 Optimal Design of Symmetrically Laminated Plates for Maximum Buckling Temperature

The laminated plates for which the optimal designs are sought have different combinations of *free* (F), *simply supported*, (S) and *clamped* (C) boundary conditions implemented at the four edges. Also the nonuniform temperature loading rules out an analytical solution. The finite element method is thus used to solve the optimal design problem. The FEM formulation is implemented using the commercial package COSMOS/M [80].

4.1.1 Finite Element Formulation

We now consider the finite element formulation of the problem. Let the region S of the plate be divided into n sub-regions S_r ($S_r \in S; r = 1, 2, ..., n$) such that

$$\Pi(u) = \sum_{r=1}^{n} \Pi^{Sr}(u) \tag{4.1}$$

where Π and Π^{Sr} are potential energies of the vessel and the element, respectively, and u is the displacement vector. Using the same shape functions associated with node i ($i = 1, 2, ..., n$), $S_i(x, y)$, for interpolating the variables in each element, we can write

$$u = \sum_{i=1}^{n} S_i(x, y) u_i \tag{4.2}$$

where u_i is the value of the displacement vector corresponding to node i, and is given by

$$u = \{u_o^{(i)}, v_o^{(i)}, w_o^{(i)}, \psi_x^{(i)}, \psi_y^{(i)}\}^T \tag{4.3}$$

The static buckling problem reduces to a generalised eigenvalue problem of the conventional form, viz.

$$([K] + \lambda[K_G])\{u\} = 0 \tag{4.4}$$

where $[K]$ is the stiffness matrix and $[K_G]$ is the initial temperature matrix. The lowest eigenvalue of the homogeneous system (4.4) yields the buckling temperature.

4.1.2 Numerical Results

The structures considered in this study are four-layered symmetrically laminated plates. The material is specified as T300/5208 graphite epoxy for which $E_1 = 181$ GPa, $E_2 = 10.34$ GPa, $E_{12} = 7.17$ GPa and $\nu_1 = 0.28$. The thermal properties are given as $\alpha_1 = 22.3 * 10^{-6}K^{-1}$, $\alpha_2 = 0.02 * 10^{-6}K^{-1}$, $k_1 = 4.5$ J /m / $^\circ K$, and $k_2 = 0.45$ J /m / $^\circ K$, where k_1 and k_2 are the coefficients of thermal conductivity in the longitudinal and transverse material directions, respectively.

Three different boundary conditions are implemented along the four plate edges (numbered 1 to 4 in Figure 2.12). These are (S,S,S,S), (C,S,C,S) and (C,C,C,C) with S representing a *simply supported* and C a *clamped* boundary, while the order refers to edges 1-4, respectively. Rotations around the x and y axes are denoted by r_x and r_y, respectively. These conditions may be explicitly described as follows:

(S,S,S,S): $v = w = r_x = 0$ at $x = 0$, a and $u = w = r_y = 0$ at $y = 0$, b.
(C,C,C,C): $u = v = w = r_x = r_y = 0$ at $x = 0$, a and $u = v = w = r_x = r_y = 0$ at $y = 0$, b.
(C,S,C,S): $u = v = w = r_x = r_y = 0$ at $x = 0$, a and $u = w = r_y = 0$ at $y = 0$, b.

The results are given for three different thermal loadings to investigate the effect of temperature distribution on the optimum design and maximum buckling temperature. These loadings can be described as follows:
i) Uniform temperature distribution across the plate.
ii) Linear temperature distribution across the plate.
iii) Nonlinear temperature distribution across the plate.

In all cases, the temperature remains constant through the thickness of the plate, and the results are non-dimensionalised using the following expression

$$T = \frac{T_{actual} H \alpha_0}{b}$$

where α_0 is specified as 1 K^{-1}, $b = 1m$ and $H = 0.01m$.

Uniform temperature loading

The first case of thermal loading consists of a uniform temperature over the surface of the plate. Figure 4.1.1 shows the graph of the critical buckling temperature T_{cr} versus the fibre angle for this loading case for a square plate. The maximum buckling temperature occurs at a different fibre angle for each support condition. For the case (S,S,S,S), the maximum is at 45°. For the clamped plate, the maxima occur at 35.7° and 54.3°. For the case (C,S,C,S), the optimal angle is 53.4°.

Figure 4.1.2 shows the graph of the maximum buckling temperature $T_{\max}$ versus the plate aspect ratio a/b. The maximum buckling temperatures for the clamped plates are seen to be lower than the (S,S,S,S) and the (C,S,C,S) plates. Under mechanical buckling loads, (C,C,C,C) plates tend to give the highest buckling loads. This contrast in the case of temperature loading can be attributed to the fact that simple support conditions provide more degrees of freedom and allow the plate to buckle at higher temperatures. The corresponding optimal fibre angles are shown in Figure 4.1.3. It is observed that the boundary conditions have a distinct influence on the optimum fibre orientation.

Linear temperature distribution

Loading two involves a linear variation of the temperature across the plate with the temperature loading along the first plate edge (edge 1, Figure 2.12) being T and that along the edge 3, 0°. The resulting temperature distribution is shown in Figure

4.1.4a schematically where the darker shade indicates the higher temperature.

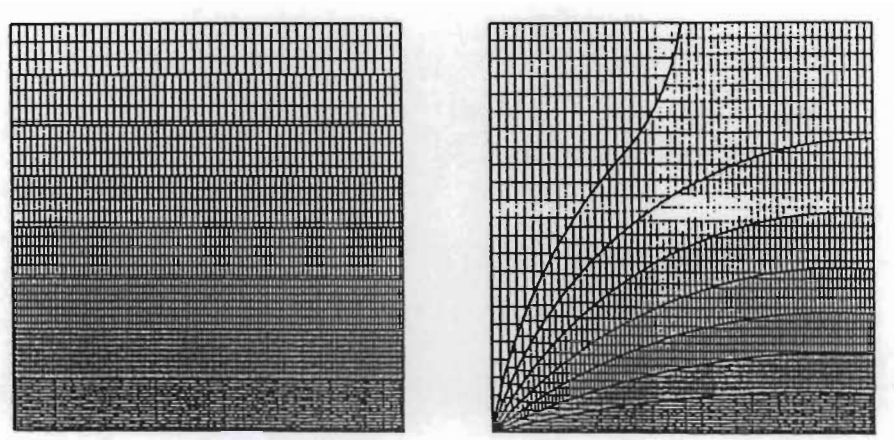

Figure 4.1.4. Temperature fields for a) loading case 2 and b) loading case 3.

Figure 4.1.5 shows the buckling temperature versus the fibre angle for various boundary conditions and for a square plate. The second loading condition causes an increase in the buckling temperatures, as compared to the first loading case, for all boundary conditions as well as small changes in the optimal fibre angle. The curves of T_{max} versus the aspect ratio are shown in Figure 4.1.6. It is observed that (S,S,S,S) gives the lowest T_{max} for $a/b \geq 1$ while under uniform loading (C,C,C,C) gives the lowest T_{max} for $a/b \geq 1.3$ as seen from Figure 4.1.2. The corresponding fibre angles are shown in Figure 4.1.7. The trends for θ_{opt} are similar to the uniform temperature case (Figure 4.1.3) with small changes in the values of θ_{opt}.

Nonlinear temperature distribution

The third loading case is obtained by setting the temperature of the edge 1 to T and keeping the edge 2 at 0°. The resulting temperature distribution is shown in Figure 4.1.4b. Curves of T_{cr} versus θ are shown in Figure 4.1.8 for square plates. It is observed that higher temperatures are needed for buckling as compared to the previous cases even though the general pattern of the curves remains the same. Curves of T_{max} versus a/b are shown in Figure 4.1.9. The corresponding optimal ply angles are shown in Figure 4.1.10. It is observed that the sharp increase in θ_{opt} in the (C,C,C,C) case is moderate as compared to the previous cases.

Bending–twisting coupling

The effect of bending–twisting coupling on the buckling temperatures is shown in Tables 4.1.1 to 4.1.3. Results are given for square plates for each of the three loading cases. It is noted that as the number of layers increases the effect of bending–twisting coupling is reduced as D_{16}, $D_{26} \rightarrow 0$ and in all cases, for the number of layers $K \geq 10$, the effect becomes negligible. It is interesting to note that the effect on the optimal fibre angle is minimal, which is in contrast to the case when the mechanical buckling load is being maximised for similar plates as described by Walker *et al* [81]. In that study, it was found that when bending–twisting coupling was neglected, the effect on the optimal fibre angle was considerable, particularly when $K \leq 10$.

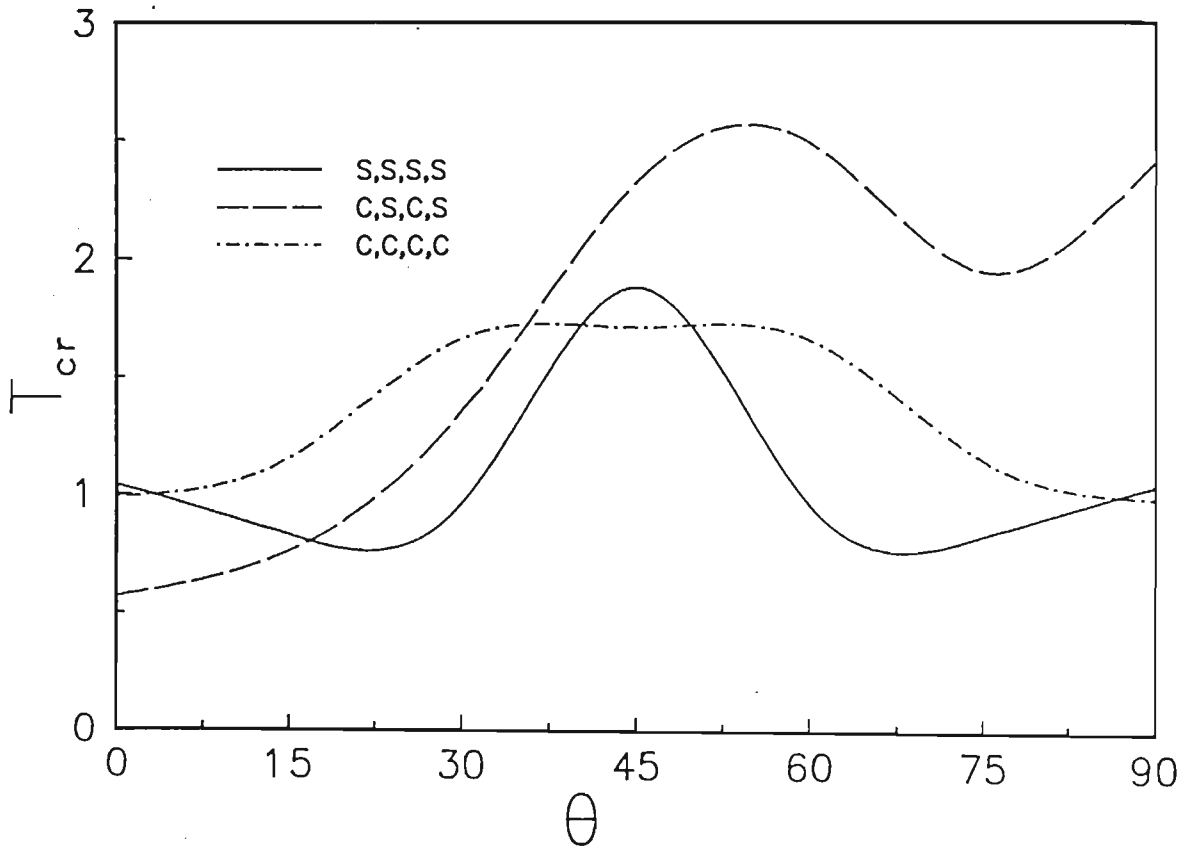

Figure 4.1.1. T_{cr} versus fibre angle θ (Uniform temperature distribution).

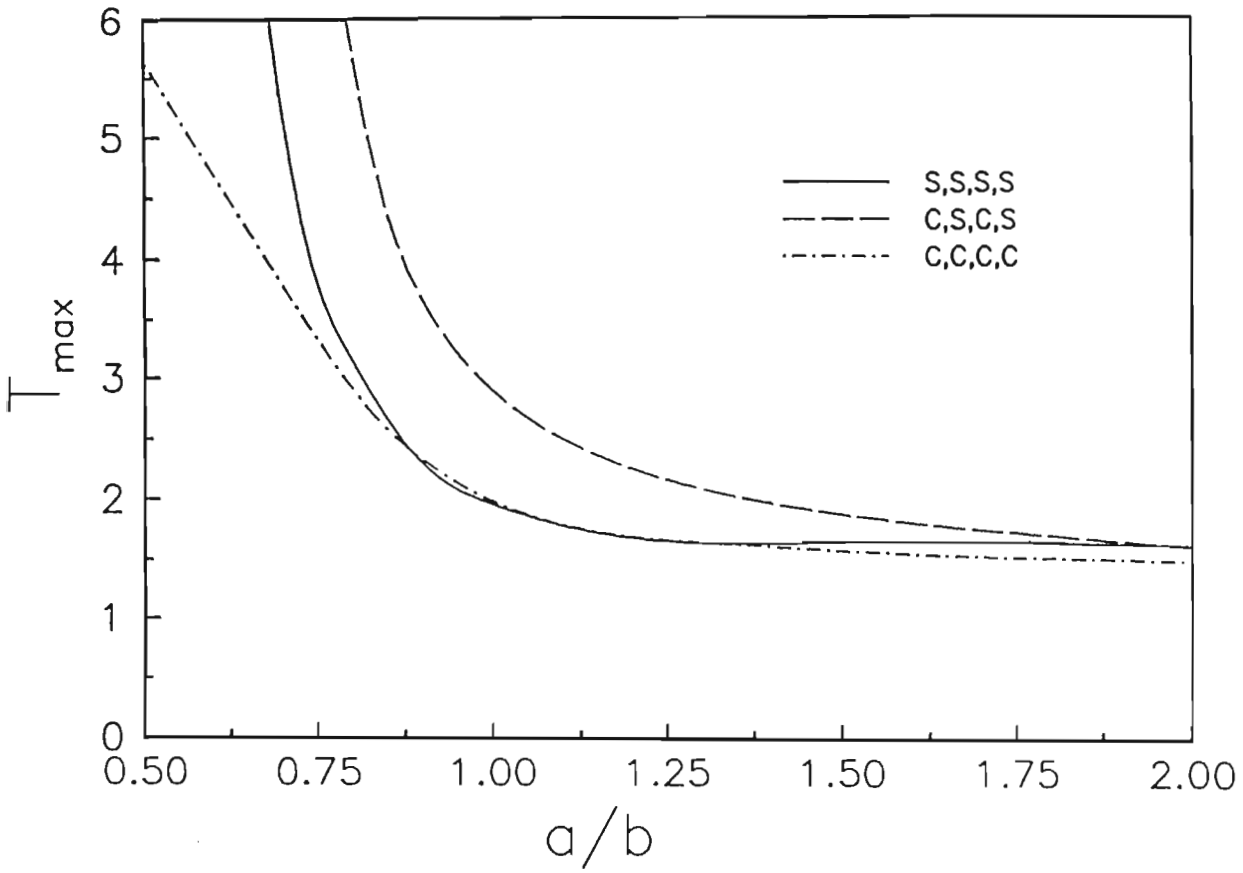

Figure 4.1.2. $T_{\max}$ versus the aspect ratio a/b (Uniform temperature distribution).

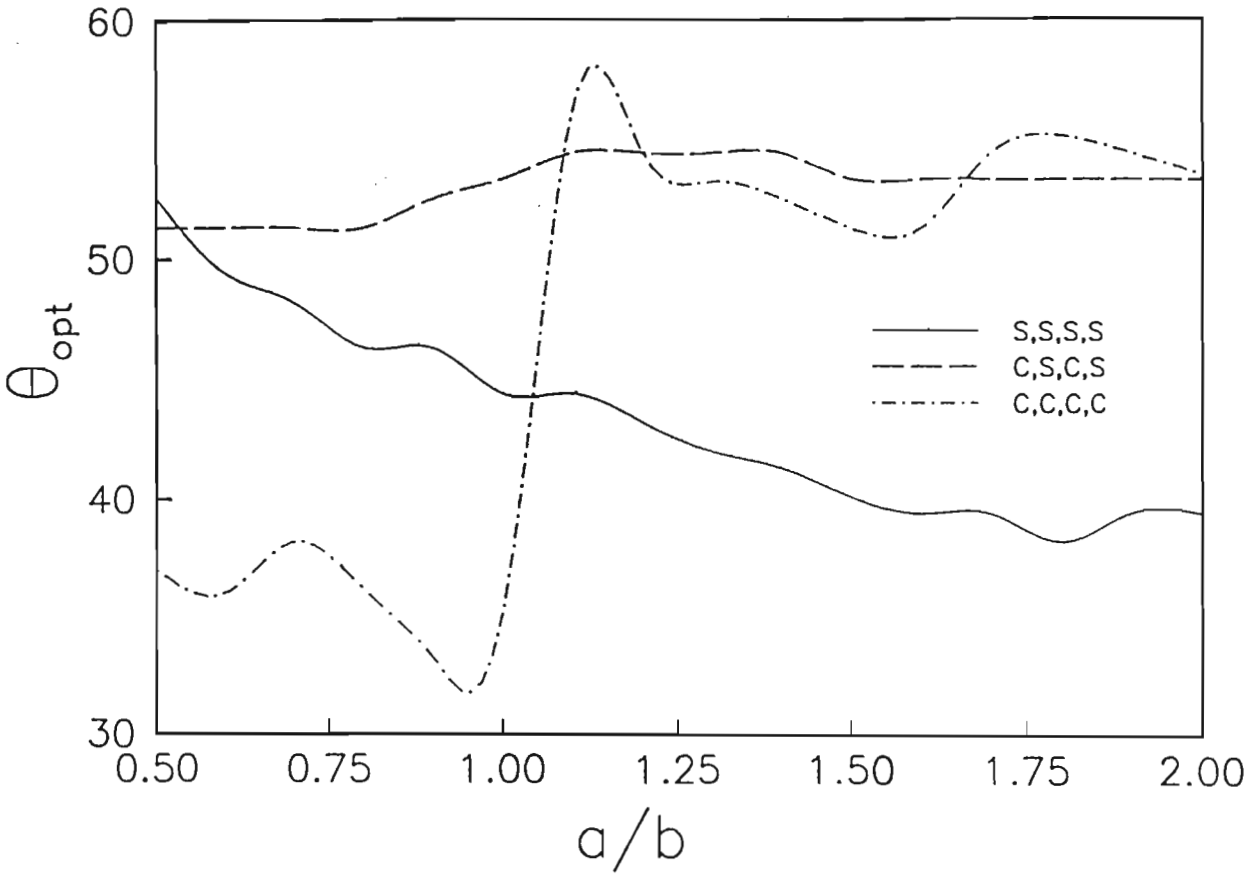

Figure 4.1.3. θ_{opt} versus the aspect ratio a/b (Uniform temperature distribution).

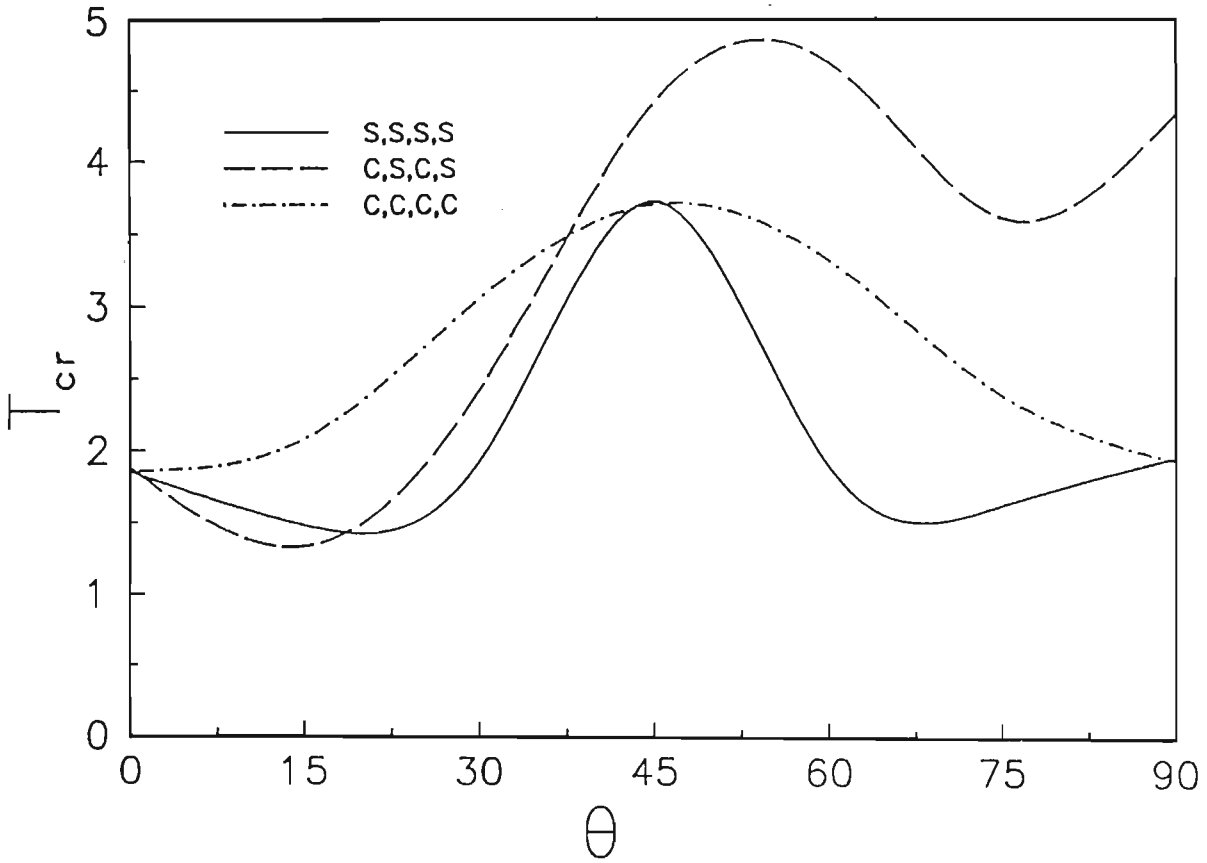

Figure 4.1.5. T^{cr} versus fibre angle θ (Linear temperature distribution).

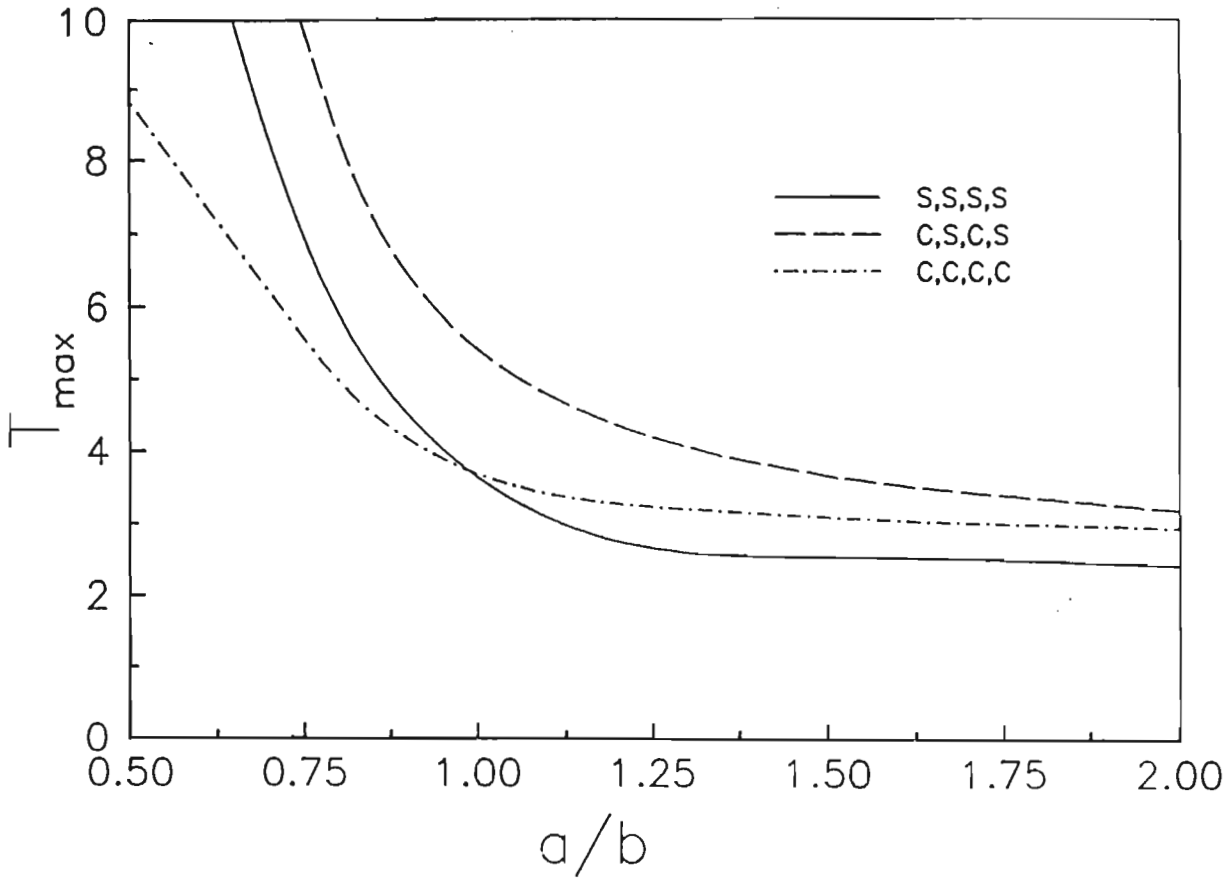

Figure 4.1.6. $T_{\max}$ versus the aspect ratio a/b (Linear temperature distribution).

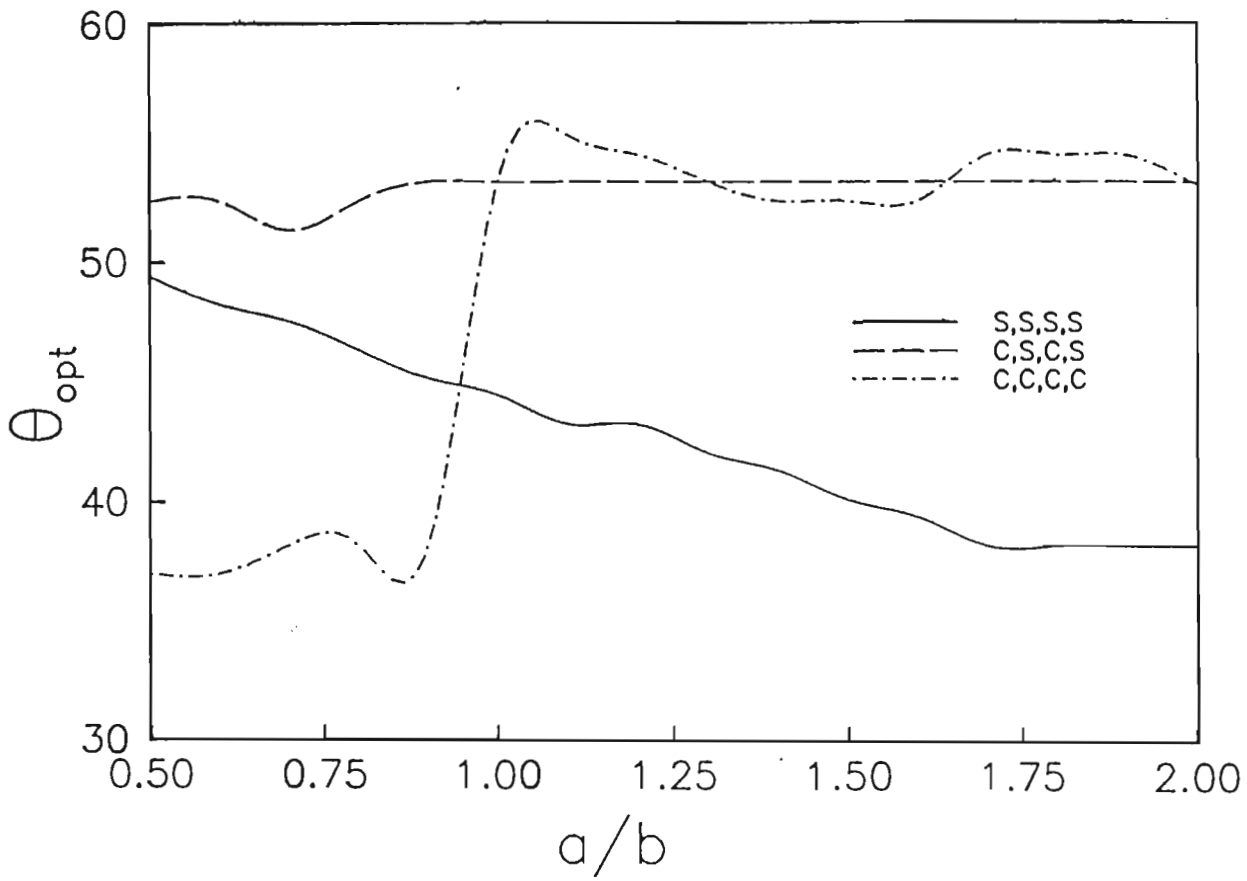

Figure 4.1.7. θ_{opt} versus the aspect ratio a/b (Linear temperature distribution).

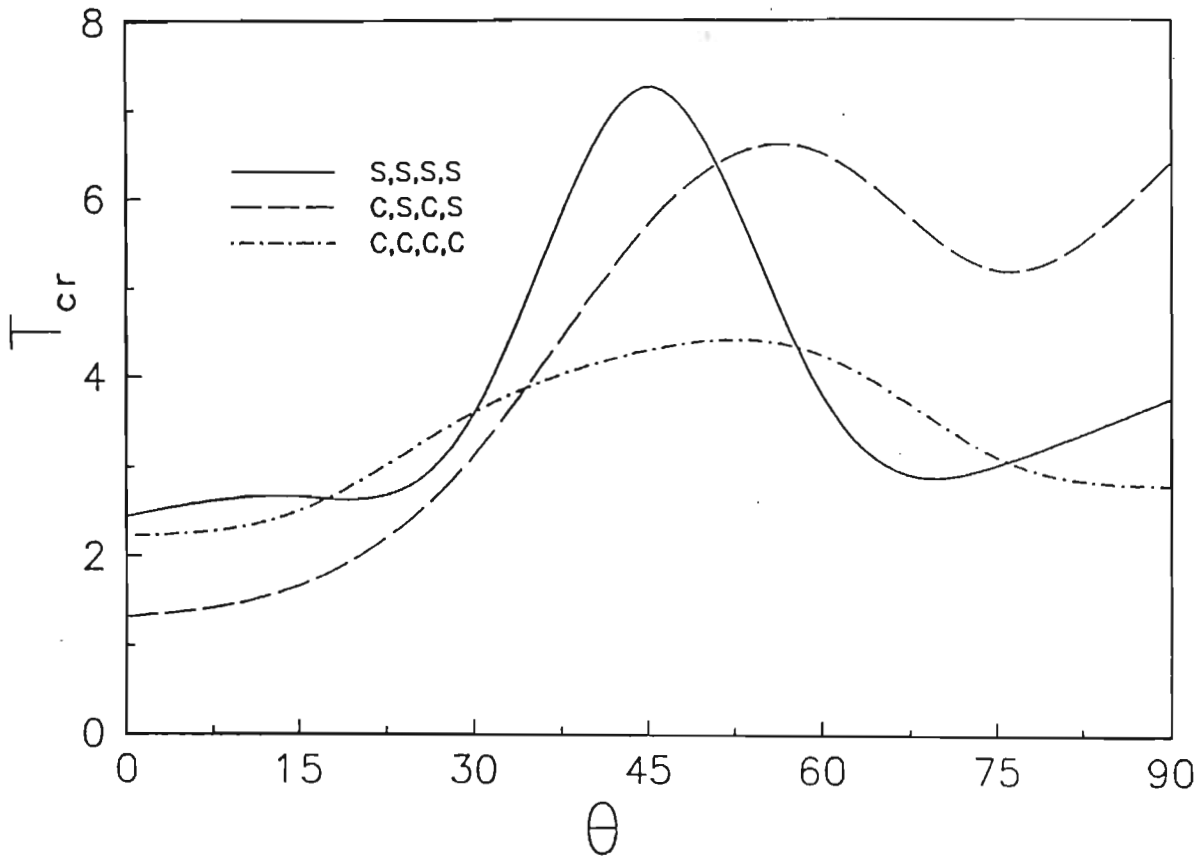

Figure 4.1.8. T_{cr} versus fibre angle θ (Nonlinear temperature distribution).

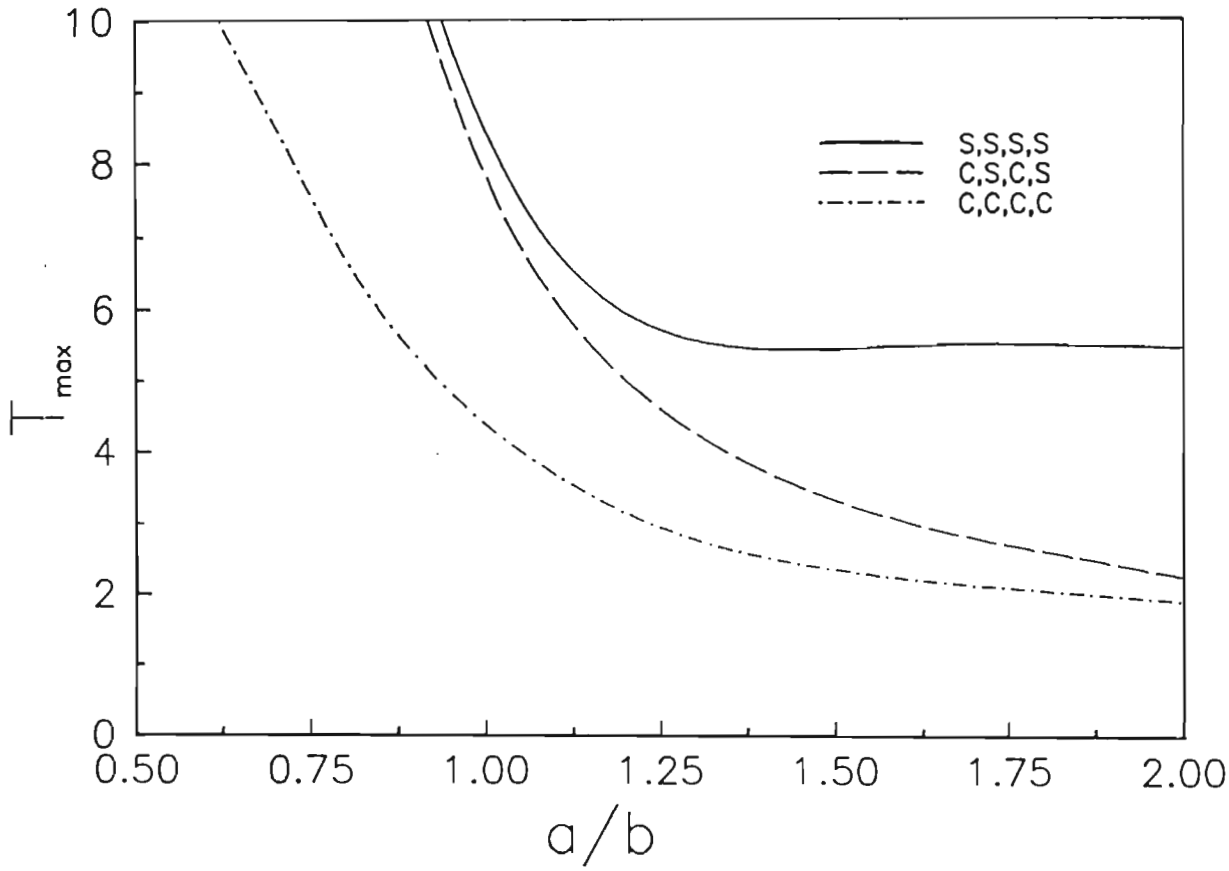

Figure 4.1.9. $T_{\max}$ versus the aspect ratio a/b (Nonlinear temperature distribution).

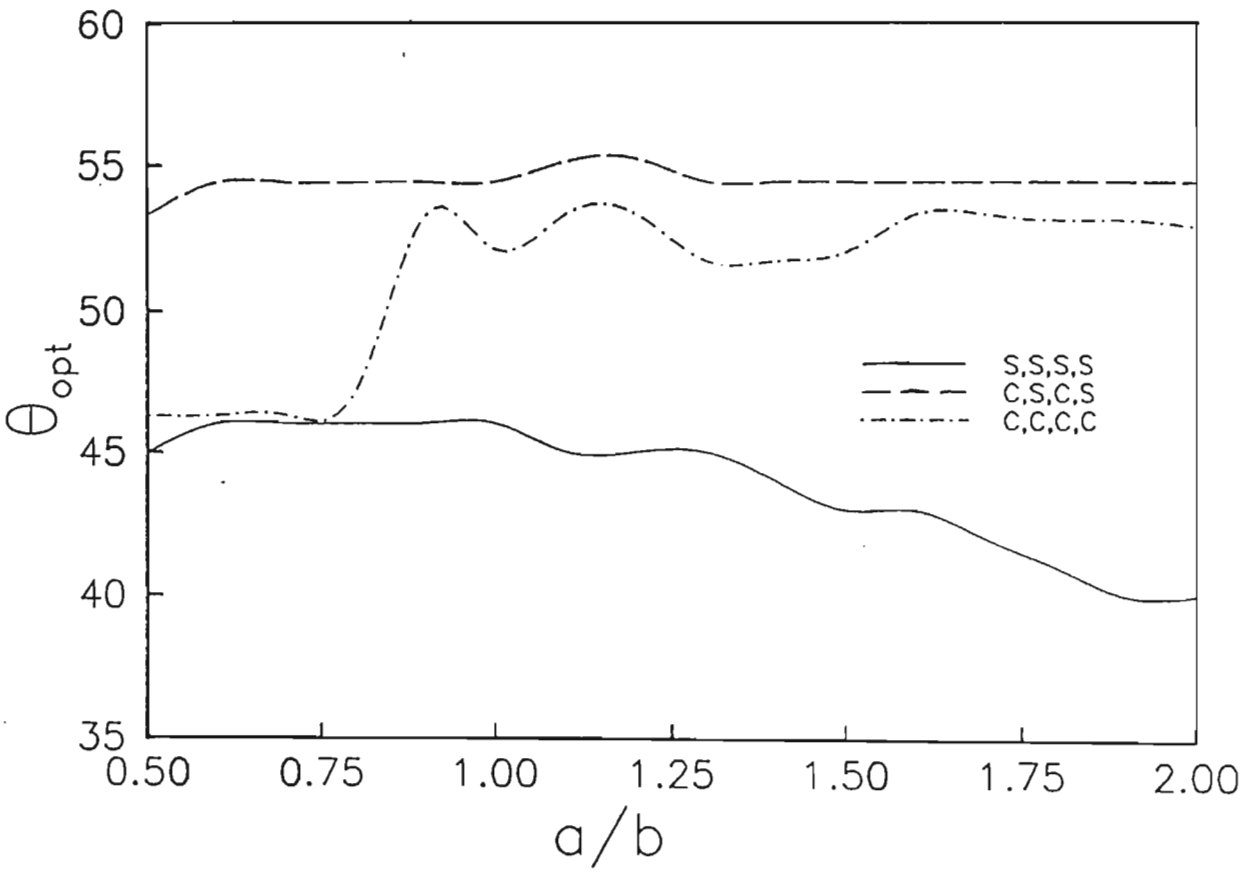

Figure 4.1.10. θ_{opt} versus the aspect ratio a/b (Nonlinear temperature distribution).

No. of Layers	T_{max} (S,S,S,S)	θ_{opt} (S,S,S,S)	T_{max} (C,C,C,C)	θ_{opt} (C,C,C,C)	T_{max} (C,S,C,S)	θ_{opt} (C,S,C,S)
4	1.88	35.1°	1.72	44.4°	2.66	53.5°
8	1.98	35.1°	1.77	44.9°	2.78	54.0°
10	2.01	35.5°	1.78	44.5°	2.80	53.7°
20	2.04	35.4°	1.78	44.4°	2.81	53.5°
50	2.05	35.3°	1.79	44.3°	2.82	53.4°

Table 4.1.1. The effect of the number of layers on $T_{\max}$ and θ_{opt} (Uniform temperature distribution).

No. of Layers	T_{max} (S,S,S,S)	θ_{opt} (S,S,S,S)	T_{max} (C,C,C,C)	θ_{opt} (C,C,C,C)	T_{max} (C,S,C,S)	θ_{opt} (C,S,C,S)
4	3.72	44.4°	3.38	53.3°	5.08	53.3°
8	3.90	44.2°	3.47	53.3°	5.30	53.2°
10	3.94	44.5°	3.50	53.3°	5.32	53.2°
20	3.96	44.5°	3.52	53.3°	5.33	53.2°
50	3.97	44.4°	3.52	53.3°	5.34	53.3°

Table 4.1.2. The effect of the number of layers on $T_{\max}$ and θ_{opt} (Linear temperature distribution).

No. of Layers	T_{max} (S,S,S,S)	θ_{opt} (S,S,S,S)	T_{max} (C,C,C,C)	θ_{opt} (C,C,C,C)	T_{max} (C,S,C,S)	θ_{opt} (C,S,C,S)
4	7.19	46.1°	6.23	52.1°	6.85	54.4°
8	7.39	46.0°	6.36	52.1°	7.07	54.4°
10	7.45	46.1°	6.38	52.1°	7.12	54.4°
20	7.47	46.1°	6.40	52.1°	7.14	54.4°
50	7.47	46.0°	6.40	52.1°	7.16	54.2°

Table 4.1.3. The effect of the number of layers on $T_{\max}$ and θ_{opt} (Nonlinear temperature distribution).

4.2 Optimal Design of Laminated Cylindrical Pressure Vessels for Maximum External Pressure

As in the design problem one, the presence of endcaps rules out an analytical solution to this design problem. A similar finite element formulation to that in the first design problem is used.

4.2.1 Numerical Results

The critical buckling loads for the pressure vessels are initially determined using the finite element method using a similar formulation to the one in section 4.1.1. The optimisation is achieved with a routine written in the C programming language. This routine is used to run the FEM software iteratively, and to extract from the output the relevant data for use in the optimisation. The buckling load found at a certain fibre angle is used in a *Golden Section* algorithm which maximises the buckling load to the accuracy required.

Verification

In order to verify the finite element formulation described above, convergence tests were carried out. For both the hemispherically and flat capped pressure vessels, the convergence testing was carried out with $L = 3m$, $R = 0.5m$ and $\theta = 30°$. Table 4.2.1 shows the dependence of the buckling pressure on the number of elements. The wall thickness is specified as $0.01m$, and the material properties are those of T300/5208 graphite epoxy. The use of 700 elements for a hemispherically capped pressure vessel provided a mesh density which was considered sufficient, and similarly for a flat capped pressure vessel 676 elements proved sufficient. Consequently, in the present study, vessels of lengths other than given here were meshed with a corresponding proportion of these numbers of elements.

Numerical results

The buckling loads for the pressure vessels are determined with a finite element software package. The optimisation, however, is achieved with a routine written in the C programming language. This routine is used to run the FEM software iteratively,

and to extract from the output the relevant data for use in the optimisation.

The thickness of all the pressure vessels considered was $H = 0.01m$. The dependence of the buckling pressure P on the fibre angle for hemispherically capped vessels is shown in Figure 4.2.1. For $L = 3m$ and $R = 0.5m$ the optimal fibre angle is 30.8° while for $L = 10m$, $R = 0.5m$, the optimal fibre angle has decreased to 0°. For $L = 3m$, $R = 0.75m$, θ_{opt} has increased to 43.2°. Figure 4.2.2 shows the equivalent results for the flat capped vessel. For $L = 3m$ and $R = 0.5m$, the optimal ply angle is 44.4°, and for the geometry $L = 3m$, $R = 0.75m$, θ_{opt} has increased to 54.4°, while for the case $L = 10m$, $R = 0.5m$, θ_{opt} decreases to 7.1°. These graphs illustrate the importance of selecting the optimal fibre angle in order to maximise the buckling pressure of these structures. Moreover it is clear that the shape of end caps has a distinct effect on the optimal ply angles.

The effect of the vessel length L on the maximum buckling pressure and optimal fibre angles is shown in Table 4.2.2. In this case the radius of the pressure vessel is specified as $R = 0.5m$ and the thickness $H = 0.01m$. The optimal fibre angle is found to fluctuate but in general decrease with increasing length and as expected, the maximum pressure corresponding to the optimal fibre angles decreases as L increases. In the case of flat capped vessels of similar lengths, θ_{opt} also decreases with increasing length, although not as rapidly as for the hemispherically capped vessel. This is also the case for the maximum buckling pressure.

Table 4.2.3 shows the effect of vessel radius on the maximum pressure and optimal angle for vessels with $L = 3m$, $H = 0.01m$. In both cases, the maximum buckling pressure is found to decrease with increasing radius. For the hemispherically capped vessel, the fibre angle does not show any trend with increasing radius, with a minimum optimal fibre angle $\theta_{opt} = 0°$ for $R = 0.3m$, and a maximum $\theta_{opt} = 40.1°$ for $R = 0.8m$. Interestingly, for the flat capped vessel, the minimum optimal angle $\theta_{opt} = 0°$ is also found at $R = 0.3m$. At radii greater than $R \geq 0.7m$, the optimal angle remains fairly constant at around 54°.

The effect of vessel wall thickness H is shown in Table 4.2.4 for a pressure vessel of length $L = 1.5m$ and radius $R = 0.5m$. As expected the buckling pressure increases with an increase in wall thickness for both vessels. No noticeable trend can be seen in the relationship between θ_{opt} and H. For the hemispherically capped vessel the minimum optimal angle is $\theta_{opt} = 0°$ for $H = 0.001m$ while for the flat capped vessels $\theta_{opt} = 0°$ for $H = 0.025m$.

The effect of bending–twisting coupling on the maximum buckling pressure and

optimal fibre angle is shown in Table 4.2.5. As the number of layers K increases, so the strength reducing effect diminishes by virtue of D_{16}, $D_{26} \to 0$. From the table it is evident that the effect of bending–twisting coupling is greatest when the pressure vessel consists of four layers, since the difference in the maximum buckling pressure as compared to that of a vessel of fifty layers is the largest. For $K \geq 8$, the effect is almost negligible.

The optimal fibre angles and maximum buckling pressure of a four layered hybrid pressure vessel (hemispherical and flat capped) with various geometries is given in Table 4.2.6. The internal layers of each vessel consist of K49 Kevlar epoxy for which $E_1 = 76\ GPa$, $E_2 = 5.50\ GPa$, $E_{12} = 2.30\ GPa$ and $\nu_{12} = 0.34$, while the outer layers remain T300/5208 graphite epoxy material. The comparison between these vessels and the one composed only of graphite epoxy shows that the hybrid vessels have slightly lower buckling pressures for all geometries considered. The optimal fibre angles also change, which indicates that a non-optimal design may be obtained for a hybrid vessel if the optimal results from a single-material design are used.

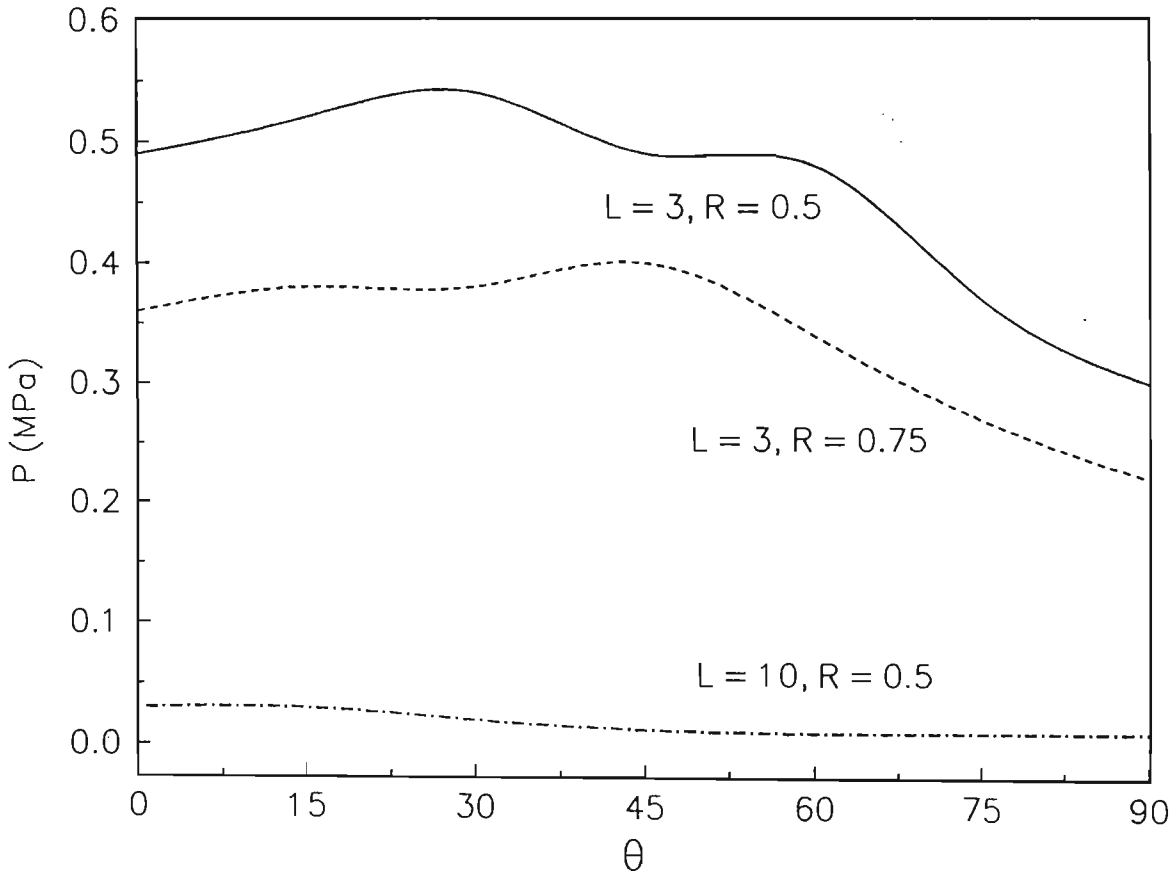

Figure 4.2.1. Graph of Buckling Pressure versus Fibre Angle for Hemispherical Vessels.

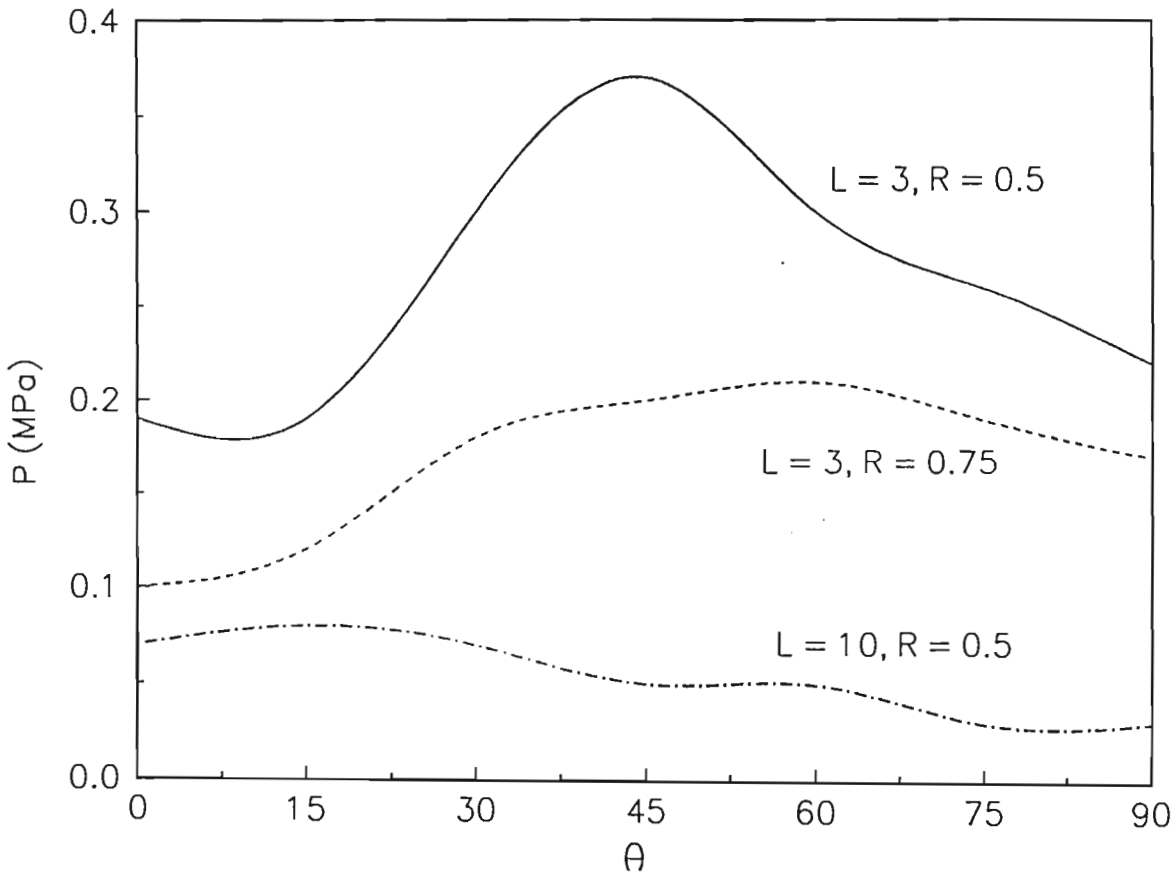

Figure 4.2.2. Graph of Buckling Pressure versus Fibre Angle for Flat Vessels.

Hemispherical		Flat	
No. of elements	P (MPa)	No. of elements	P (MPa)
440	0.38	465	0.21
500	0.46	505	0.29
540	0.51	588	0.38
620	0.53	636	0.39
700	0.54	676	0.39

*Number of elements around the periphery is 20 for all cases

Table 4.2.1. Dependence of critical buckling pressure on the number of elements with $L = 3.0m$, $R = 0.5m$ and $\theta = 30°$.

	Hemispherical		Flat	
L (m)	θ_{opt}	P_{max} (MPa)	θ_{opt}	P_{max} (MPa)
1.50	41.6°	4.07	54.7°	0.65
1.75	27.7°	2.61	55.2°	0.65
2.00	22.2°	1.73	55.2°	0.65
2.25	17.2°	1.11	45.9°	0.57
2.50	20.1°	0.85	42.0°	0.51
2.75	25.1°	0.67	38.9°	0.45
3.00	30.8°	0.54	37.3°	0.39
3.25	26.0°	0.46	41.3°	0.33
3.50	18.7°	0.37	44.4°	0.28
3.75	10.8°	0.31	31.9°	0.24
4.00	7.6°	0.28	23.2°	0.23
4.25	5.3°	0.26	21.5°	0.22
4.50	4.1°	0.24	20.1°	0.21
4.75	2.2°	0.23	18.4°	0.20
5.00	1.0°	0.22	17.2°	0.20
10.0	0°	0.21	9.2°	0.19

Table 4.2.2. The effect of length on the optimal fibre angle and maximum buckling pressure with $R = 0.5m$.

	Hemispherical		Flat	
R (m)	θ_{opt}	P_{max} (MPa)	θ_{opt}	P_{max} (MPa)
0.1	16.5°	9.54	21.1°	8.11
0.2	5.7°	2.58	4.6°	2.31
0.3	0°	1.00	0°	0.94
0.4	11.0°	0.60	19.2°	0.46
0.5	30.8°	0.54	37.3°	0.39
0.6	18.4°	0.47	45.4°	0.31
0.7	15.0°	0.40	54.4°	0.21
0.8	40.1°	0.39	54.0°	0.14
0.9	33.5°	0.36	54.4°	0.10
1.0	25.8°	0.33	54.4°	0.07

Table 4.2.3. The effect of radius on the optimal fibre angle and maximum buckling pressure with $L = 3.0m$.

	Hemispherical		Flat	
H (m)	θ_{opt}	P_{max} (MPa)	θ_{opt}	P_{max} (MPa)
0.001	0°	0.0045	55.9°	0.00024
0.01	30.8°	0.538	37.3°	0.387
0.025	8.8°	3.61	0.0°	3.45
0.05	7.9°	19.83	4.6°	19.93
0.075	10.8°	51.59	9.1°	51.66
0.1	13.1°	97.21	11.5°	96.53

Table 4.2.4. The effect of thickness on the optimal fibre angle and maximum buckling pressure with $L = 3.0m$ and $R = 0.5m$.

	Hemispherical		Flat	
K	θ_{opt}	P_{max} (MPa)	θ_{opt}	P_{max} (MPa)
4	41.6°	4.07	54.7°	0.654
8	43.2°	4.22	55.2°	0.699
10	43.5°	4.26	55.5°	0.705
20	43.9°	4.28	55.2°	0.701
50	44.4°	4.29	54.7°	0.698

Table 4.2.5. The effect of the number of layers on the optimal fibre angle and maximum buckling pressure with $L = 3.0m$ and $R = 0.5m$.

Hemispherical				
	Graphite		Graphite/Kevlar	
Geometry	θ_{opt}	P_{max} (MPa)	θ_{opt}	P_{max} (MPa)
L = 3.0m, R = 0.5m	30.8°	0.54	22.0°	0.43
L = 3.0m, R = 0.75m	12.1°	0.39	15.6°	0.36
L = 5.0m, R = 0.5m	1.0°	0.22	0°	0.16
Flat				
	Graphite		Graphite/Kevlar	
Geometry	θ_{opt}	P_{max} (MPa)	θ_{opt}	P_{max} (MPa)
L = 3.0m, R = 0.5m	37.3°	0.39	35.5°	0.38
L = 3.0m, R = 0.75m	54.4°	0.21	41.0°	0.21
L = 5.0m, R = 0.5m	17.2°	0.20	8.3°	0.18

Table 4.2.6. The effect of hybrid construction on the optimal fibre angle and maximum buckling pressure.

4.3 Multiobjective Design of Laminated Cylindrical Shells for Maximum Torsional and Axial Loads

The results reported in this section are for eight-layered symmetrically laminated cylinders with simply supported ends. The material properties used in the design are those of T300/5208 graphite epoxy. In the numerical results, the weighting factors are constrained as $\alpha + \beta = 1$ so that $\beta = 1 - \alpha$, $0 \leq \alpha \leq 1$. In Figures 4.3.1–4.3.12, the plate thickness is taken as $H = 0.05m$ and the accuracy is specified as $0.1°$.

Single objective designs

Results for the single objective designs involving the maximisation of either N^*_{xy} or N_{cr} are given first. Figure 4.3.1 shows the effect of cylinder length on the optimal fibre angles for N_{cr} ($\alpha = 0$) and maximum N^*_{xy} ($\alpha = 1$) with $R = 1m$. For the axial loading case, θ_{opt} generally decreases with increasing length. The discontinuity is due to a change in the buckling mode integers m and n. The optimal fibre angle for torsional loading is $90°$ for all L. This is explained by the form of equation (2.97), from which it may be seen that, since L and R are independent of the fibre angle, the optimal angle is the same for all L, R. Figure 4.3.2 shows the corresponding performance indices plotted against length L. The curves for the optimal fibre angles plotted against cylinder radius R are shown in Figure 4.3.3 where $L = 15m$. The curve is stepped, again due to changes in the buckling mode. Figure 4.3.4 shows the corresponding curves for the design objectives. It is observed that N_{cr}/N_0 decreases as the length L or radius R of the shell increases.

Multiobjective designs

The dependence of the performance index J on the fibre angle is investigated in Figure 4.3.5 for four weighting cases with $\alpha = 0,\ 1/3,\ 2/3,\ 1$ indicating the dependence of N_{cr} and N^*_{xy} on the fibre orientation. For this figure, the cylinder length was specified as $L = 15m$ and the radius as $R = 1m$ For $\alpha = 1.0$, the graph rises monotonically with a maximum at $90°$ and this is the optimal θ for maximum N^*_{xy}. As α decreases the graphs become less monotonic and the maximum is found

at decreasing fibre angles. For $\alpha = 2/3$, the optimal angle is 77.21^o, for $\alpha = 1/3$, the optimal angle is 74.73^o, and for $\alpha = 0$, θ_{opt} is 24.22^o, which is the optimal θ for maximum N_{cr}. It is interesting to note that at 54.78^o the four curves intersect.

Figure 4.3.6 illustrates the effect of cylinder length on the optimal fibre angle for a cylinder of radius $R = 1m$ and $h = 0.05m$, for three different weightings. For $\alpha = 1/3$, the value of the optimal fibre angle lies between 68^o and 83^o, whereas for $\alpha = 1/2$, θ_{opt} varies between 47^o and 78^o. The optimal fibre angles for $\alpha = 2/3$ again are correspondingly less, and vary across a greater range. All three of these curves show discontinuities at various values of L, and this is due to mode changes.

Figure 4.3.7 shows the performance index $J(\alpha, \beta; \theta)$ corresponding to the optimal fibre angles shown in Figure 4.3.6. For $\alpha = 1/3$ and $\alpha = 1/2$, the performance index J generally decreases with increasing cylinder length L. For $\alpha = 2/3$, the index remains fairly constant.

The curves for θ_{opt} versus cylinder radius R are shown in Figure 4.3.8 for the three weightings with $L = 15m$. As α decreases, the optimal angle is generally lower for all values of R. The discontinuities in the graphs of θ_{opt} vs R are once again due to mode changes. The corresponding curves for J (Figure 4.3.9) show that the performance index fluctuates as α decreases. The performance index J generally decreases with increasing R for all three values of α.

Figure 4.3.10 shows the dependence of θ_{opt} on the value of the weighting factor α for three different cases of L and R. As the proportion of the torsional load increases, viz. as α increases, so θ_{opt} correspondingly approaches 90^o, and for all three cases of L and R, $\theta_{opt} = 90^o$ at $\alpha = 1$, corresponding to maximum N^*_{xy}. θ_{opt} values for $\alpha = 0$ are different for different values of L and R indicating that N_{cr} reaches its maximum at different values of θ_{opt} depending on L and R.

Figure 4.3.11 shows the corresponding values of the performance index J. In all three cases, the trends show a minimum between $\alpha = 0.65$ and $\alpha = 0.8$. At $\alpha = 1$, the loading is purely torsional, and thus $J = N^*_{xy}/N^*_0$, which is independent of R and L (see eqn. (2.97)). Therefore in all three cases the performance index converges to the same value $J = 2.05$.

Table 4.3.1 shows the values of the performance index J and θ_{opt} for various values of H, with $L = 15m$ and $R = 1m$. The performance index increases with increasing H. Also, θ_{opt} generally decreases with increasing H for both values of α.

Figure 4.3.12 shows the trade-off curve for N^*_{xy} and N_{cr} with $L = 15m$ and $R = 1m$. The individual loadings N_{cr} and N^*_{xy} are evaluated separately at the

optimal fibre angles θ_{opt} corresponding to the range of weightings $0 < \alpha < 1$. The non-weighted contributions of these loads are plotted against each other to give the trade-off between the weightings $\alpha = 0$ and $\alpha = 1$.

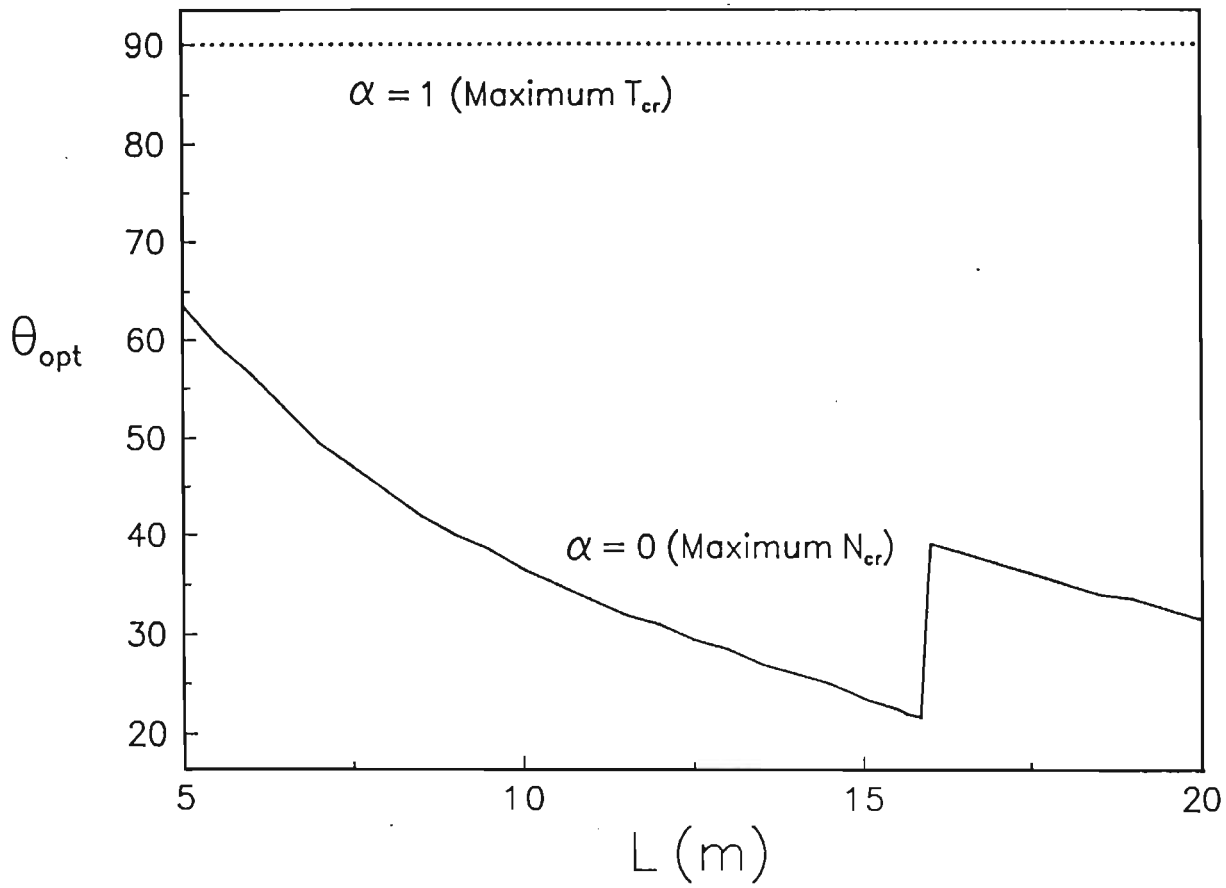

Figure 4.3.1. θ_{opt} versus L with $R = 1m$ (single objective design).

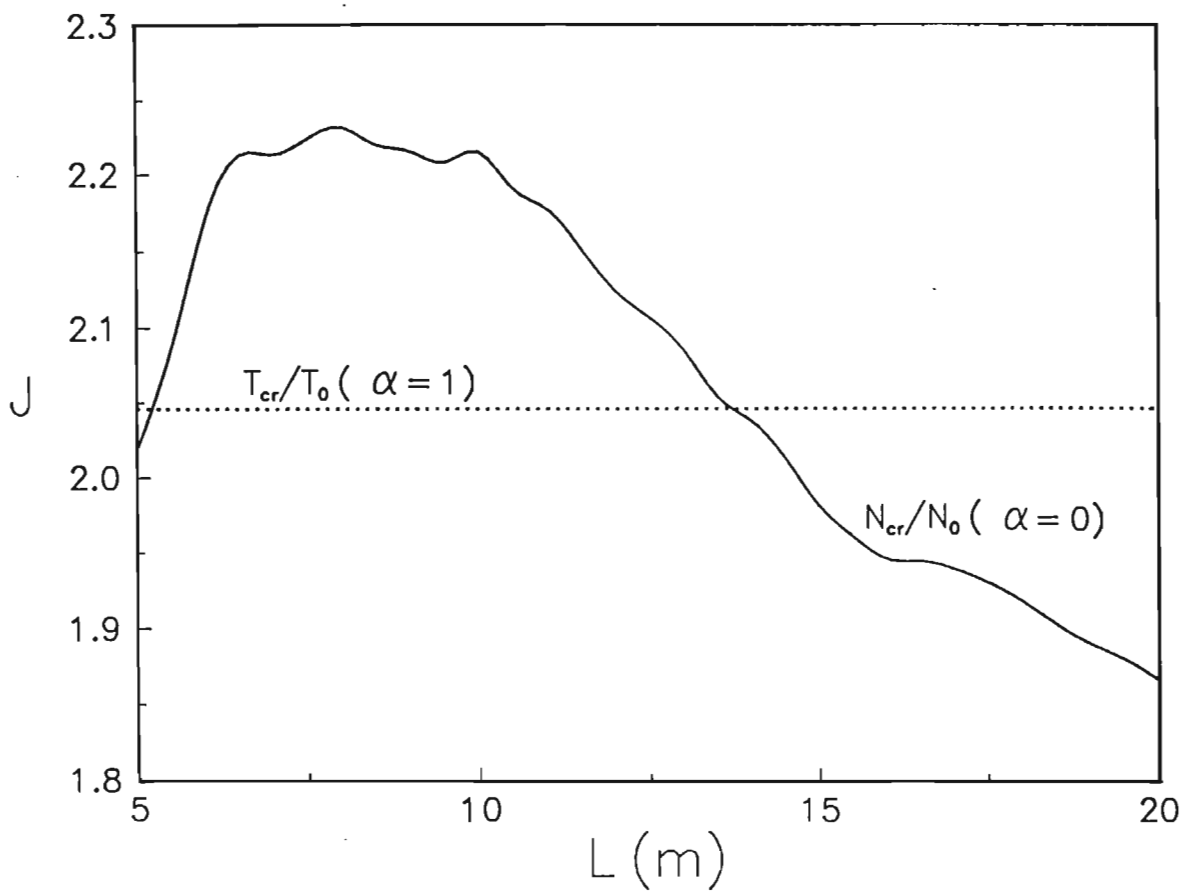

Figure 4.3.2. J versus L with $R = 1m$ (single objective design).

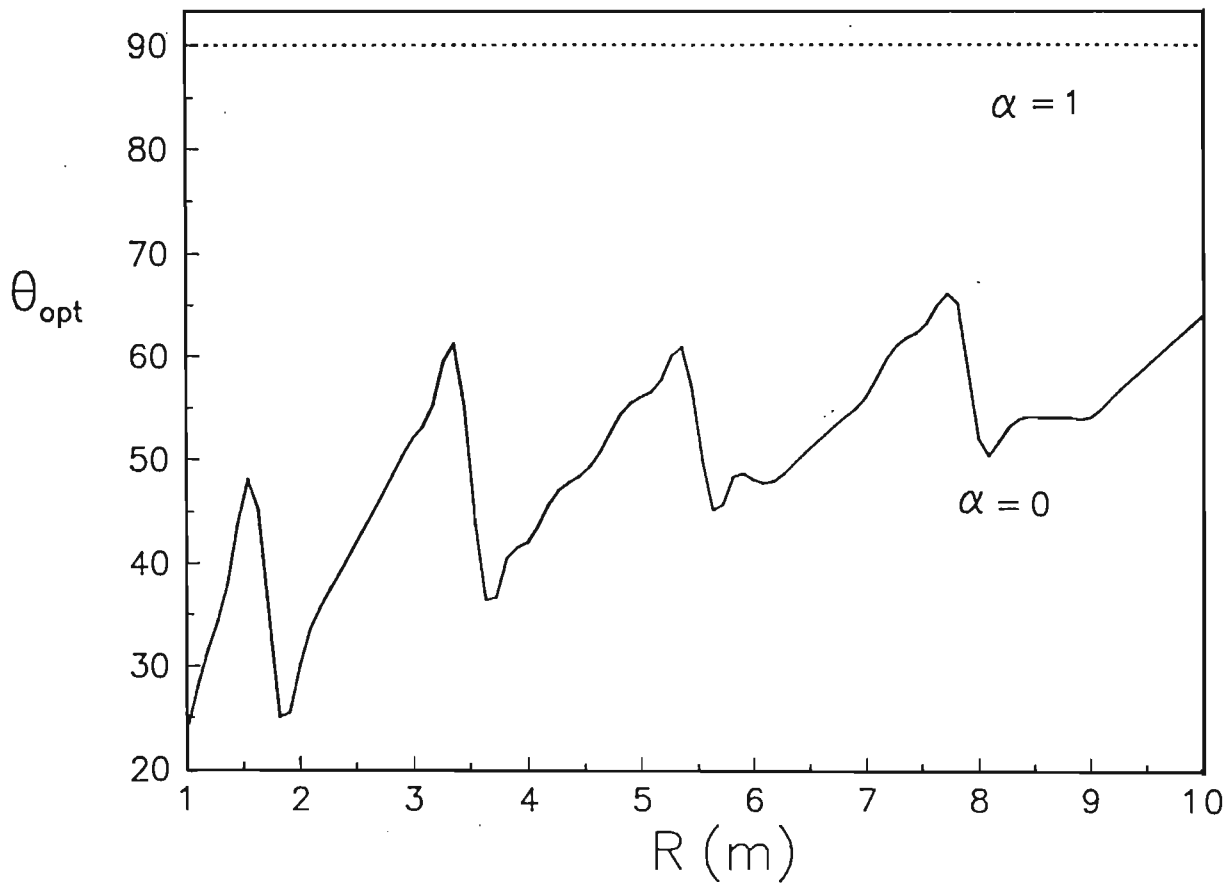

Figure 4.3.3. θ_{opt} versus R with $L = 15m$ (single objective design).

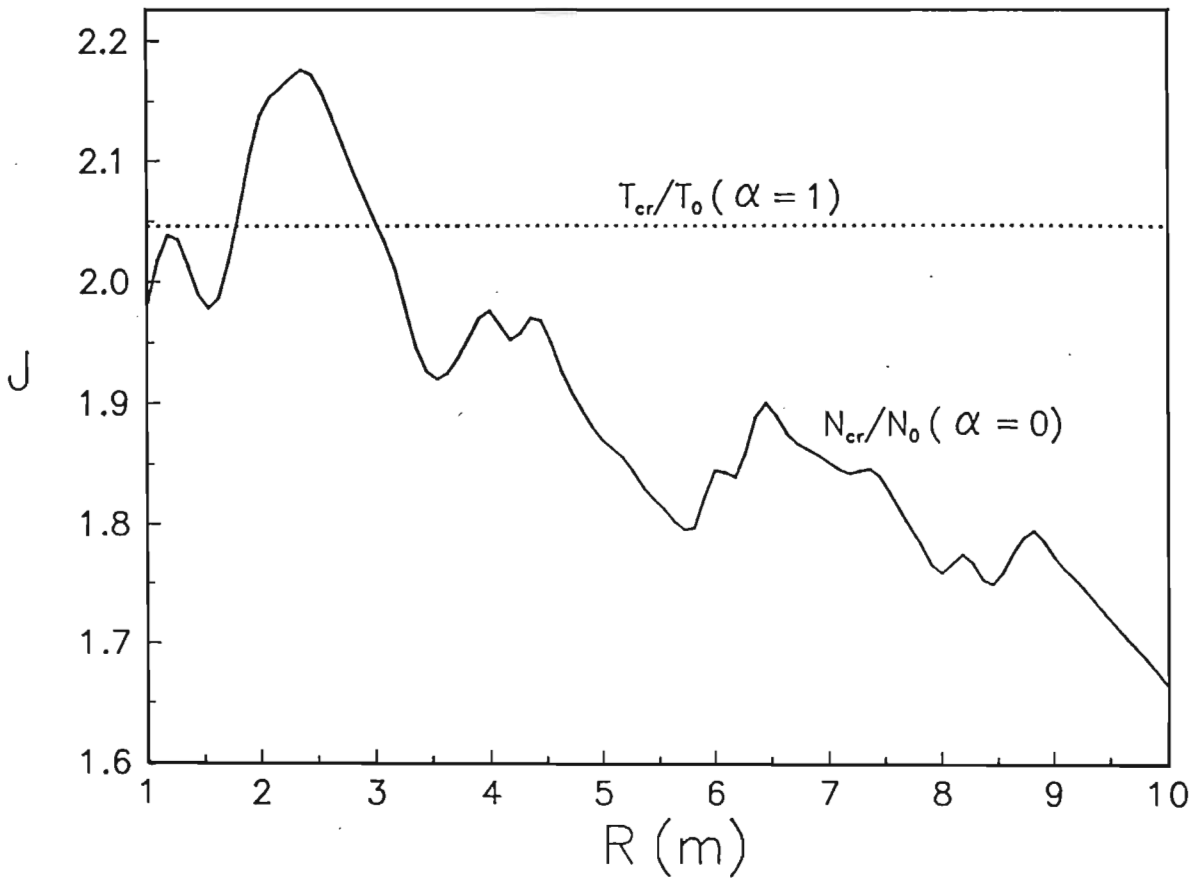

Figure 4.3.4. J versus R with $L = 15m$ (single objective design).

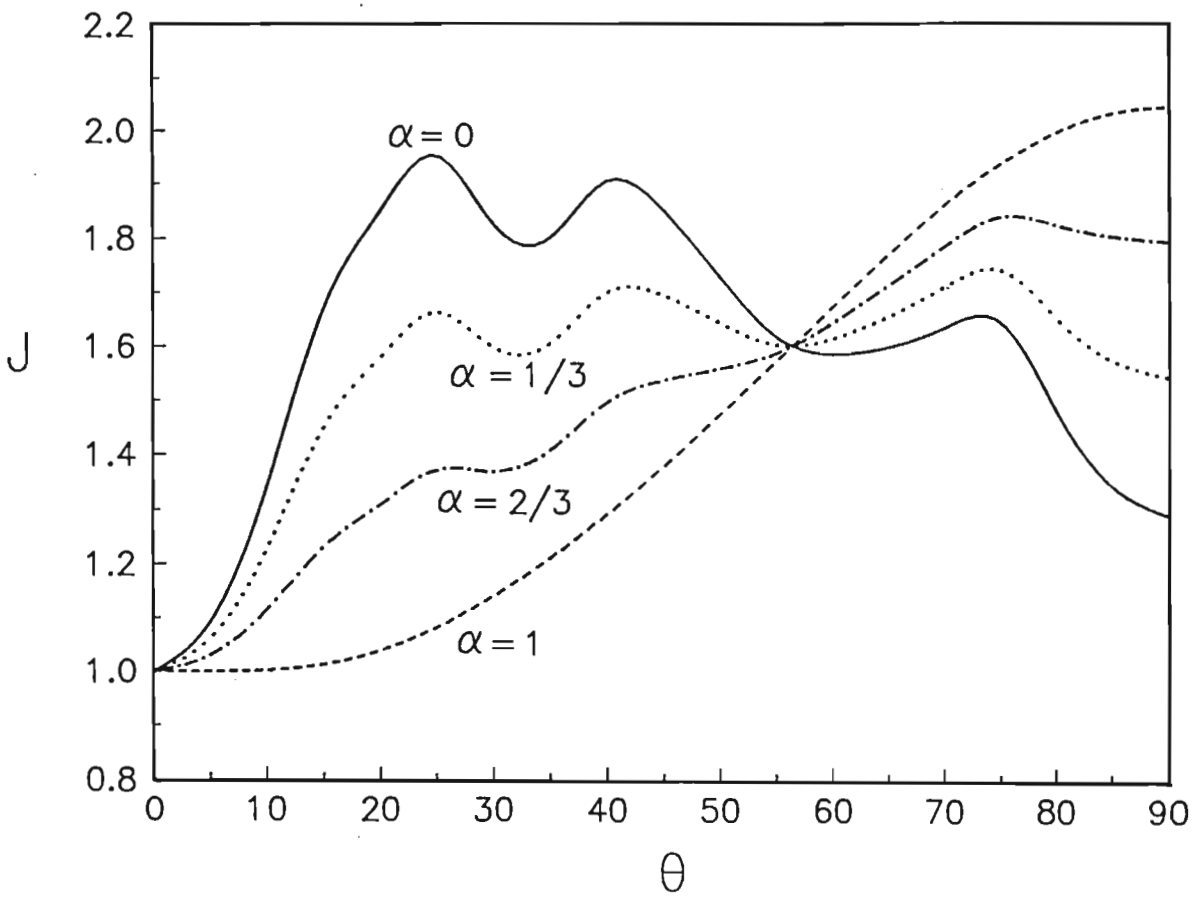

Figure 4.3.5. J versus θ for various values of α with $R = 1m$.

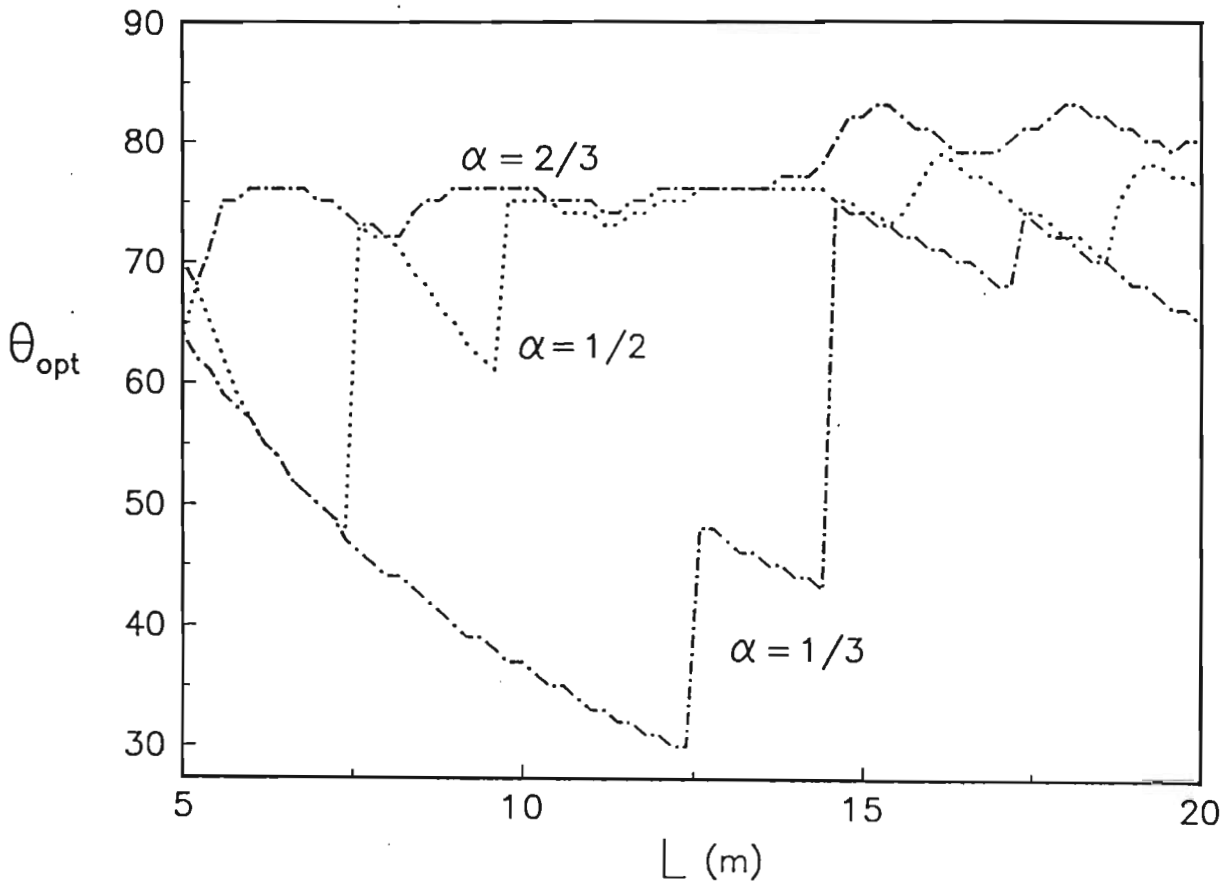

Figure 4.3.6. θ_{opt} versus L with $R = 1m$ (multiobjective design).

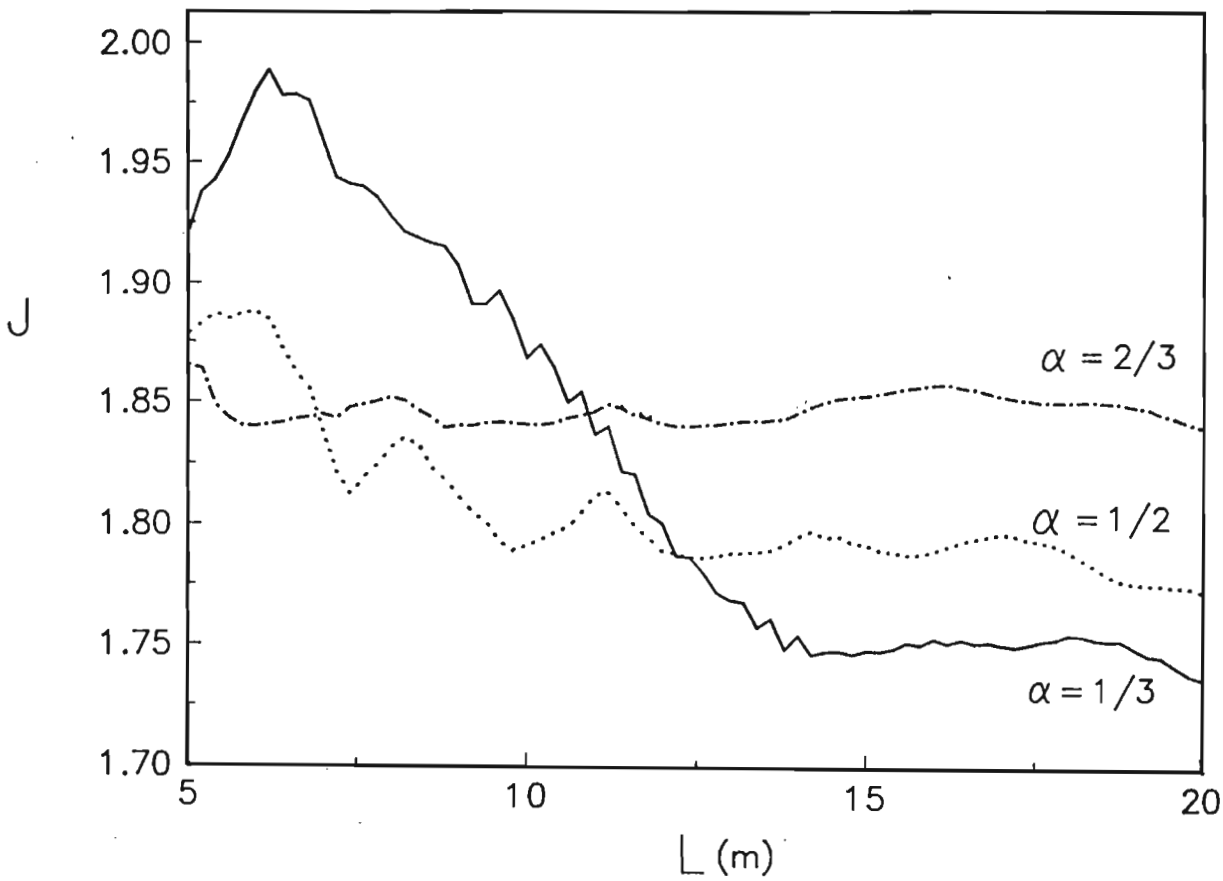

Figure 4.3.7. J versus L with $R = 1m$ (multiobjective design).

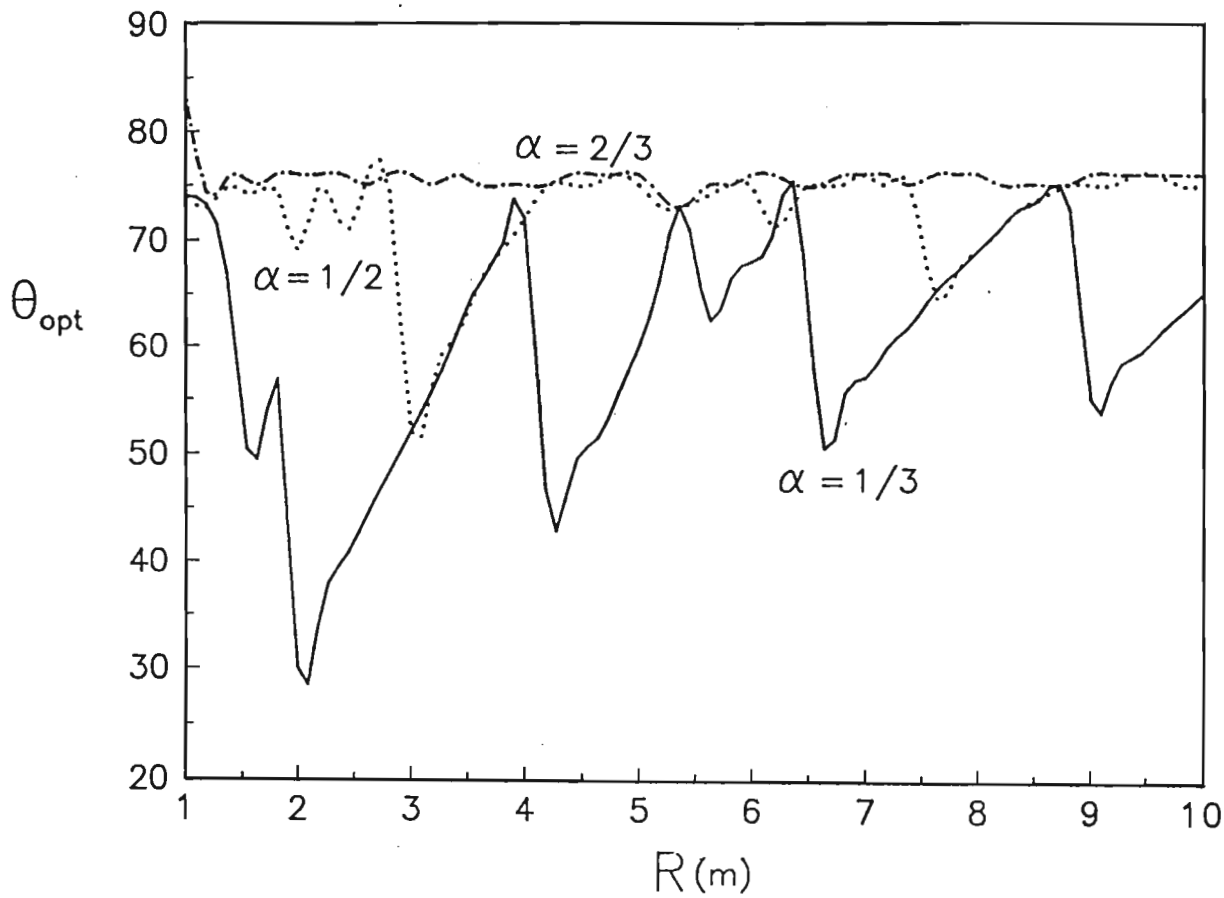

Figure 4.3.8. θ_{opt} versus R with $L = 15m$ (multiobjective design).

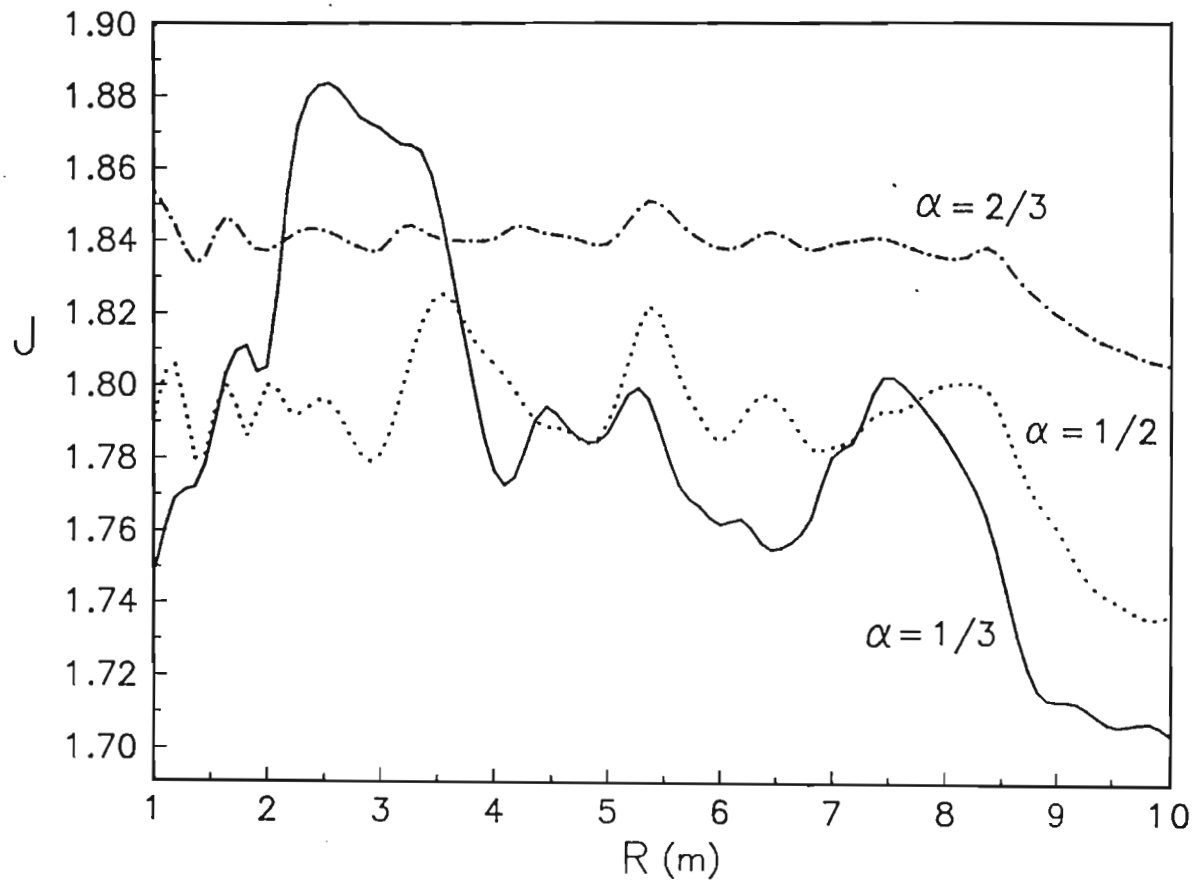

Figure 4.3.9. J versus R with $L = 15m$ (multiobjective design).

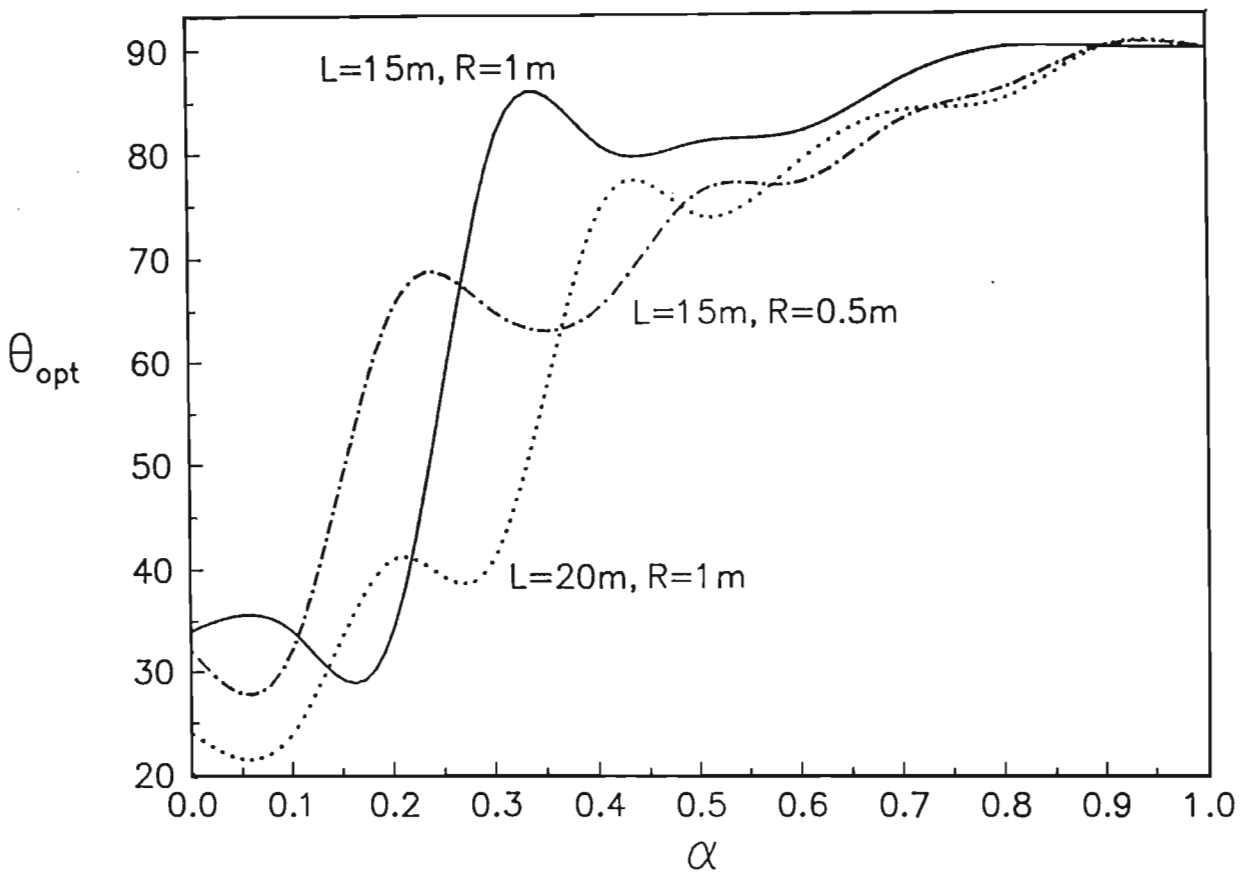

Figure 4.3.10. θ_{opt} versus α (multiobjective design).

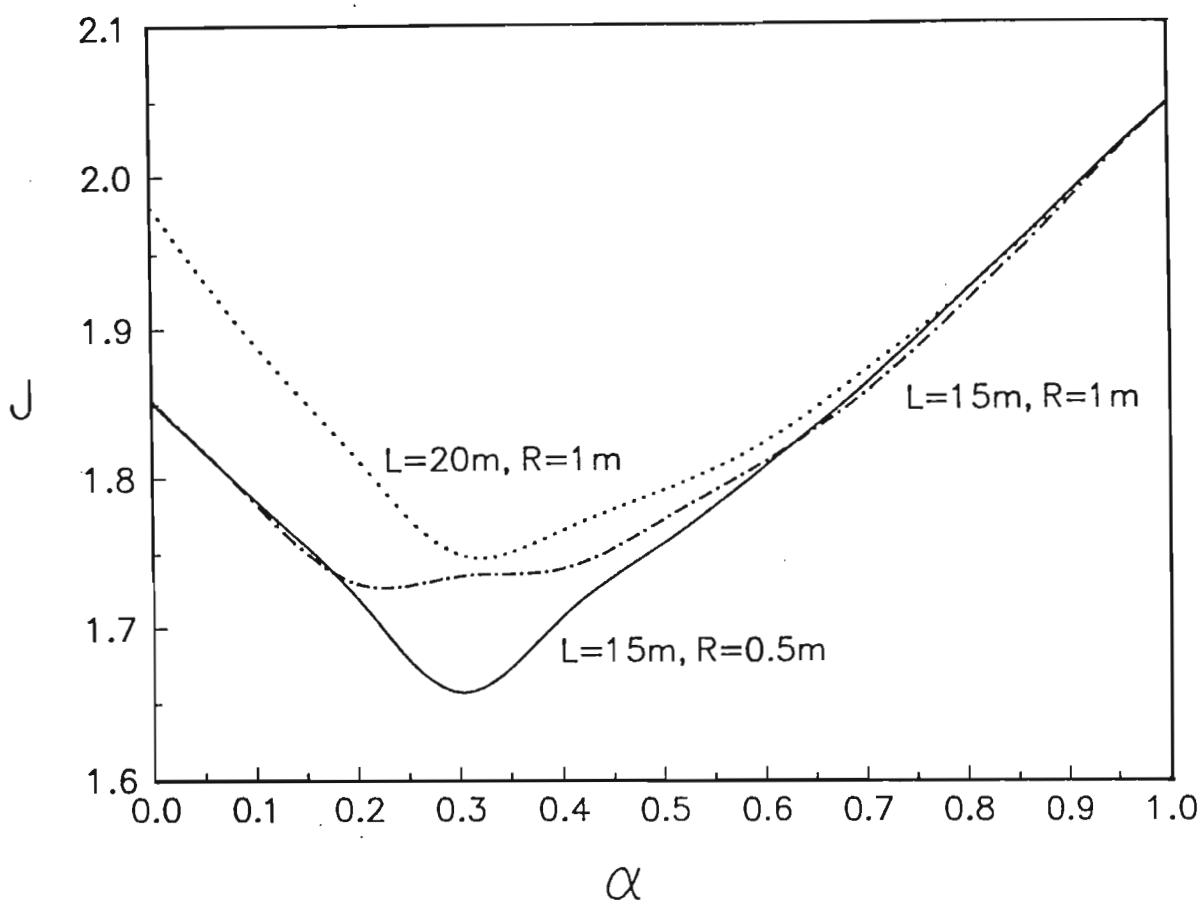

Figure 4.3.11. J versus α (multiobjective design).

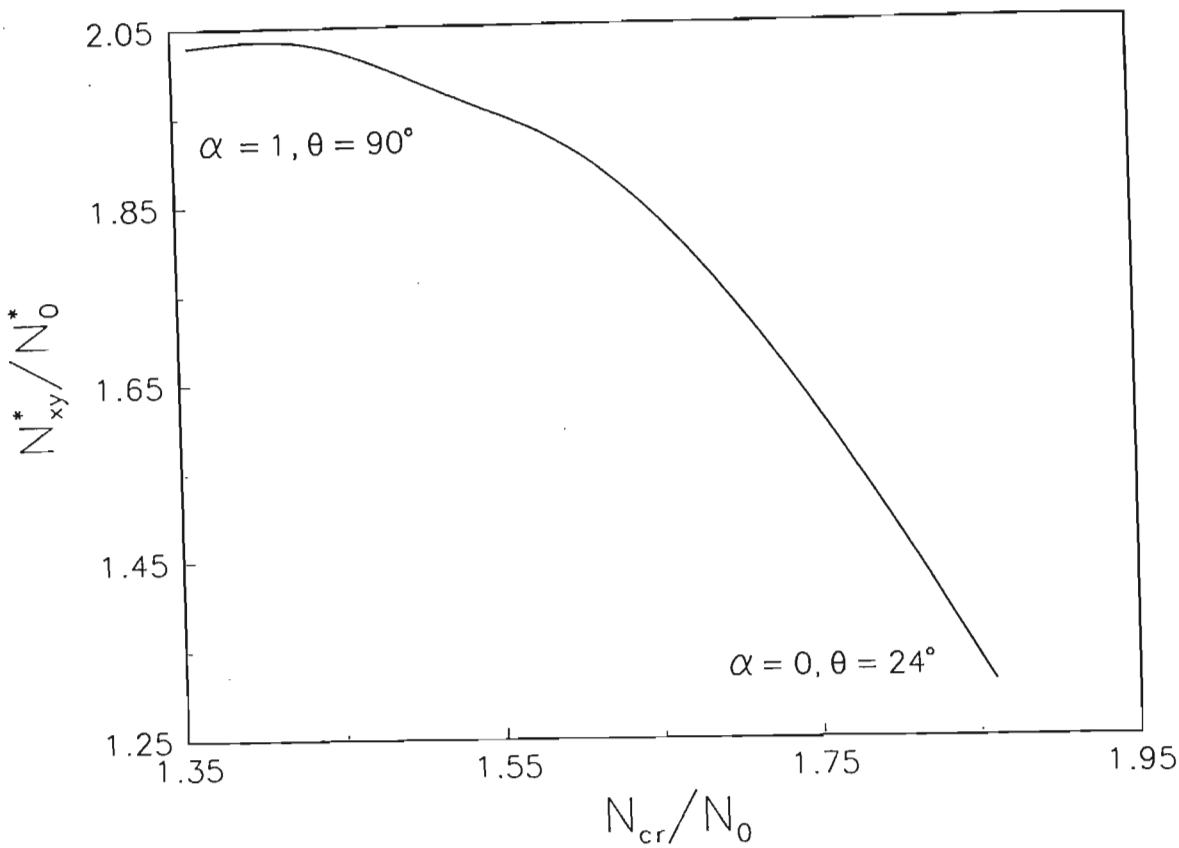

Figure 4.3.12. Trade-off curves of $\frac{N^*_{xy}}{N^*_0}$ versus $\frac{N_{cr}}{N_0}$.

H (m)	$J(\alpha = 1/3)$	$\theta_{opt}(\alpha = 1/3)$	$J(\alpha = 2/3)$	$\theta_{opt}(\alpha = 2/3)$
0.001	1.37	88.73°	1.71	90°
0.005	1.54	78.44°	1.78	90°
0.01	1.62	76.33°	1.81	84.86°
0.05	1.75	74.73°	1.85	83.88°
0.1	1.88	63.68°	1.84	70.83°

Table 4.3.1. The design index J versus H with $L = 15m$ and $R = 1m$, for different values of α.

4.4 Minimum Weight and Cost Design of Hybrid Laminated Plates

4.4.1 Method of Solution

The design space S contains a combination of continuous and discrete variables complicating the formulation of an optimisation procedure. Moreover, the high number of available design parameters suggests that conventional optimisation algorithms will be time consuming and possibly fail to find the global design point. To overcome these difficulties and in order to increase the accuracy of the solution, a sequential design procedure is formulated. The basic idea in this technique is to determine the optimal variables in a sequence and work with these variables (as they become available), as the solution progresses. This approach generates several trial solutions which are optimal with respect to one or more of the design parameters. The final design is chosen among these trial solutions. It is noted that the method of solution has no bias toward a hybrid construction and the final solution could produce a hybrid or non-hybrid laminate depending on the minimum buckling load or maximum cost (weight).

The procedure involves two stages of optimisation with the first stage yielding the optimum θ_k and t_{ref} and the second stage the optimum γ_i and the material combinations. Next, the steps in each stage are discussed.

First stage of optimisation

Step 1. For a given combination of materials, input the thickness parameters γ_i.

Step 2. For a given set of θ_k, $k = 1, ..., K/2$, compute the lowest t_{ref} satisfying the buckling constraint (3.10).

Step 3. Minimise the weight (cost) over θ_k by a suitable optimisation routine.

Note that t_{ref} varies for every set of θ_k values and is determined as part of the solution at this stage of the optimisation.

At the end of the first stage, a laminate is obtained which is optimal with respect to ply angles and satisfies the buckling constraint by virtue of the computation of t_{ref} accordingly. However γ_i are not determined optimally as they are input parameters at this stage and the material of each layer has been chosen a priori.

Second stage of optimisation

Step 4. The weight (cost) of a given laminate is to be minimised over the thickness parameters γ_i subject to the maximum cost (weight) constraint. This

can be done by any constrained optimisation routine which involves solving the problem (3.15), (3.16) (or (3.17), (3.18)) with respect to γ_i only as the optimal θ_k and t_{ref} are computed in steps 2 and 3 with the buckling constraint (3.10) already satisfied.

For a hybrid laminate with two different materials only, this process is illustrated in Figure 4.4.1. In this case $\gamma = t/t_{ref}$ where t is the layer thickness of the second material. The curves of weight versus γ and cost versus γ are plotted for each combination and the cost constraint C_0 is indicated on the figure. Cross-sections of $C = C_0$ and $C = C(\gamma)$ curves (lines d, e, f) indicate the points of active constraint for laminates 1, 2, 3 and the points to the left are feasible design points to minimise the weight.

Similarly the line $W = W_0$ gives the weight constraint and lines a, b and c are drawn from active constraint points. The cross-sections of lines a, b and c with $C = C(\gamma)$ curves, gives the optimal γ and the corresponding minimum cost for laminates 1, 2 and 3, respectively.

At the end of this step, the optimal γ values for minimum weight (cost) are determined for every material combination. Note that $\gamma = 0$ produces a non-hybrid laminate as the solution.

Step 5. The best material combination is determined by comparing the weights (costs) of laminates obtained in step 4. For example Figure 4.4.1 shows that minimum weight design is given by laminate 3 with the weight indicated by the line $W_{\min}$. Similarly, the minimum cost is marked by $C_{\min}$ corresponding to laminate 3. In this step the optimisation results are obtained for all material combinations by applying steps 1-4 to different hybrid constructions. A final comparison of $W_{\min}$ ($C_{\min}$) values for each construction yields the best design among competing laminates.

The solution process determines one of the design variables optimally at each step of the optimisation and the discrete variable (material combination) is determined by a comparison of candidate designs.

4.4.2 Numerical Results

The results are given for two-material hybrid constructions with eight layers [82], [83]. Three different materials, namely, T300/5208 graphite, Kevlar 49 and E-glass epoxies are selected which produces G/K, G/E and K/E combinations with G, K and E indicating the graphite (T300/5208), kevlar (Kevlar 49) and glass (E-glass)

laminates with epoxy matrix, respectively. The elastic constants, specific densities ρ and cost factors for these materials are given in Table 4.4.1 which are taken from Reference [79]. The fibre volume fractions are given as $v_f = 0.70$ for the graphite/epoxy, $v_f = 0.70$ for the Kevlar/epoxy and $v_f = 0.45$ for the glass/epoxy.

Material Specification	E_1(GPa)	E_2(GPa)	G_{12}(GPa)	ν	ρ	p
Graphite/Epoxy (T300/5208)	181	10.30	7.17	0.28	1.60	1
Kevlar/Epoxy (Kevlar49)	76	5.50	2.30	0.34	1.46	1/3
Glass/Epoxy (E-Glass)	38.60	8.27	4.14	0.26	1.80	1/20

Table 4.4.1 Elastic Constants of Materials

In Table 4.4.1, the cost factors p_i are computed as $p_i = P_i/P_{gr}$ where P_{gr} indicates the cost per unit weight of graphite/epoxy. The results are given in terms of non-dimensional quantities by introducing the variables W and C defined by

$$W = \frac{W_T}{\rho_w a b T_0} \quad , \quad C = \frac{C_T}{P_{gr}\rho_w a b T_0} \tag{4.5}$$

where $\rho_w = 1000 kg/m^3$ and $T_0 = 0.01m$. The buckling load is also nondimensionalised by defining

$$N_{cr} = \frac{N b^2}{E_0 T_0^3} \tag{4.6}$$

where $E_0 = 1\ GPa$ is a reference modulus. The stacking sequences are shown as $(G/G/K/K)_s$ etc., where the subscript s indicates a symmetric lay-up. It is noted that the buckling load (2.89) is a function of D_{ij} which gives the highest value when the stronger material is in the surface layers and the weak material is in the core layers due to sandwich effect (see Ref [55]). Thus two-material combinations out of three different materials yield 3 different hybrid constructions to optimise and compare, namely, G/K, G/E and K/E combinations.

In the numerical results the ply angles are taken as $(\theta/-\theta/\theta/-\theta)_s$ and $\gamma = t/t_{ref}$ with t_{ref} taken as the layer thickness of the stronger material. Thus $t_{ref} = t_{gr}$ for graphite/kevlar and graphite/glass combinations with $t = t_k$ and t_{gl}, respectively. In the kevlar/glass combination $t_{ref} = t_k$ and $t = t_{gl}$. In the rest of the paper N_0 is specified as $N_0 = 10^3$, $\lambda = 1$ (biaxial loading).The thickness constraint is specified as $\gamma \leq 3.0$ in all cases.

The effect of the fibre orientation on the weight and the cost is investigated in Figures 4.4.2 and 4.4.3 which show the curves of W and C plotted against θ,

respectively, with $a/b = 1.5$, $\gamma = 1.0$ (equal layer thicknesses) for various material combinations. In the figures, laminations $(G/G/K/K)_s$, $(G/G/E/E)_s$, etc. are indicated as GGKK, GGEE and so on. Note that the buckling constraint (3.10) is satisfied at every point by virtue of determining t_{ref} from (3.10). The minimum weight and cost occur approximately at the same ply angle for all materials which is about $\theta = 62^o$ (Figures 4.4.2 and 4.4.3). The curves indicate that optimisation with respect to θ is an important part of the design process as the weight and cost at $\theta = 0°$ and $\theta = \theta_{opt}$ may differ as much as 35% for some laminates. It is observed that the G/K combination yields the lowest weight while the lowest cost laminate is given by a glass/epoxy one.

The effect of the buckling constraint on the weight and cost are studied in Figures 4.4.4 and 4.4.5 which show the curves of weight and cost versus N_0 for $a/b = 1.5$ for different layer thicknesses. It is observed that layer thicknesses have varying degrees of effect on different material combinations. Furthermore their effect on weight and cost also differs with the change in γ affecting cost more than weight for all material combinations. Note that $\theta = \theta_{opt}$ at every point on the curves given in Figures 4.4.4 and 4.4.5. This is also the case for Figures 4.4.6 and 4.4.7.

Next the curves of weight and cost plotted against γ are studied. Figures 4.4.6 and 4.4.7 show these curves for the various material combinations with $a/b = 1.5$. Increasing γ indicates an increase in the thickness of kevlar and glass layers for G/K and G/E combinations and glass layers for K/E combinations since $t_{ref} = t_{gr}$ or t_k. Although the general trend is increasing weight as γ increases (Figure 4.4.6), the graphite/kevlar combination displays quite a different weight versus γ behaviour. As γ increases, i.e., as t_k increases relative to t_{gr}, the weight decreases up to a minimum value before increasing again suggesting the existence of an optimal γ value for minimum weight design in the graphite/kevlar combination. Figure 4.4.7 shows the corresponding curves for the cost function. In this case increase in the thickness of inexpensive layers leads to decrease in cost. However $KKKK$ and $GGEE$ laminates show different cost values at different γ.

The solutions are given in Tables 4.4.2 and 4.4.3 for the minimum weight problem and in Tables 4.4.4 and 4.4.5 for the minimum cost problem for different aspect ratios.

C_0	$H\ (mm)$	θ_{opt}	γ_{opt}	optimal layup	W_{min}
5	26.0	45°	2.93	KKEE	44.50
10	20.9	45°	2.90	GGEE	36.52
15	19.3	45°	1.20	GGEE	33.03
20	18.9	45°	0.95	GGKK	29.01
25	18.7	45°	0.67	GGKK	28.94
30	18.7	45°	0.67	GGKK	28.94

Table 4.4.2 Minimum weight designs for various cost constraints with $a/b = 1.0$ and $\lambda = 1$.

C_0	$H\ (mm)$	θ_{opt}	γ_{opt}	optimal layup	W_{min}
5	—	—	—	—	—
10	27.0	60.90°	0.41	KKEE	42.01
15	21.5	62.01°	1.46	GGEE	36.89
20	21.1	61.87°	1.40	GGKK	32.09
25	20.4	61.96°	0.51	GGKK	31.75
30	20.4	61.96°	0.51	GGKK	31.75

Table 4.4.3 Minimum weight designs for various cost constraints with $a/b = 1.5$ and $\lambda = 1$.

Tables 4.4.2 and 4.4.3 indicate that as the cost constraint is relaxed graphite/kevlar combinations provide the best lay-ups. At lower costs kevlar/glass gives the optimal solution due to the inexpensive nature of E-glass accompanied by higher weight. The decrease in weight as the cost increases tapers off as C_0 exceeds $C_0 = 20$ as the last column indicates. This shows that higher expenditure on material leads to diminished returns as far as the weight is concerned and higher cost is possibly not justified after a certain point.

The increase in the weight constraint leads to an initial drop in cost which again tapers off after a certain point as the last columns of Table 4.4.4 and 4.4.5 indicate. No constraint was imposed on the total thickness of the laminates and H depends on the cost and the weight. Obviously a constraint on H would lead to different optimal designs in many cases.

W_0	$H\ (mm)$	θ_{opt}	γ_{opt}	optimal layup	C_{min}
30	19.9	45°	2.37	GGKK	16.27
35	20.4	45°	2.28	GGEE	11.21
40	24.7	45°	0.79	KKEE	7.70
45	26.0	45°	3.00	KKEE	4.92
50	26.0	45°	3.00	KKEE	4.92

Table 4.4.4 Minimum cost designs for various weight constraints with $a/b = 1.0$ and $\lambda = 1$.

W_0	$H\ (mm)$	θ_{opt}	γ_{opt}	optimal layup	C_{min}
30	—	—	—	—	—
35	22.4	61.71°	3.00	GGKK	17.01
40	22.9	62.05°	2.87	GGEE	10.99
45	27.4	60.99°	1.12	KKEE	7.60
50	28.5	61.23°	3.00	KKEE	5.47

Table 4.4.5 Minimum cost designs for various weight constraints with $a/b = 1.5$ and $\lambda = 1$.

The optimal designs are given by hybrid laminates in all cases indicating the extra tailoring capability gained by admitting hybrid constructions into the design space. At this stage it is useful to compare the optimal designs with optimal non-hybrid designs in order to assess the differences quantitatively. For this purpose the following efficiency indices are introduced:

$$\eta_{gr} = \frac{W_{gr} - W_{min}}{W_{min}} \times 100 \ , \ \eta_k = \frac{W_k - W_{min}}{W_{min}} \times 100 \ , \ \eta_{gl} = \frac{W_{gl} - W_{min}}{W_{min}} \times 100 \tag{4.7}$$

to compute the reduction in weight obtained by choosing a hybrid design. In Equation (4.7) W_{gr}, W_k and W_{gl} denote the weight of one-material optimal laminates made out of graphite, kevlar or glass, respectively. The results are shown in Table 4.4.6 which gives the weight efficiency indices in percentages for various cost constraints for the same input parameters as in Tables 4.4.2 and 4.4.3. It is observed that hybrid designs lead to substantial weight savings as compared to glass constructions. In the case of kevlar constructions, the weight savings are about 20%. In many cases, a non–hybrid laminate satisfying the design constraints is not available.

	$a/b = 1.0$			$a/b = 1.5$		
C_0	η_{gr}	η_k	η_{gl}	η_{gr}	η_k	η_{gl}
5	NA^*	NA^*	14.50	NA^*	NA^*	NA^*
10	NA^*	NA^*	30.08	NA^*	NA^*	26.62
15	NA^*	7.43	36.76	NA^*	5.94	35.56
20	2.09	18.69	44.46	1.23	18.33	43.98
25	1.86	18.50	44.32	3.60	20.19	45.33
30	2.33	18.89	44.59	3.05	19.73	45.01

*NA indicates that a non-hybrid design is not available for this cost constraint.

Table 4.4.6. Comparison of minimum weights for hybrid and non–hybrid constructions

Similarly the reduction in cost obtained opting for a hybrid construction can be assessed from the indices given by

$$\mu_{gr} = \frac{C_{gr} - C_{min}}{C_{min}} \times 100 \ , \ \mu_k = \frac{C_k - C_{min}}{C_{min}} \times 100 \ , \ \mu_{gl} = \frac{C_{gl} - C_{min}}{C_{min}} \times 100 \quad (4.8)$$

where C_{gr}, C_k and C_{gl} denote the costs of the one-material optimal laminates made out of graphite, kevlar or glass, respectively. The results are given in Table 4.4.7 which shows the cost indices for various weight constraints and for the same input parameters as Tables 4.4.4 and 4.4.5. Hybrid laminates provide cost savings of more than 80% in some cases and highlight the tailoring capabilities obtained by selecting optimal material combinations for design purposes.

	$a/b = 1$			$a/b = 1$		
W_0	μ_{gr}	μ_k	μ_{gl}	μ_{gr}	μ_k	μ_{gl}
30	45.09	NA^*	NA^*	NA^*	NA^*	NA^*
35	62.17	5.72	NA^*	47.61	NA^*	NA^*
40	74.01	35.24	NA^*	66.15	15.91	NA^*
45	83.40	58.62	NA^*	76.59	41.85	NA^*
50	83.40	58.62	NA^*	83.15	58.15	NA^*

*NA indicates that a non-hybrid design is not available for this weight constraint.

Table 4.4.7. Comparison of minimum costs for hybrid and non–hybrid constructions

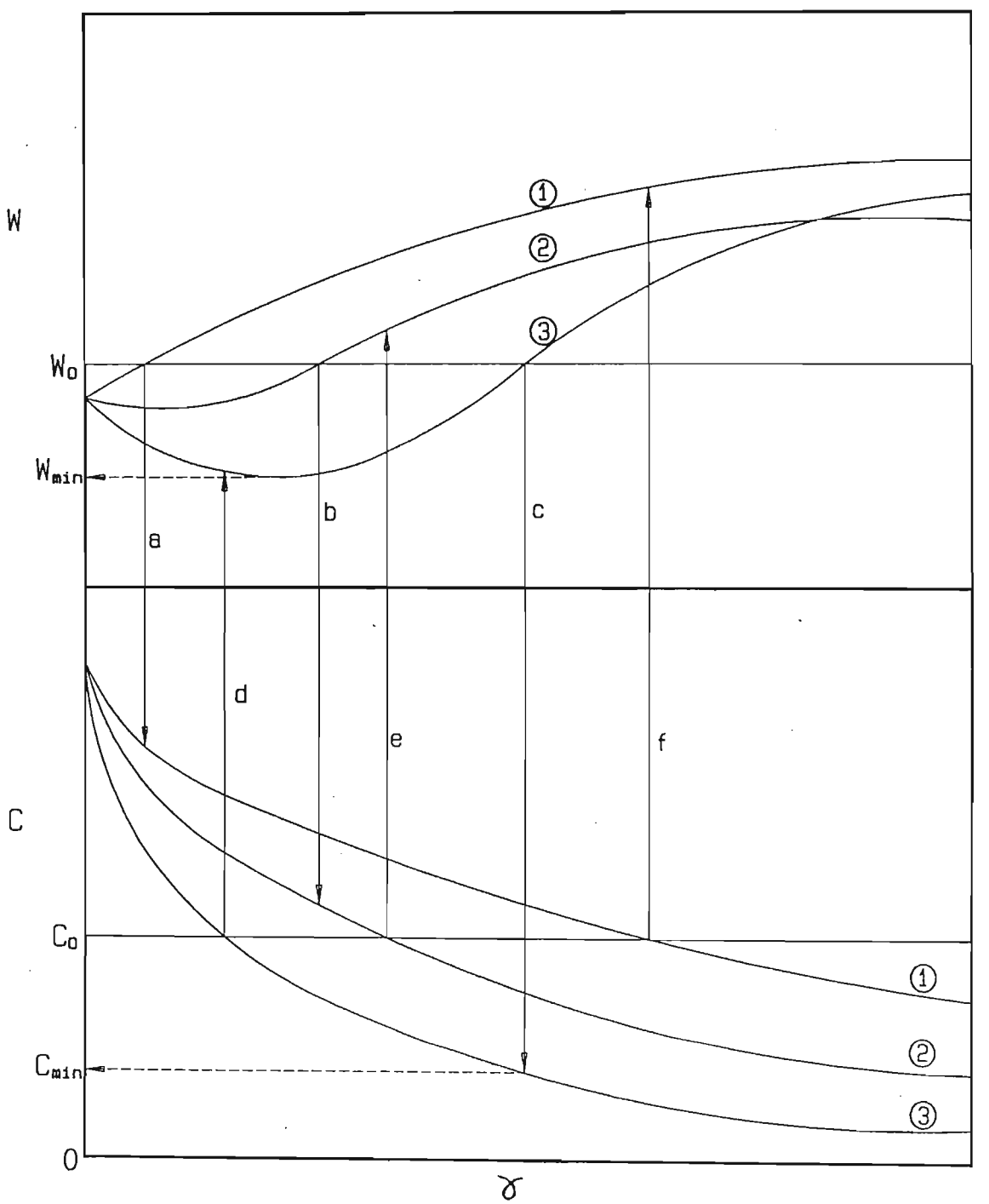

Figure 4.4.1. Curves of weight and cost versus the relative layer thickness γ

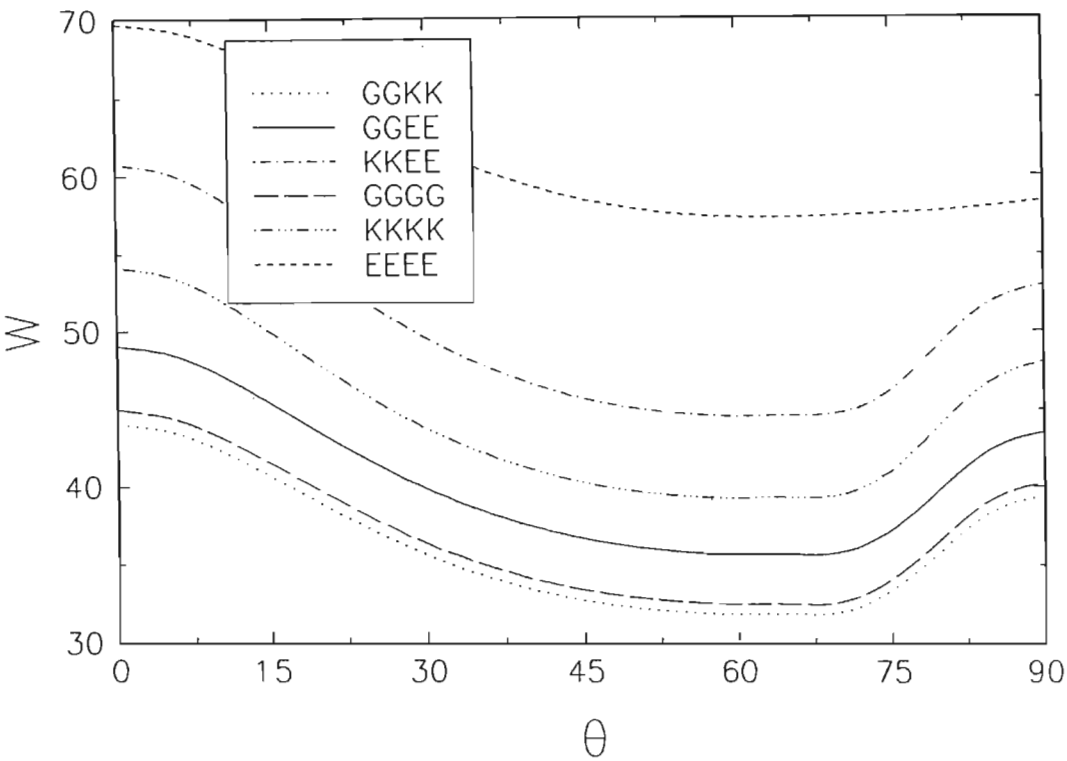

Figure 4.4.2. Weight versus θ curves for hybrid and non–hybrid laminates with $\lambda = 1$, $a/b = 1.5$, and $\gamma = 1.0$.

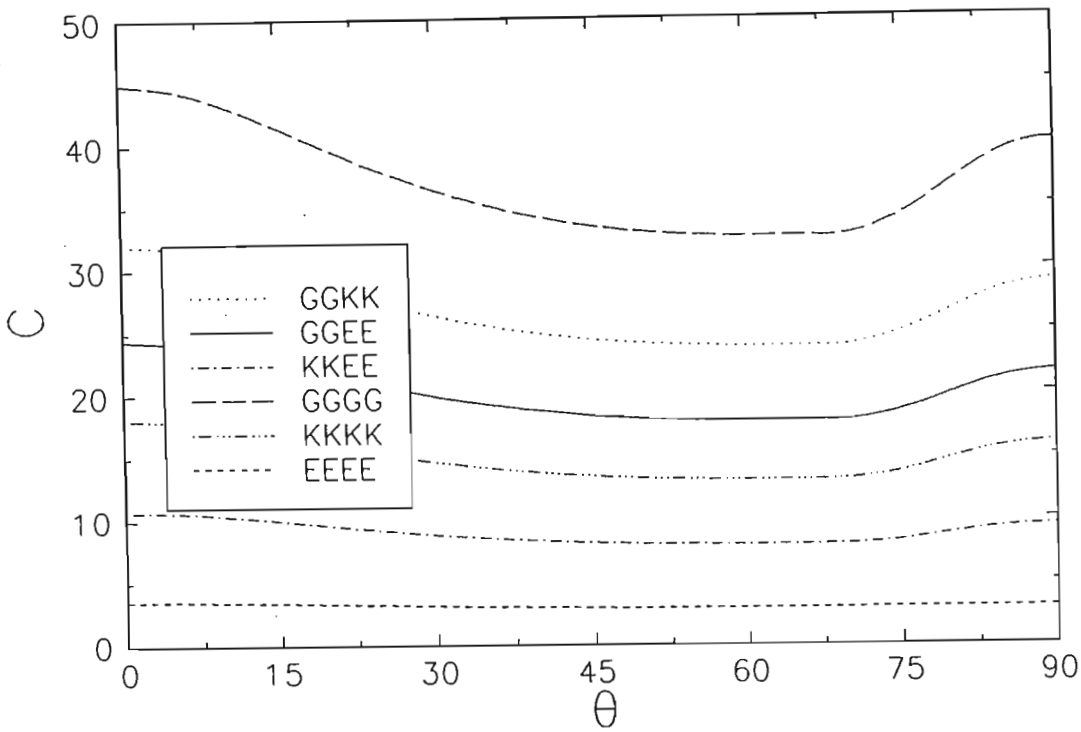

Figure 4.4.3. Cost versus θ curves for hybrid and non–hybrid laminates with $\lambda = 1$, $a/b = 1.5$, and $\gamma = 1.0$.

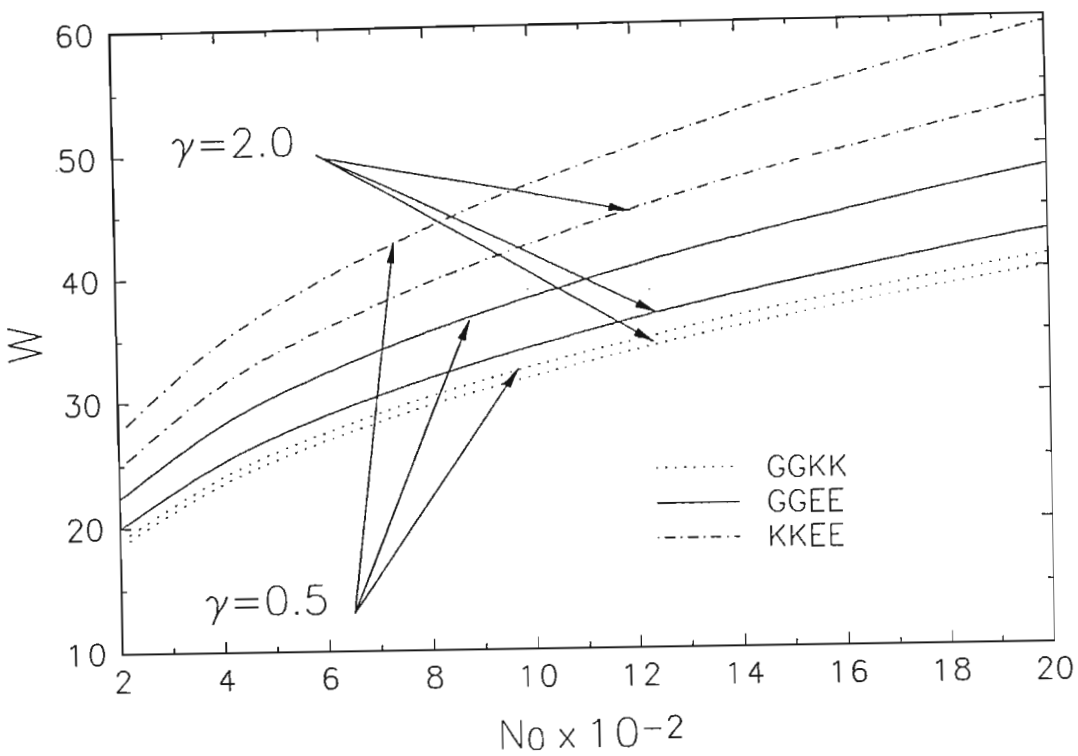

Figure 4.4.4. Weight versus buckling constraint for hybrid laminates with $a/b = 1.5$, and $\lambda = 1.0$

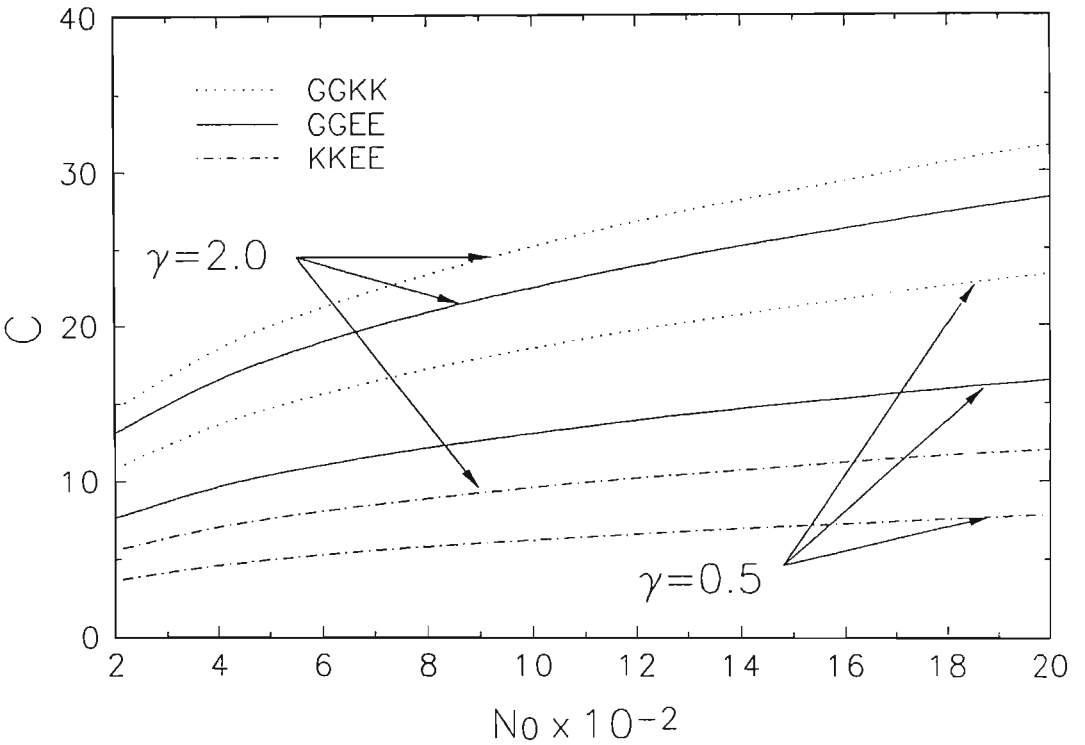

Figure 4.4.5. Cost versus buckling constraint for hybrid laminates with $a/b = 1.5$, and $\lambda = 1.0$

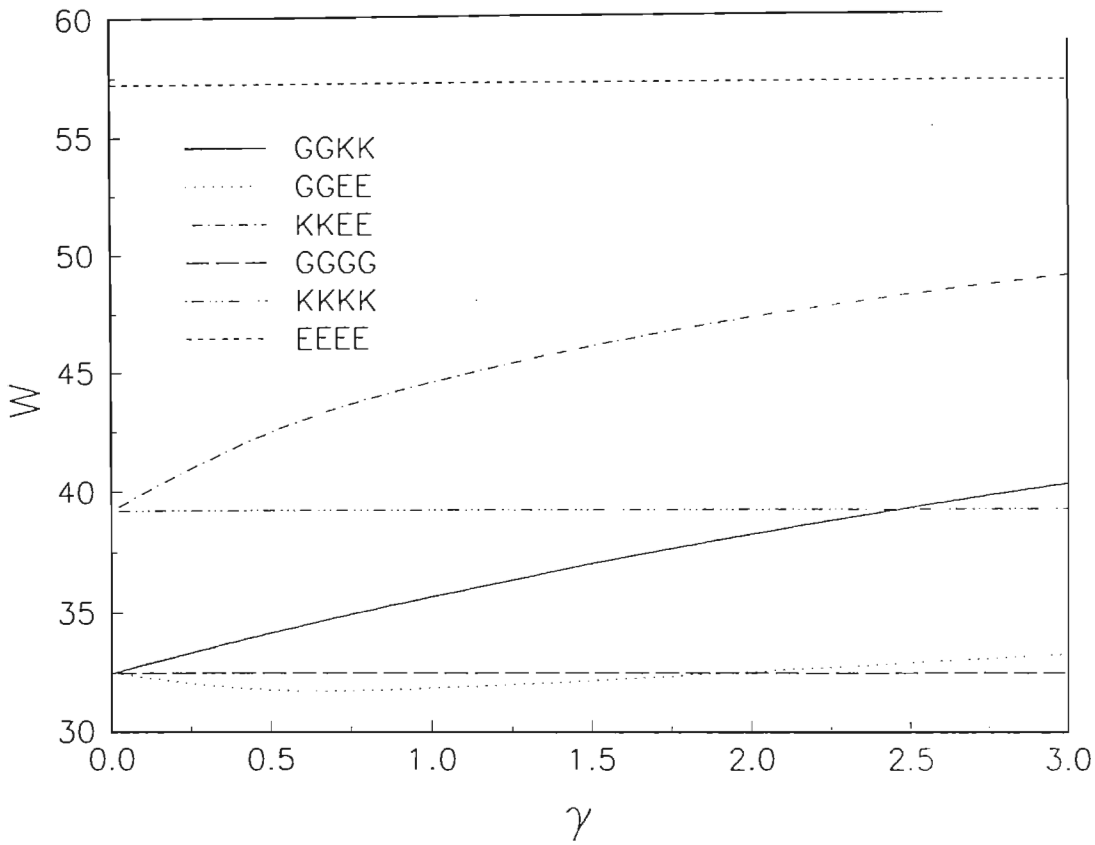

Figure 4.4.6. Weight versus γ curves for various material combinations with $a/b = 1.5$, and $\lambda = 1.0$

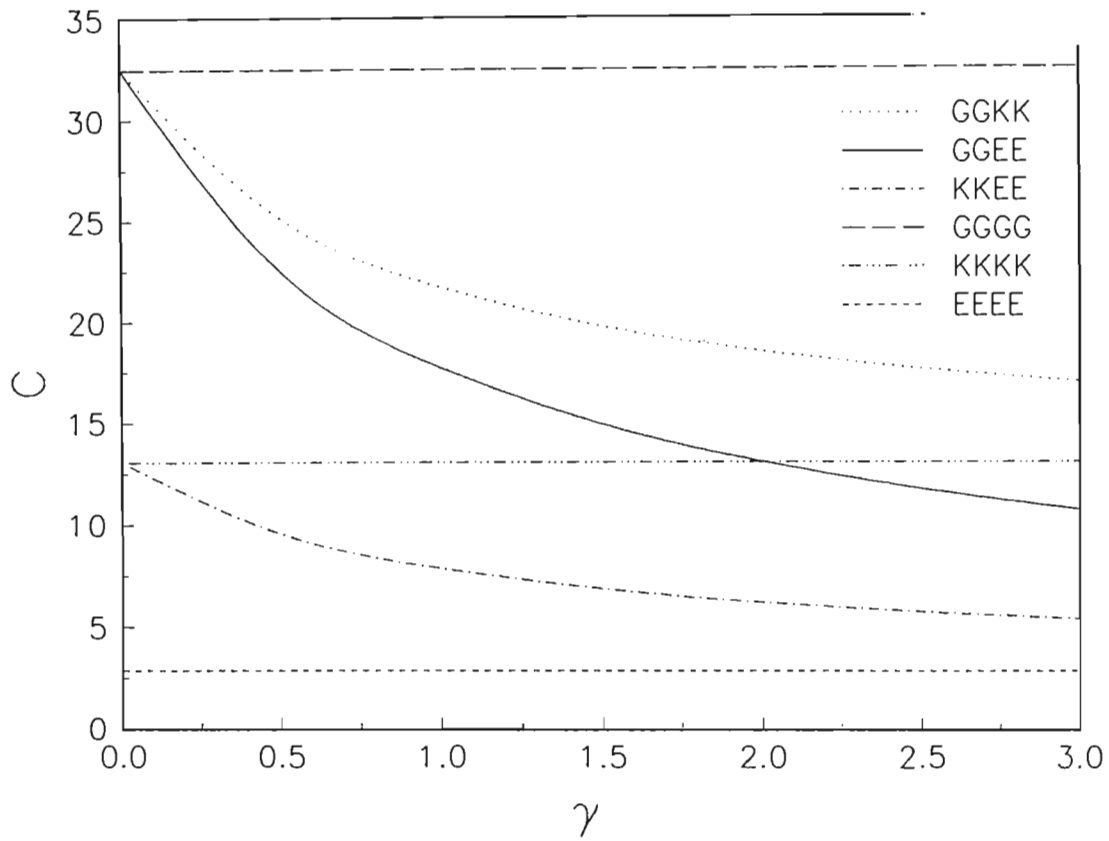

Figure 4.4.7. Cost versus γ curves for various material combinations with $a/b = 1.5$, and $\lambda = 1.0$

4.5 Optimal Design of Symmetrically Laminated Plates for Minimum Deflection and Weight

The plates considered in this design problem are subjected to a combination of free, simply supported and clamped boundary conditions. This fact and the presence of nonuniform transverse loads necessitate a numerical approach to the solution of the problem. The FEM formulation used is given below.

4.5.1 Finite Element Formulation

We now consider the finite element formulation of the problem [84]. Let the region S of the plate be divided into n sub-regions S_r ($S_r \in S; r = 1, 2, ..., n$) such that

$$\Pi(u) = \sum_{r=1}^{n} \Pi^{Sr}(u) \tag{4.9}$$

where Π and Π^{Sr} are potential energies of the plate and the element, respectively, and u is the displacement vector. Using the same shape functions associated with node j ($j = 1, 2, ..., n$), $S_j(x, y)$, for interpolating the variables in each element, we can write

$$u = \sum_{j=1}^{n} S_j(x, y) u_j \tag{4.10}$$

where u_j is the value of the displacement vector corresponding to node j, and is given by

$$u = \{u^{(j)}, v^{(j)}, w^{(j)}, \phi_1^{(j)}, \phi_2^{(j)}\}^T \tag{4.11}$$

The displacements $\{u, v, w, \phi_1, \phi_2\}$ are approximated as

$$u = \sum_{j=1}^{n} u_j \psi_j(x, y) \ , \ v = \sum_{j=1}^{n} v_j \psi_j(x, y) \ , \ w = \sum_{j=1}^{n} w_j \psi_j(x, y)$$

$$\phi_1 = \sum_{j=1}^{n} S_j^1 \psi_j(x, y) \ , \ \phi_2 = \sum_{j=1}^{n} S_j^2 \psi_j(x, y) \tag{4.12}$$

where ψ_j are Lagrange family of interpolation functions. From the equilibrium equations of the first order theory, and equations (4.12), we obtain the finite element model of the first-order theory,

$$\sum_{\beta=1}^{5} \sum_{j=1}^{n} K_{ij}^{\alpha\beta} \Delta_j^{\beta} - F_i^{\alpha} = 0 \ , \ (\alpha = 1, 2, ..., 5) \tag{4.13}$$

or

$$[K]\{\Delta\} - \{F\} = \{0\} \tag{4.14}$$

where K and F are the stiffness and force coefficients respectively, and the variable Δ denotes the nodal values of w and its derivatives.

4.5.2 Numerical Results

The structures considered in this study are four-layered symmetrically laminated plates. The material properties used for the analysis of these shells is T300/5208 graphite epoxy. The strength values used in the Tsai-Wu failure criterion are $X_t = 1500\ MPa$, $X_c = 1500\ MPa$, $Y_t = 40\ MPa$, $Y_c = 68\ MPa$ and $S = 246\ MPa$. The values for the material properties are taken from reference [79].

For the first part of the study, where minimum deflection/minimum weight is the design priority (part A.), two loading conditions are considered. The first is a uniform pressure over the whole surface of the plate of magnitude $q = 100KPa$. The second is a patch load of uniform pressure over one quarter of the plate. In this case, the magnitude of the pressure is the same as before.

Four different boundary conditions are implemented along the four plate edges (numbered 1 to 4 in Figure 2.13). These are (S,S,S,S), (C,S,C,S), (C,C,C,C) and (C,S,F,S) with S representing simply supported, C clamped and F free, while the order refers to edges 1 - 4, respectively. Rotations around the x and y axes are denoted by r_x and r_y, respectively. These conditions may be explicitly described as follows:

(S,S,S,S): $w = r_x = 0$ at $x = 0,\ a$ and $w = r_y = 0$ at $y = 0,\ b$.
(C,C,C,C): $w = r_x = r_y = 0$ at $x = 0,\ a$ and $w = r_x = r_y = 0$ at $y = 0,\ b$.
(C,S,C,S): $w = r_x = r_y = 0$ at $x = 0,\ a$ and $r_y = 0$ at $y = 0,\ b$.
(C,S,F,S): $w = r_x = r_y = 0$ at $x = 0$ and $w = r_y = 0$ at $y = 0,\ b$.

For the results where the priority is the minimum weight (design problem 2), only two cases of boundary conditions, viz. (S,S,S,S) and (C,C,C,C) are studied for comparative purposes.

The accuracy for the optimal fibre angle, θ_{opt}, is $0.1°$ and that for the minimum laminate thickness, $H_{\min}$, is $0.1\,mm$.

Minimum deflection/minimum weight design

1. Uniform load

First the maximum deflection of a square plate versus the fibre angle is determined at an arbitrary thickness $H = 0.01m$ in order to study the effect of fibre orientation on the deflection. These curves are shown in Figure 4.5.1, which indicates that the optimum θ depends heavily on the boundary conditions and may be 0°, 45° or 90° depending on these conditions. Figure 4.5.2 shows the maximum deflection of the plate versus the fibre angle θ for a square plate under a uniformly distributed load where the thickness at every θ is determined subject to the failure criterion. Due to the symmetry of the loading and boundary conditions, the minimum deflection for (C,C,C,C) is found at two fibre angles namely 0° and 90°. For (C,S,C,S) and (C,S,F,S) the optimal fibre angle is found at 0°, while for (S,S,S,S) the minimum deflection occurs at 45°. The corresponding minimum thicknesses are shown in Figure 4.5.3. Figure 4.5.4 shows the curves of minimum deflection plotted against the aspect ratio. At low aspect ratios ($a/b \leq 1.2$), w_{min} is not monotonic. However at higher values of the aspect ratio, w_{min} tends to increase for all the boundary conditions. The minimum thicknesses corresponding to the deflections shown in Figure 4.5.4 are shown in Figure 4.5.5. For all boundary conditions, H_{min} generally increases with increasing aspect ratio. The optimal fibre angles corresponding to w_{max} are shown in Figure 4.5.6. At higher aspect ratios, θ_{opt} for (S,S,S,S), (C,C,C,C) and (C,S,F,S) all tend to 90° while for (C,S,C,S) the optimal fibre angles are found at 0°. All the curves exhibit discontinuities, although no suitable explanation for this can be given.

2. Patch load

The curves of maximum deflection versus fibre angle for a square plate of thickness $H = 0.01m$ are shown in Figure 4.5.7. Figure 4.5.8 shows the variation of deflection with fibre angle for a square plate with the minimum thickness subject to the failure criterion. As expected, the deflections for all boundary conditions are slightly less than for the first loading case. Although for the square plate the optimal fibre angle for (S,S,S,S), (C,C,C,C) and (C,S,C,S) remain the same as for the uniform load, the optimal fibre angle for (C,S,F,S) is found at about 20°. The minimum thicknesses are plotted against θ in Figure 4.5.9. The minimum deflections

versus the plate aspect ratio are shown in Figure 4.5.10. As before, the minimum deflections generally increase with increasing a/b, although it is interesting to note that none of the curves is monotonic, as it could be expected that deflection would increase as the plate surface area increases.The corresponding minimum thicknesses and optimal fibre angles are shown in Figures 4.5.11 and 4.5.12. It is observed that the optimal θ displays several jump discontinuities as for the uniform load.

Minimum weight design

The results for the minimum weight design under the uniform pressure loading condition are given in Tables 4.5.1 and 4.5.2, together with the equivalent results for the first design problem. For the case (S,S,S,S) the second design problem leads to a decrease in the thickness of around 10 % for all aspect ratios with an increase in the deflection of approximately the same magnitude. In the case of clamped plates (C,C,C,C), minimising the weight only results in an increase in the deflection of about 170 % for an aspect ratio of $a/b = 0.5$ reducing to an increase of about 25 % for $a/b = 2.0$.

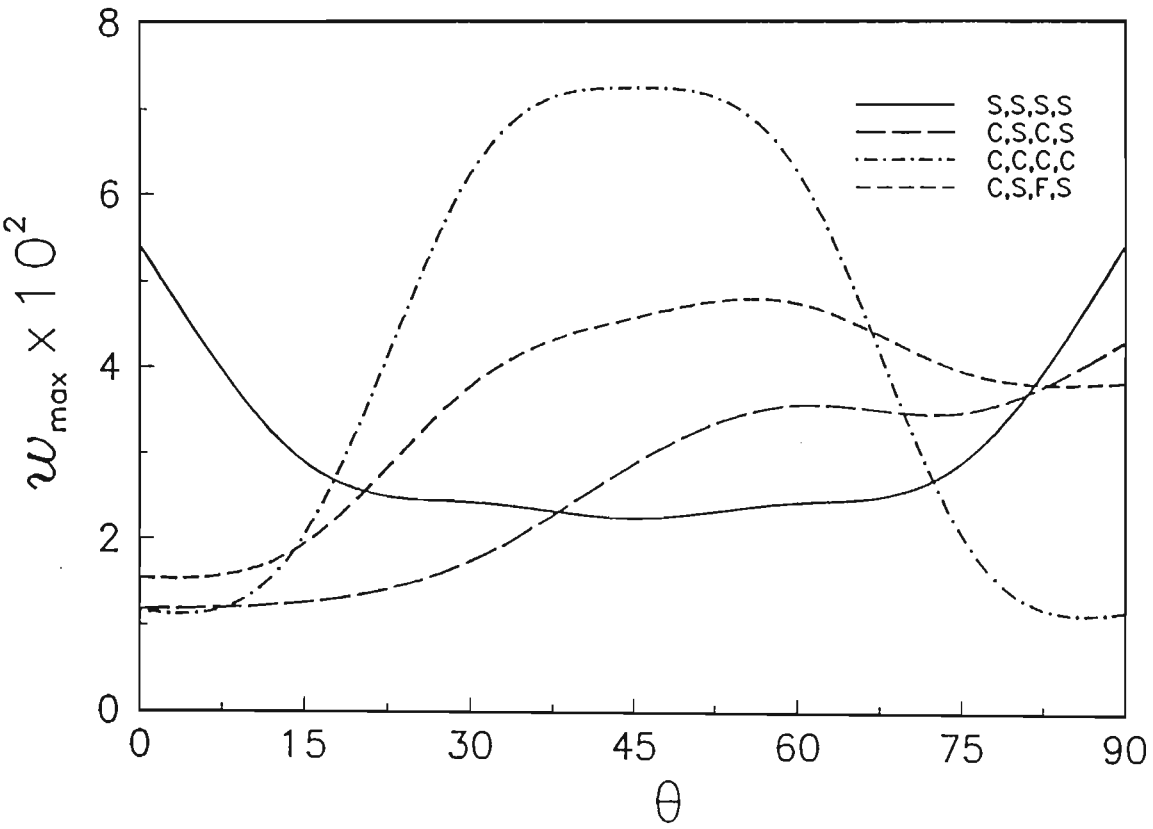

Figure 4.5.2. w_{max} versus θ with $a/b = 1$ and $F(\theta) = 1$ (uniformly distributed load).

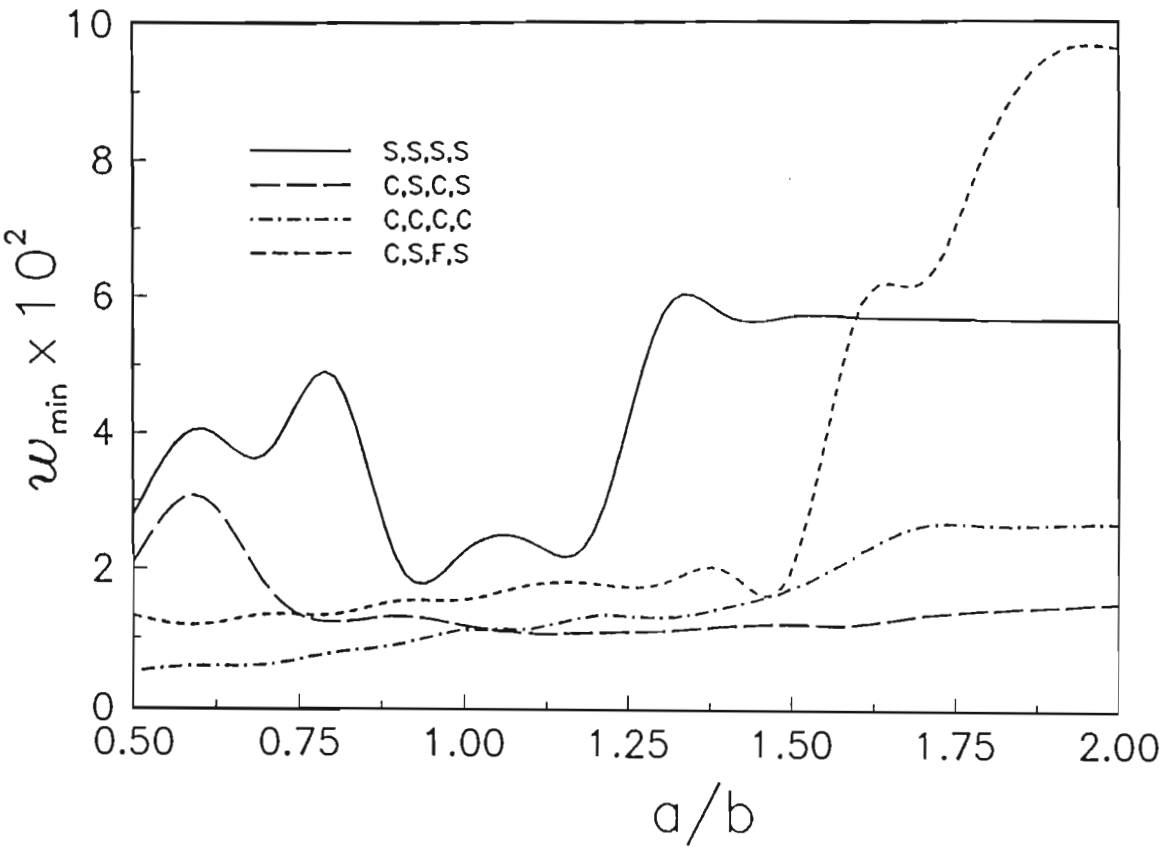

Figure 4.5.4. w_{min} versus a/b with $F(\theta) = 1$ (uniformly distributed load).

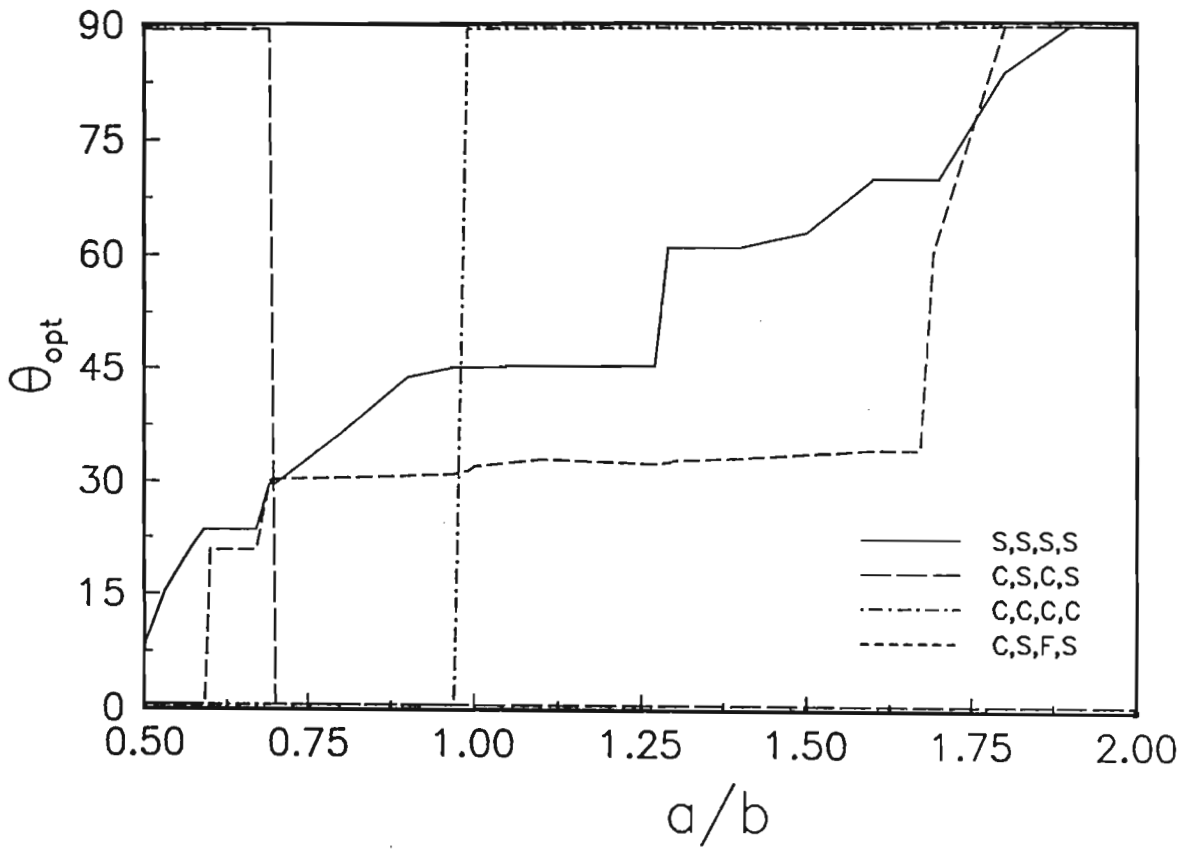

Figure 4.5.6. θ_{opt} versus a/b (uniformly distributed load).

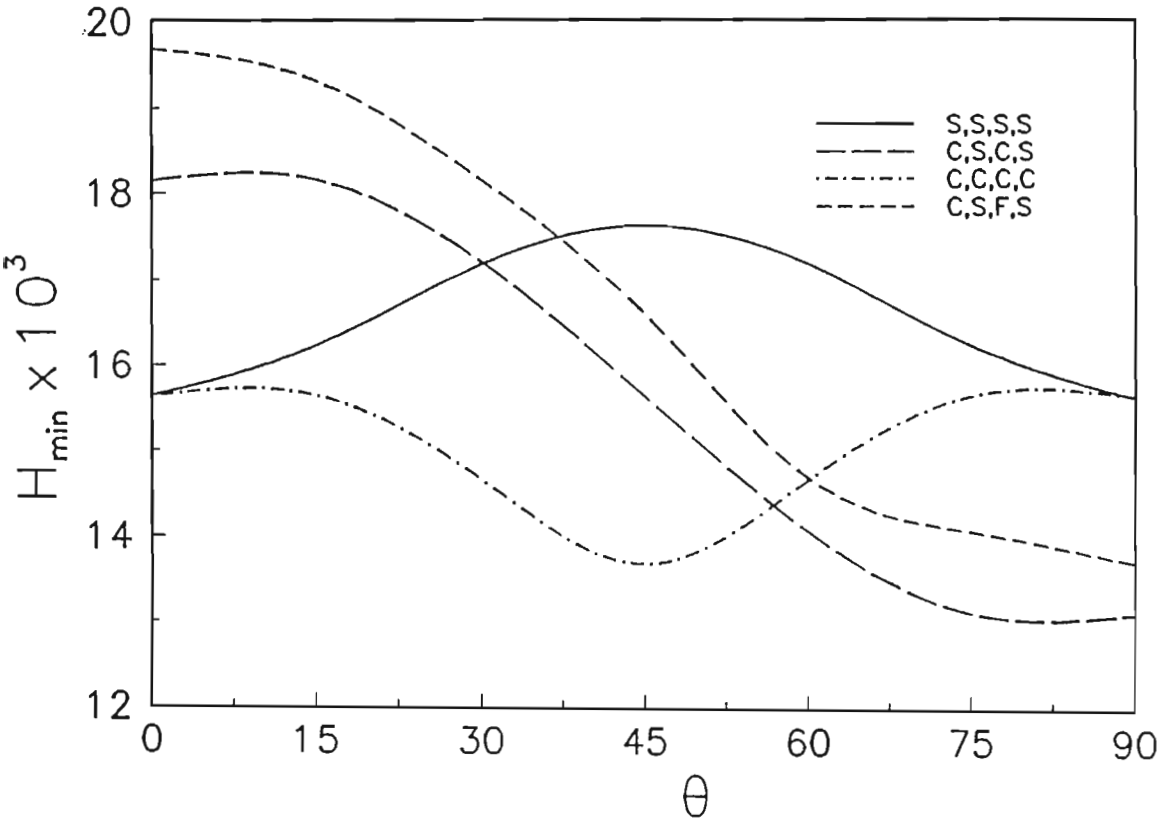

Figure 4.5.3. H_{min} versus θ with $a/b = 1$ (uniformly distributed load).

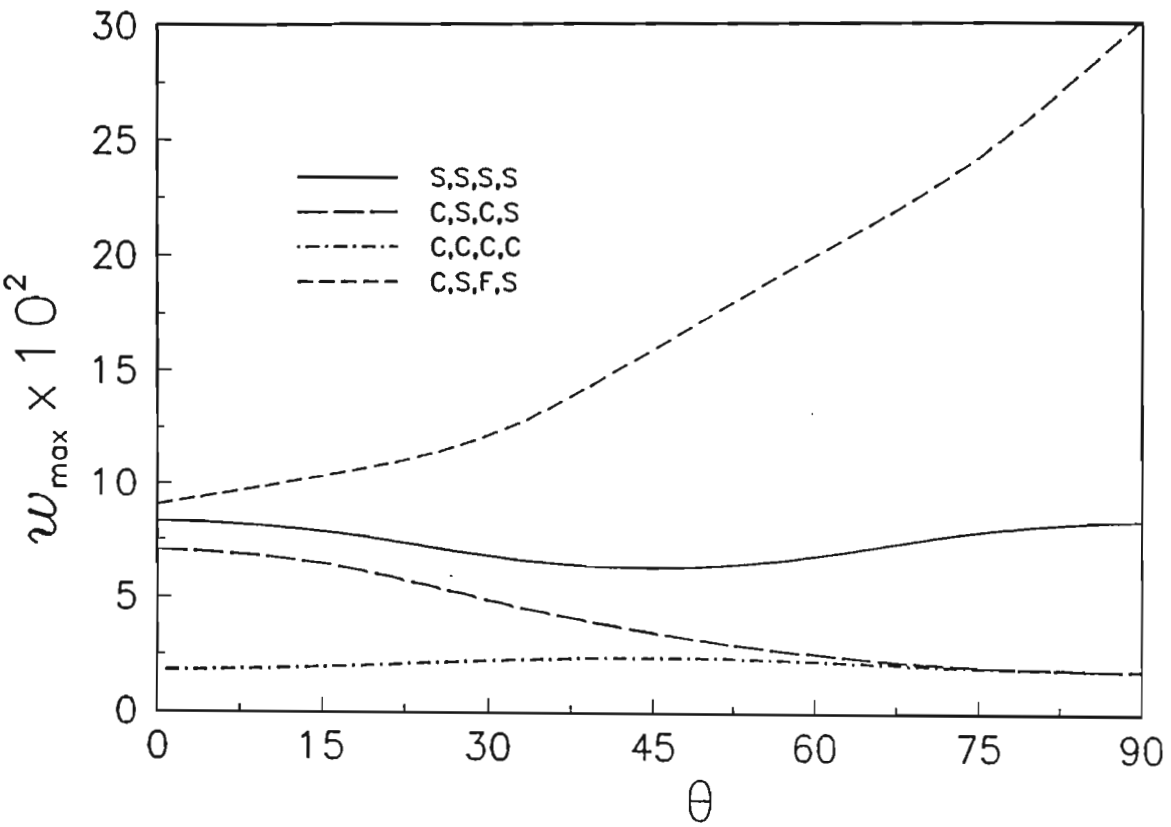

Figure 4.5.1. w_{max} versus θ with $a/b = 1$ and $H = 0.01m$ (uniformly distributed load).

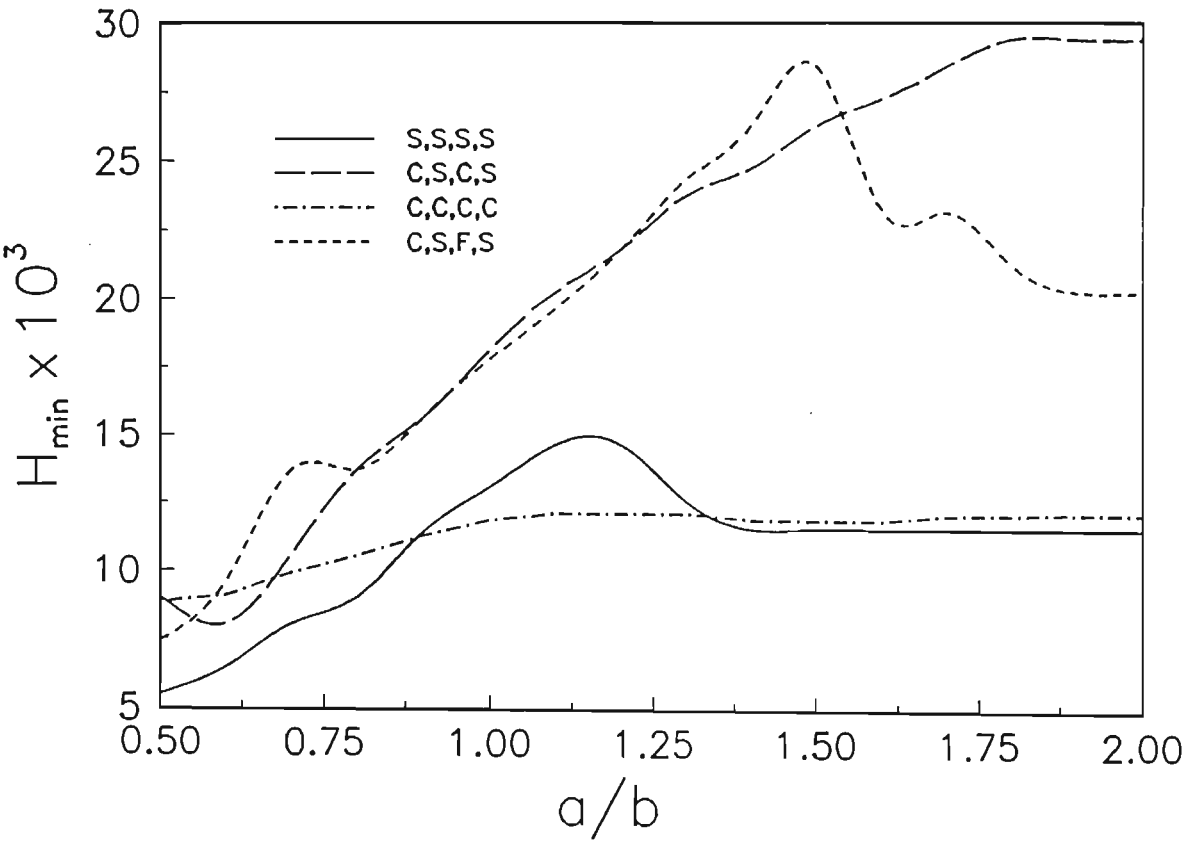

Figure 4.5.5. H_{min} versus a/b (uniformly distributed load).

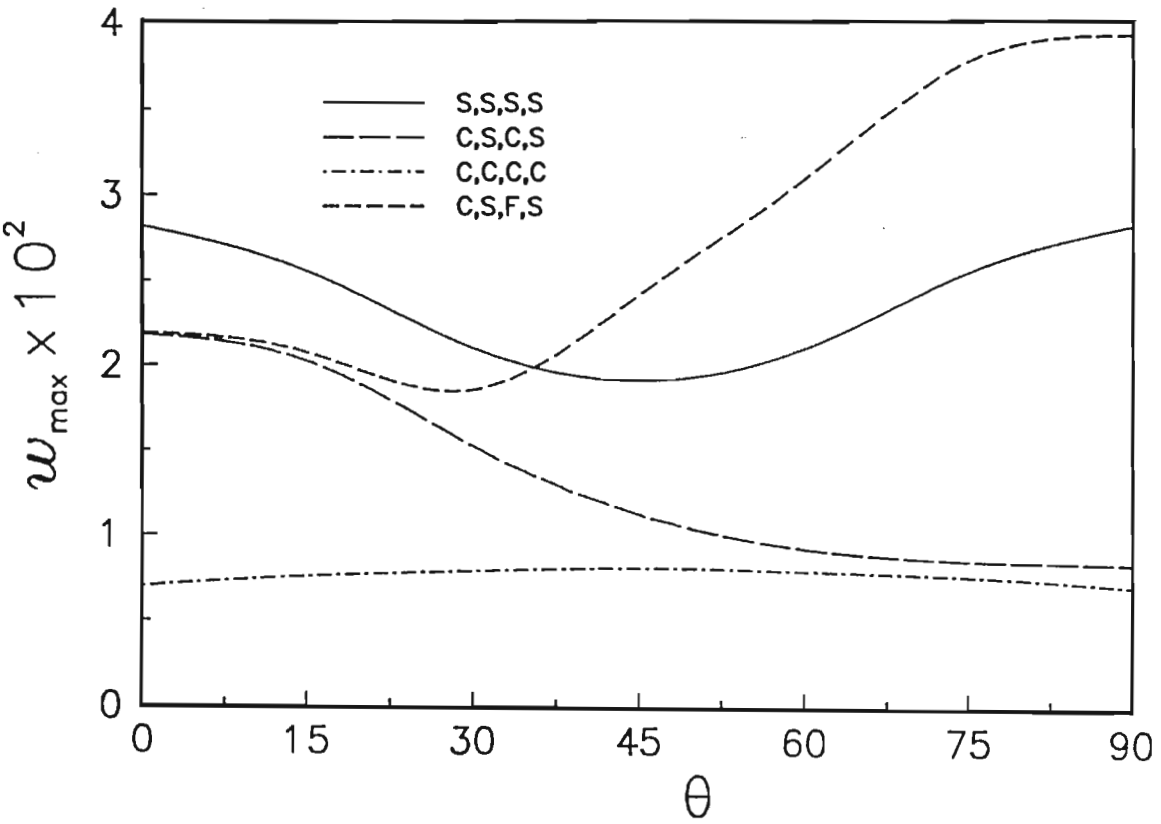

Figure 4.5.7. w_{max} versus θ with $a/b = 1$ and $H = 0.01m$ (patch load).

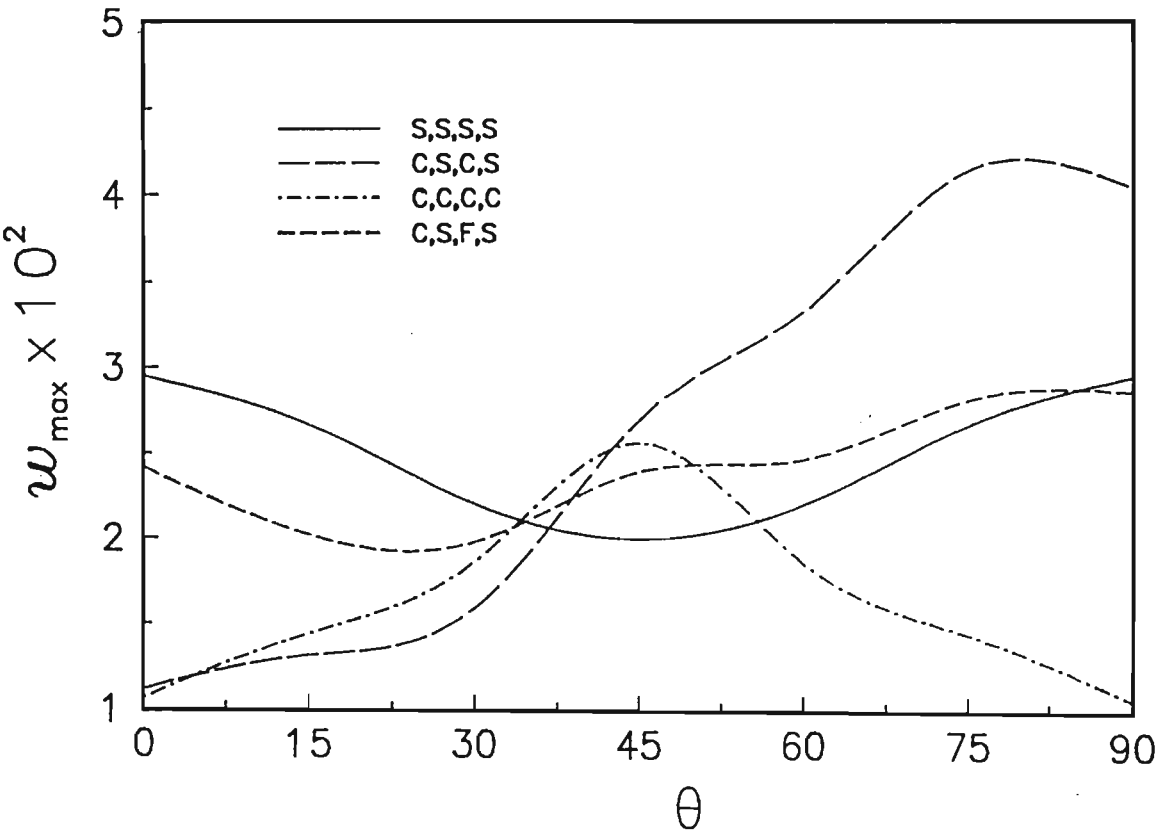

Figure 4.5.8. w_{max} versus θ with $a/b = 1$ and $F(\theta) = 1$ (patch load).

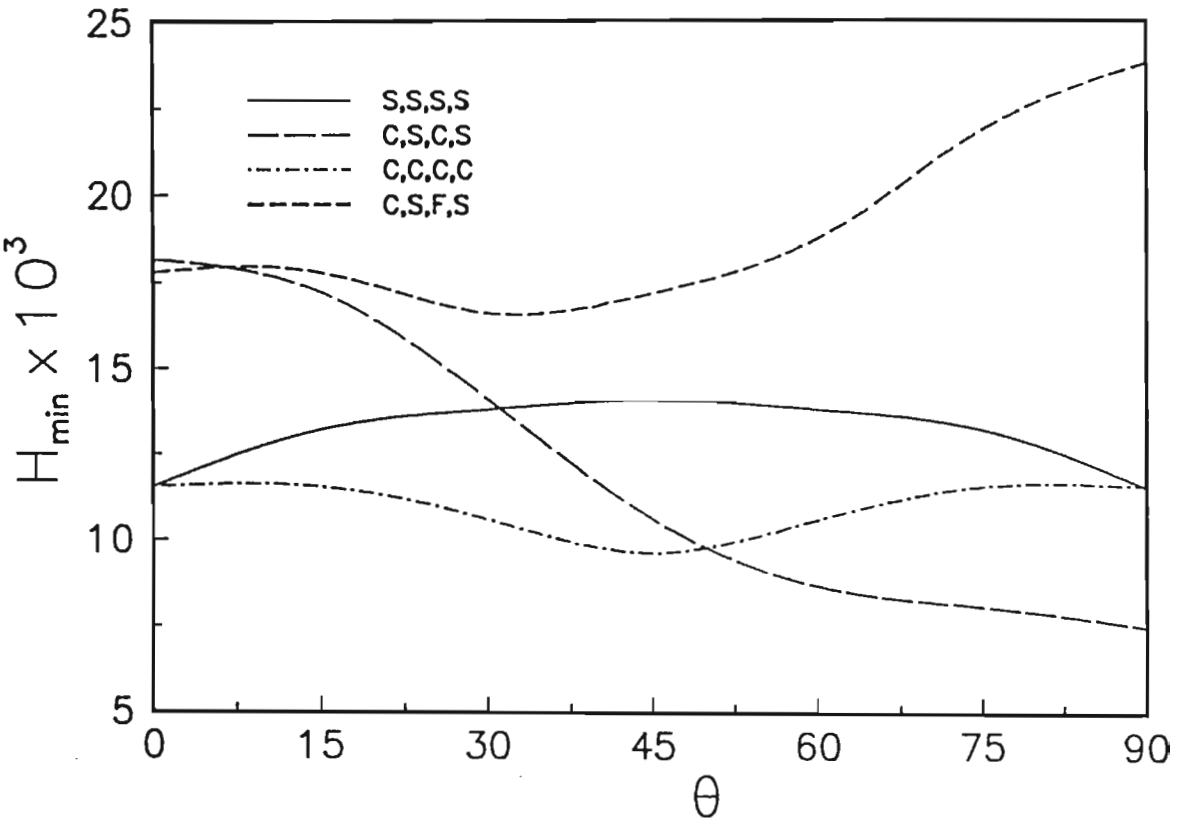

Figure 4.5.9. H_{min} versus θ with $a/b = 1$ (patch load).

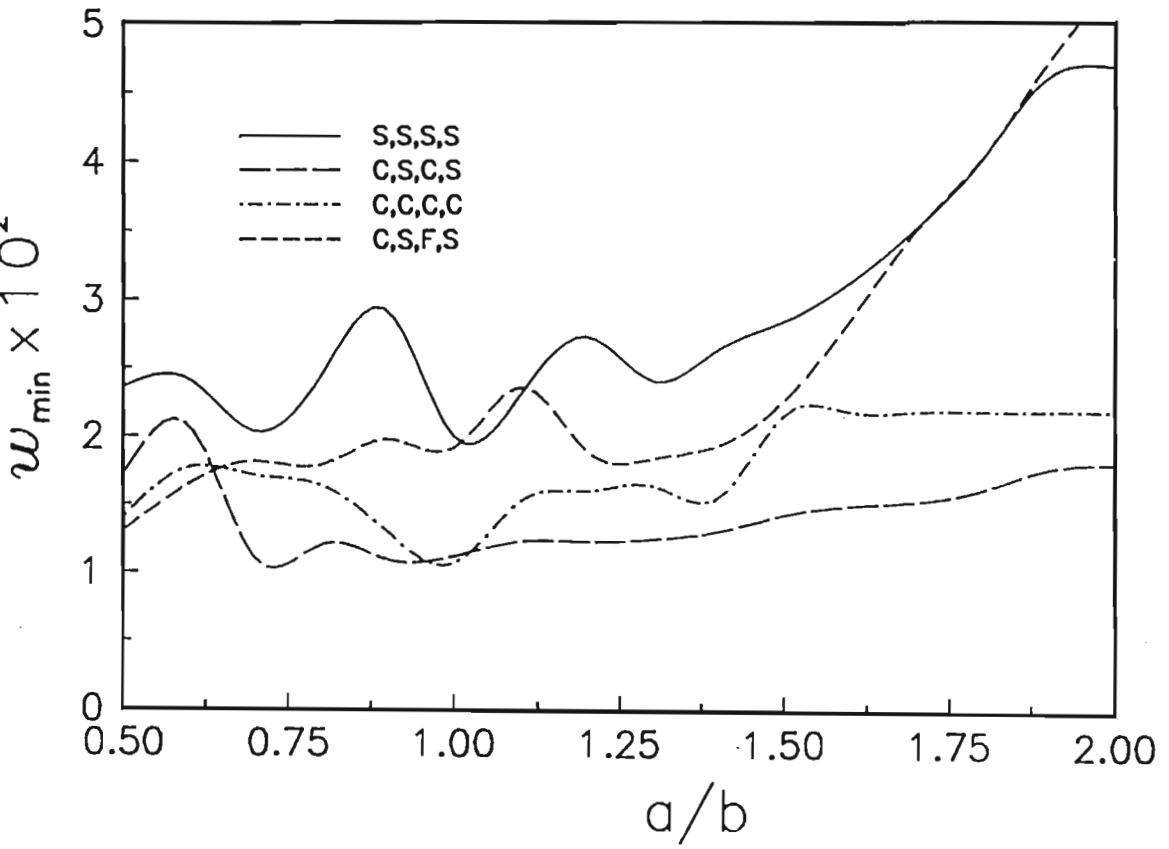

Figure 4.5.10. w_{min} versus a/b with $F(\theta) = 1$ (patch load).

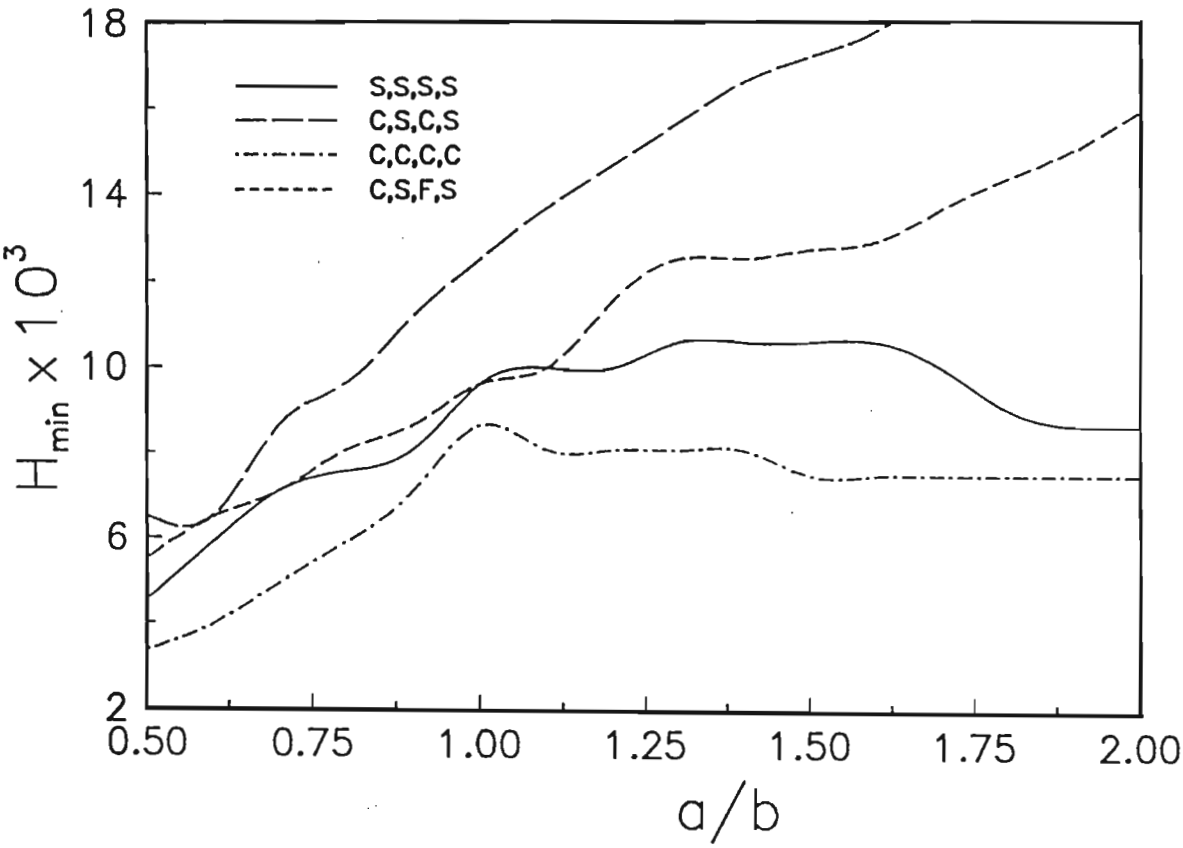

Figure 4.5.11. H_{min} versus a/b (patch load).

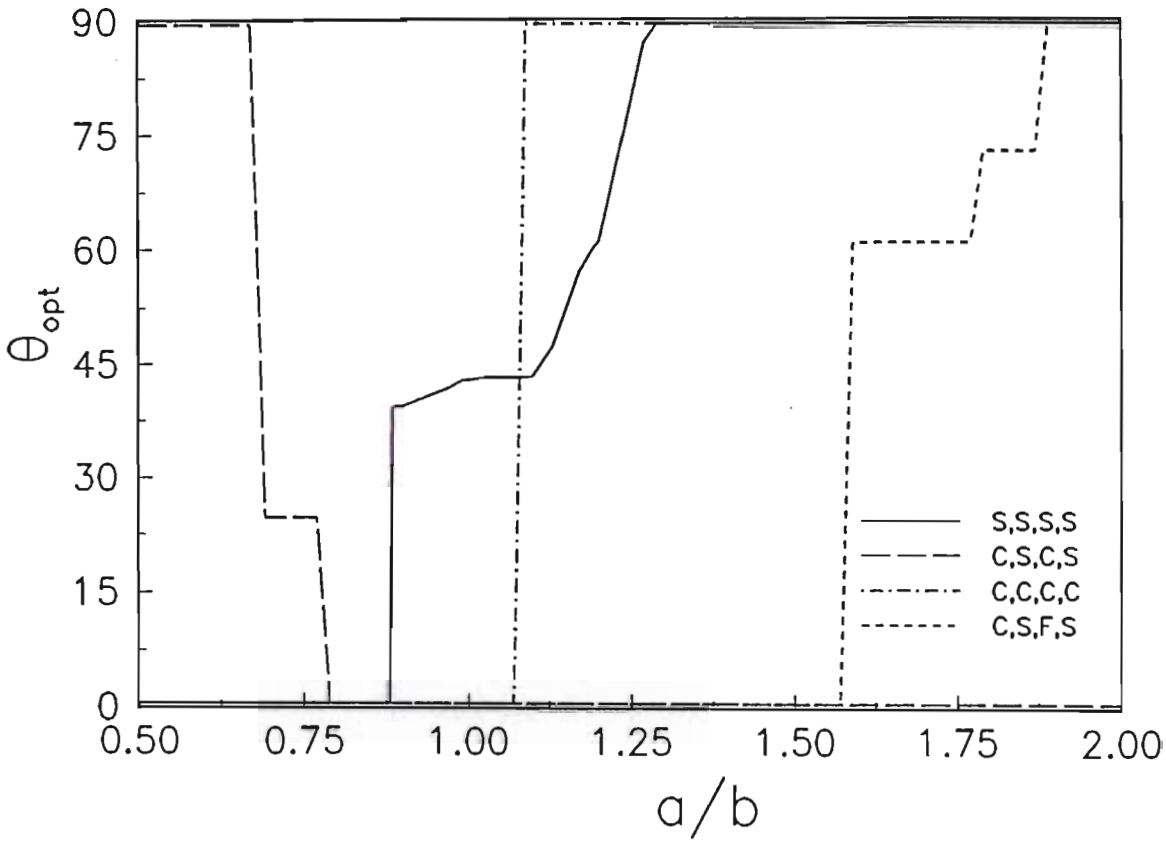

Figure 4.5.12. θ_{opt} versus a/b (patch load).

	DESIGN PROBLEM 1			DESIGN PROBLEM 2		
a/b	$w_{min} * 10^{-2}$	$H_{min} * 10^{-3}$	θ_{opt}	$w_{min} * 10e^{-2}$	$H_{min} * 10^{-3}$	θ_{opt}
0.50	3.03	5.09	10.4°	2.79	5.52	0.0°
0.75	4.57	8.04	0.0°	4.21	8.52	0.0°
1.00	5.09	11.69	90.0°	2.25	13.09	43.4°
1.25	5.38	11.68	90.0°	3.11	13.02	61.1°
1.50	5.89	10.68	90.0°	5.70	11.54	90.0°
1.75	6.09	10.29	90.0°	5.66	11.54	90.0°
2.00	6.06	10.29	90.0°	5.64	11.54	90.0°

Table 4.5.1. Effect of design priority on the maximum deflection and minimum weight for simply supported laminates.

	DESIGN PROBLEM 1			DESIGN PROBLEM 2		
a/b	$w_{min} * 10^{-2}$	$H_{min} * 10^{-3}$	θ_{opt}	$w_{min} * 10e^{-2}$	$H_{min} * 10^{-3}$	θ_{opt}
0.50	2.28	4.51	37.2°	0.52	8.85	0.0°
0.75	2.75	7.25	41.3°	0.71	10.21	0.0°
1.00	3.09	9.19	47.5°	1.12	11.86	90.0°
1.25	2.35	9.99	62.2°	1.31	12.10	90.0°
1.50	3.50	9.58	54.2°	1.72	11.85	90.0°
1.75	3.21	9.58	57.9°	2.64	12.04	90.0°
2.00	3.33	9.71	60.1°	2.66	12.11	90.0°

Table 4.5.2. Effect of design priority on the maximum deflection and minimum weight for clamped laminates.

Chapter 5

Conclusions

5.1 Optimal Design of Symmetrically Laminated Plates for Maximum Buckling Temperature

The optimal thermal buckling design for symmetrically laminated plates was determined. The solutions were obtained using the finite element method in conjunction with an optimisation routine to solve the analysis and design problems, respectively. Results are presented for various temperature loadings and different combinations of boundary conditions.

The effect of optimisation on the buckling load was investigated by plotting the buckling load against the fibre orientation. The results show that the difference in the buckling loads of optimal and non-optimal plates could be quite substantial, emphasising the importance of optimisation for fibre composite structures. The optimal ply angles and the corresponding buckling temperatures were given for the aspect ratios $0.5 \leq a/b \leq 2.0$. It was observed that the boundary conditions have a major effect on the optimal ply angle. However, the temperature distributions do not show the same influence on θ_{opt}. On the other hand, the temperature distribution affects the maximum buckling load considerably.

The effect of bending–twisting coupling on the maximum buckling temperature and optimal fibre angles was also investigated. This effect was found to decrease with increasing numbers of layers and become negligible for $K \geq 10$. Overall, the bending–twisting coupling has a minor effect on θ_{opt} and $T_{\max}$ and this contrasts with the results obtained for laminates under mechanical buckling loads [81]. In this study it was found that both the maximum buckling load and optimal angle at

which it was found changed considerably when the number of layers in the laminate was increased.

5.2 Optimal Design of Laminated Cylindrical Pressure Vessels for Maximum External Pressure

Finite element solutions for the optimal design of laminated composite pressure vessels for maximum buckling pressure are presented. The numerical approach employed in the study is necessitated by the fact that the inclusion of factors such as the effect of end caps and bending–twisting coupling rule out an analytical approach.

These results were obtained using the finite element method coupled with an optimisation routine, and the results are presented for vessels with hemispherical and flat caps of varying length, radius, wall thickness, layer numbers and hybridisation.

As expected, when the vessel length and radius are increased, the maximum buckling pressure corresponding to the optimal fibre angles decreases, while an increase in the wall thickness results in an increase in the buckling pressure. The effect of bending–twisting coupling on the optimal fibre angle and buckling pressure was demonstrated by increasing the number of layers and the effect was seen to be negligible when the vessel was composed of eight or more layers. Hybridisation results in different optimal fibre angles as opposed to single material designs, in addition to causing changes in buckling pressures due to the different materials used.

5.3 Multiobjective Design of Laminated Cylindrical Shells for Maximum Torsional and Axial Loads

A multiobjective design is given for simply supported laminated cylindrical shells subject to a combination of axial and torsional buckling loads. The objective is defined as the maximisation of the performance index specified by the sum of the non-dimensionalised weighted loadings. Results for single objective and multiobjective designs are presented. The effect of cylinder length, radius, wall thickness and weighting on the optimal fibre angle is investigated.

The mode changes which result due to the nature of the loading lead to designs

whose trends are not unimodal with regard to parameters such as the length and radius. Further, it is noted that the optimal fibre angle has a large effect on the maximum buckling load and varies markedly with geometry.

It is observed that at single-objective designs, the other objective becomes quite low. This drawback is overcome by choosing a suitable intermediate value of the weighting α in order to achieve the required compromise design. Studies of this type are thus essential if an optimal design for a certain shell geometry is to be obtained.

5.4 Minimum Weight and Cost Design of Hybrid Laminated Plates

Optimal designs of symmetrically laminated plates are obtained taking the weight or the cost as the objective function to be minimised and by imposing a minimum buckling load constraint. Moreover, the designs are subject to maximum cost or weight constraints. By admitting hybrid constructions into the design space, the tailoring capabilities of composite materials are expanded and the design requirements can be met as one-material laminates fail to satisfy the constraints in many cases.

A sequential optimisation procedure is devised in order to obtain the optimal values of the ply angles, total thickness, layer thicknesses as well as to determine the best material combinations. At each stage of the solution, one set of the variables is computed optimally which carries on to the next stage. The final design is determined by comparing several material combinations and selecting the one with the minimum weight or cost. Initial stages of the design involving continuous design variables require constrained optimisation routines to obtain the optimal solutions satisfying the problem constraints. Each material combination is subjected to this process in order to compare their relative advantages.

It is found that the use of a limited amount of kevlar reduces the weight of graphite constructions leading to not only weight but also to cost savings. However, if the thickness of kevlar layers exceeds a certain amount, the weight again increases as kevlar has lower stiffness as compared to graphite. It was also observed that different material combinations affect the weight and cost differently. Thus experimenting with different hybrid constructions may lead to substantially improved designs from either weight or cost viewpoints.

It is observed that the optimal material combinations depend on the cost constraint leading to the use of more glass layers for low cost constructions and more graphite layers for high cost ones. An assessment was made in Tables 6 and 7 in order to determine the weight and cost savings obtained by opting for hybrid rather than non-hybrid designs. In those cases where a single-material laminate can be found, the weight of the corresponding hybrid construction could be up to 45% less than its non-hybrid counterpart, and the cost 80% less.

5.5 Optimal Design of Symmetrically Laminated Plates for Minimum Deflection and Weight

The minimum deflection/minimum weight designs of symmetrically laminated plates are given as well as designs for minimum weight only. Plates of various aspect ratios and with different boundary conditions are studied. Two loading conditions are considered. In the case of the minimum deflection design it is found that for an increasing aspect ratio the minimum deflection does not always increase monotonically. At higher aspect ratios however, for both the loading conditions, the deflection generally does increase with increasing plate size.

The second design problem which involves the minimisation of the weight only shows that an entirely different optimal design may result as compared to the first design problem especially for certain boundary conditions as a result of taking the weight as the only design objective. It is shown that the boundary conditions have a substantial effect on the optimal fibre orientation of a plate as well as on its weight.

This type of study is important since the non–standard loading and boundary conditions considered lead to unpredictable trends in both the minimum deflection and weight.

Bibliography

[1] Oden, J. T. & Reddy, J. N., (1976), '*An Introduction to the Mathematical Theory of Finite Elements*', John Wiley and Sons, New York.

[2] Huebner, K. H. and Thornton, E. A., (1982), '*The Finite Element Method for Engineers*', John Wiley and Sons, Toronto.

[3] Hildebrand, F. B., (1965), '*Methods of Applied Mathematics*', Prentice–Hall, Englewood Cliffs, N.J.

[4] Oden, J. T. & Somogyi, D., (1969), 'Finite Element Applications in Fluid Dynamics', *Proc. ASCE J. Eng. Mech. Div.*, Vol. 95, EM3.

[5] Felippa, C. A. & Clough, R. W., (1970), 'The Finite Element Method in Solid Mechanics', in *SIAM-AMS Proceedings*, Vol. 2, American Mathematical Society, Providence, R.I, pp. 210-252.

[6] Oliveira, E. R. A., (1968), 'Theoretical Foundations of the Finite Element Method', *Int. J. Solids Struct.*, Vol. 4, pp. 929-952.

[7] Wang, T. Y., (1986), '*Finite Element Structural Analysis*, Prentice–Hall, Englewood Cliffs, N.J.

[8] Zienkiewicz, O. C. and Cheung, Y. K., (1965), 'Finite Elements in the Solution of Field Problems', *Engineer*, Vol. 220, 1965.

[9] Pian, T.H.H. & Tong, P., (1969), 'Basis of Finite Element Methods for Solid Continua', *Int. J. Numer. Methods Eng.*, Vol. 1, No. 1, p. 26.

[10] Zienkiewicz, O. C., (1977), '*The Finite Element Method*', 3rd Ed., McGraw-Hill Book Company, New York.

[11] Gibson, R. F., (1994), *Principles of Composite Material Mechanics*, McGraw Hill, New York.

[12] Narita, Y. and Leissa, A. W., (1990), 'Buckling studies for simply supported symmetrically laminated rectangular plates', *International Journal of Mechanical Sciences*, Vol. 32, No. 11, pp. 909–924.

[13] Vinson, J. R. & Sierakowski, R. L., (1986), '*The Behaviour of Structures Composed of Composite Materials*', Martinus Nijhoff, Dordrecht. and C.T. Sun, Technomic Publishing Company, Inc., Lancaster, Pennsylvania, 267-273.

[14] Ishikawa, T., Koyama, K., and Kobayashi, S., (1978), 'Thermal Expansion Coefficients of Unidirectional Composites', *Journal of Composite Materials*, Vol. 12, pp. 153–168.

[15] Schapery, R. A., (1968), 'Thermal Expansion Coefficients of Composite Materials based on Energy Principles', *Journal of Composite Materials*, Vol. 2, pp. 380–404.

[16] Cairns, D. S. & Adams, D. F., (1984), 'Moisture and Thermal Expansion Properties of Unidirectional Composite Materials and the Epoxy Matrix', in G. S. Springer (ed.), *Environmental Effects on Composite Materials: Volume 2*, pp. 300–316, Technomic Publishing Co., Lancaster, PA.

[17] Weinstein, F., Putter, S. & Stavsky, Y., (1983), 'Thermoelastic stress analysis of anisotropic composite sandwich plates by finite element method', *Computers and Structures*, Vol. 17, No. 1, pp. 31-36.

[18] Reddy, J. N. & Hsu, Y. U., (1980), 'Effects of shear deformation and anisotropy on the thermal bending of layered composite plates', *Journal of Thermal Stresses*, Vol. 3, pp. 475-493.

[19] Jonnalagadda, K. D., Tauchert, T. R. & Blandford, G. E., (1993), 'High-order thermoelastic plate theories: An analytic comparison',*Journal of Thermal Stresses*, Vol. 16, pp. 265-284.

[20] Tauchert, T. R. & Adibhatla, S., (1985), 'Optimum thermoelastic design of laminated plates', *Journal of Thermal Stresses* , Vol. 8, pp. 11-24.

[21] Tauchert, T. R., (1995), 'Temperature and absorbed moisture' in *Buckling and Postbuckling of Composite Plates*, Edited by G. J. Turvey and I. H. Marshall, Chapman and Hall, London, pp. 190 - 226.

[22] Tauchert, T. R. & Huang, N. N., (1987), 'Thermal buckling of symmetric angle-ply laminated plates', *Composite Structures 4*, edited by I.H. Marshall. Elsevier Applied Science, London.

[23] Adali, S. & Duffy, K. J., (1990), 'Optimal design of antisymmetric hybrid laminates against thermal buckling', *Journal of Thermal Stresses*, Vol. 13, pp. 57-71.

[24] Adali, S. & Duffy, K. J., (1990), 'Multi-criteria thermo-elastic design of anti-symmetric angle-ply laminates', *Multi-criteria Design Optimization*, edited by H. Eschenauer, J. Koski and A. Osyczka, Springer-Verlag, Berlin, pp. 417-428.

[25] Thangaratnam, K. R., Palaninhatan & Ramachandran, J., (1989), ' Thermal buckling of composite laminated plates', *Journal of Thermal Stresses*, Vol. 32, No. 5, pp. 117.

[26] Chandrashekhara, K., (1992), 'Thermal buckling of plates using a shear flexible finite element', *Finite Elements in Analysis and Design*, Vol. 12, pp. 51-61.

[27] Sherrer, R. E., (1967), 'Filament-Wound Cylinders with Axial-Symmetric Loads',*Journal of Composite Materials*, Vol. 1, pp. 344 - 355.

[28] Reuter, R. C., (1972), 'Analysis of Shells Under Internal Pressure', *Journal of Composite Materials*, Vol. 6, pp. 94 - 113.

[29] Hu, H. T., (1991), 'Influence of Shell Geometry on Buckling Optimisation of Fiber-Composite Laminate Shells', *Journal of Pressure Vessel Technology*, Vol. 113, pp. 465 - 470.

[30] Onoda, J., (1985), 'Optimal Laminate Configurations of Cylindrical Shells for Axial Buckling', Vol. 23, No. 7, pp. 1093 - 1099.

[31] Tripathy, B. & Rao, K. P., (1993), 'Stiffened Composite Axisymmetric Shells-Optimum Layup for Buckling by Ranking', *Computers and Structures*, Vol. 46, No. 2, pp. 299 - 309.

[32] Yamaki, N., (1984), 'Elastic stability of circular cylindrical shells', in *Applied Mathematics and Mechanics* (E. Becker, B. Budianski, H. A. Lauwrier and W. T. Koiter), New York: North Holland.

[33] Nshanian, Y. S. & Pappas, M., (1983), 'Optimal laminated composite shells for buckling and vibration',*AIAA Journal*, Vol. 21, No. 3, pp. 430-437.

[34] Adali, S., Richter, A. & Verijenko, V. E., 'Multiobjective Design of Laminated Cylindrical Shells for Maximum Pressure and Buckling Load', *submitted to Composite Structures.*

[35] Sun, G. & Hansen, J. S., (1988), 'Optimal design of laminated composite circular-cylindrical shells subjected to combined load', *Journal of Applied Mechanics*, Vol. 55, pp. 136 - 142.

[36] Tennyson, R. C. & Hansen, J. S., (1983), '*Optimum design for buckling of laminated cylinders', Collapse: The Buckling of Structures in Theory and Practice*, edited by J. M. T. Thompson & G. W. Hunt, Cambridge University Press, pp. 409 - 429.

[37] Kumar, N. & Tauchert, T. R., (1992), 'Multiobjective design of symmetrically laminated plates', *Transactions of ASME*, Vol. 114, pp. 620 - 625.

[38] Grandhi, R. V., Bharatram, G. & Venkayya, V. B., (1993), 'Multiobjective optimisation of large- scale structures', *AIAA Journal*, Vol. 31, pp. 1329 - 1337.

[39] Rao, S. S., Sundararaju, K., Balakrishna, C. & Prakash, B. G., (1992), 'Multiobjective insensitive design of structures', *Computers and Structures*, Vol. 45, pp. 349 - 359.

[40] Saravanos, D. A. & Chamis, C. C., (1992), 'Multiobjective shape and material optimisation of composite structures including damping', *AIAA Journal*, Vol. 30, pp. 805 - 813.

[41] Reissner, E. (1987), 'On a Certain Mixed Variational Theorem and Laminated Shell Theory', *Refined Dynamical Theory of Beams, Plates and Shells*, Springer Verlag, pp. 17–26.

[42] Urazgil'dyeav, K. U., (1977), 'Design of Equal-Strength Cylindrical Shell of Composite Materials', *Prikladnaya Mekhanika*, Vol. 13, No. 7, pp. 121 - 124.

[43] Eckold, G. C., (1985), 'A Design Method for Filament Wound GRP Vessels and Pipework', *Composites*, Vol. 16, No. 1, pp. 41 - 47.

[44] Fukunaga, H. & Uemura, M., (1983), 'Optimum Design of Helically Wound Composite Pressure Vessels', *J. Comp. Structures*, Vol. 1, pp. 31 - 49.

[45] Karandikar, H., Srinivasan, R., Mistree, F. & Fuchs, W. J., (1989), 'Compromise: An Effective Approach for the Design of Pressure Vessels Using Composite Materials', *Computers and Structures*, Vol. 33, No. 6, pp. 1465 - 1477.

[46] Tauchert, T. R., (1981), Optimum Design of a Reinforced Cylindrical Pressure Vessel, *J. of Composite Materials*, Vol. 15, pp. 390 - 402.

[47] Adali, S., Summers, E. B. & Verijenko, V. E. (1993), 'Optimisation of laminated cylindrical pressure vessels under strength criterion', *Composite Structures*, Vol. 25, pp. 305 - 312.

[48] Huang, S. N. & Alspaugh, D. W., (1974), 'Minimum Weight Sandwich Beam Design', *AIAA Journal*, Vol. 12, No. 12, pp. 1617 - 1618.

[49] Paydar, N. & Park, G.-J., (1990), 'Optimal Design of Sandwich Beams', *Computers and Structures*, Vol 13., pp. 523–530.

[50] Triantafillou, T. C., Kim, P. & Meier, U., (1991), 'Optimisation of hybrid aluminium / c.f.r.p. box beams.', *International Journal of Mechanical Sciences*, Vol. 33, No. 9, pp. 729 - 739.

[51] Phillips, J. L., & Gurdal, Z., (1990), 'Analysis and Optimal Design of Geodesically Stiffened Composite Panels', *Free University of Brussels / Wessex Institute of Technology CAD in Composite Material Technology 2nd International Conference, Belgium*, 25 - 27 April.

[52] Min, K. T. & de Charenteney, F. X., (1986), 'Optimum Weight Design of Sandwich Cylinders with Orthotropic Facings and Core under Combined Loads, *Computers and Structures*, Vol. 24, No. 2, pp. 313 - 322.

[53] Ostwald, M., (1990), 'Optimum Weight Design of Sandwich Cylindrical Shells under Combined Loads', *Computers and Structures*, Vol. 11, pp. 247–254.

[54] Shin, D. K., Gürdal, Z. & Griffin, O. H.,'Minimum Weight Design of Laminated Plates for Postbuckling Performance', *Proc. 32nd AIAA/ASME/ASCE/ AHS/ASC Structures, Structural Dynamics, and Materials Conf.*, Baltimore, Maryland, 8–10 April, pp. 267–274.

[55] Adali, S. & Duffy, K. J., (1991), 'Optimal Hybridization of Antisymmetric Laminates Undergoing Free Vibrations', *Engineering Optimization*, Vol. 18,pp. 287–301.

[56] Adali, S. & Duffy, K. J., (1992), 'Minimum Cost Design of Vibrating Laminates by Hybridization', *Engineering Optimization*, Vol. 19, pp. 255–267.

[57] Adali, S. & Duffy, K. J., (1989), 'Design of Antisymmetric Hybrid Laminates for Maximum Buckling Load: I. Optimal Fibre Orientation, *Composite Structures*, Vol. 14, pp. 49–60.

[58] Adali, S. & Duffy, K. J., (1989), 'Design of Antisymmetric Hybrid Laminates for Maximum Buckling Load: II. Optimal Layer Thickness, *Composite Structures*, Vol. 14, pp. 113–124.

[59] Miki, M. & Tonomura, K., (1987), 'Optimum Design of Hybrid Fibrous Laminated Composite Plates Subject to Axial Compression', *Composite Structures*, 4, Vol. 1, ed. I. H. Marshall. Elsevier Applied Science, London, pp.368–377.

[60] Jiang, Y. & Chiang, Y.-C., (1983), 'Optimum design of fibre reinforced (composite) materials', *Proceedings of the 4th Intl. Conf. on Mechanical Behaviour of Materials - IV* ed. J. Carlson and N. G. Ohlson, Stockholm, Sweden, Vol. 1, pp. 439 - 441.

[61] Johnson, A. F. & Sims, G. D., (1983), 'Simplified design procedures for composite plates under flexural loading', *Composite Structures 2*, ed. I. H. Marshall. Applied Science Publishers, London, pp. 302 - 325.

[62] Rao, S. S. & Singh, K, (1979), 'Optimum design of laminates with natural frequency constraints', *J. Sound Vib.*, Vol 67, pp. 101 - 112.

[63] Iyengar, N. G. & Umeratiya, J. R., (1984), 'Optimisation of hybrid laminated composite plates', ICAS, pp. 1172 - 1178.

[64] Kogiso, N., Watson, L. T., Gurdal, Z., Haftka, R. T., & Nagendra, S., (1994), 'Design of Composite Laminates by a Genetic Algorithm with Memory', *Mechanics of Composite Materials and Structures*, Vol. 1, pp. 95 - 117.

[65] Adali, S., Richter, A., and Verijenko, V. E., (1995), 'Minimum weight design of symmetric angle-ply laminates under multiiple uncertain loads', *Structural Optimisation*, Vol. 9, pp. 89 - 95.

[66] Quian, B., Reiss, R., & Aung, W., (1990), 'The maximum stiffness design of rectangular symmetric angle-ply laminates', *Proceedings of the 2nd Int. Conf. on Computer Aided Design in Composite Material Technology*, Free University of Brussels / Wessex Institute of Technology, Computational Mechanics Publications, Southampton, pp. 451 - 464.

[67] Kengtung, C., (1986), 'Sensitivity analysis and a mixed approach to the optimization of symmetric layered composite plates', *Engineering Optimization*, Vol. 9, pp. 233 - 248.

[68] Kam, T. Y., & Chang, R. R., (1992), 'Optimum layup of thick laminated composite plates for maximum stiffness', *Engineering Optimization*, Vol. 19, pp. 237 - 249.

[69] Adali, S., Summers, E.B., & Verijenko, V. E., (1994), 'Minimum Weight and Deflection Design of Thick Sandwich Laminates via Symbolic Computation', *Composite Structures*, Vol. 29, pp. 145 - 160.

[70] Walker, M., Reiss, T., Adali, S. & Verijenko, V. E., 'Optimal Design of Symmetrically Laminated Plates for Maximum Buckling Temperature', to appear in *Journal of Thermal Stresses.*

[71] Walker, M., Reiss, T. & Adali, S., 'Optimal Design of Laminated Cylindrical Pressure Vessels for Maximum External Pressure', to appear in *ASME Journal of Pressure Vessel Technology.*

[72] Walker, M., Reiss, T. & Adali, S., 'Optimal Design of Hemispherically Capped Laminated Composite Pressure Vessels for Maximum Buckling Pressure', *Pro-*

ceedings of FEMSA 95, Stellenbosch, South Africa, 18-20 January 1995, Vol. 2, pp. 719–729.

[73] Walker, M., Reiss, T. & Adali, S., 'Optimal Design of Laminated Composite Pressure Vessels with Flat and Hemispherical End-caps for Maximum Buckling Pressure', *Proceedings of International Conference on Computational Engineering Science*, Hawaii, USA, 30 July - 3 August 1995.

[74] Pareto, V., (1896), 'Cours d'Economie Poltique', F. Rouge, Lausanne.

[75] Adali, S., (1983), 'Pareto Optimal Design of Beams Subjected to Support Motions', *Computers & Structures*, Vol. 16, No. 1–4, pp. 297–303.

[76] Walker, M., Reiss, T. & Adali, S., 'Multiobjective Design of Laminated Cylindrical Shells for Maximum Torsional and Axial Buckling Loads', to appear in *Composite Structures.*

[77] Walker, M., Reiss, T., Adali, S. & Weaver, P. M., 'Application of MATHEMATICA to the Optimal Design of Composite Shells for Improved Buckling Strength', submitted to *Engineering with Computers.*

[78] Walker, M., Reiss, T., Adali, S., 'Optimal Design of Symmetrically Laminated Plates for Minimum Deflection and Weight', submitted to *AIAA Journal.*

[79] Tsai, S., (1985), 'Composites Design', Think Composites, Dayton , Ohio.

[80] COSMOS/M Version 1.70, 1993, Structural Research and Analysis Corporation, Santa Monica, California.

[81] M. Walker, S. Adali & V. E. Verijenko, 'Optimisation of Symmetric Laminates for Maximum Buckling Load Including the Effects of Bending–Twisting Coupling' *to appear in Computers and Structures.*

[82] Walker, M., Reiss, T. & Adali, S., 'A Procedure to Select the Best Material Combinations and Optimally Design Hybrid Composite Plates for Minimum Weight and Cost', to appear in *Computers and Structures.*

[83] Walker, M., Reiss, T., Adali, S. & Verijenko, 'Minimum Weight Design of Composite Hybrid Shells via Symbolic Computation', to appear in *Journal of the Franklin Institute.*

[84] Ochoa, O. O, and Reddy, J. N., (1992), *Finite Element Analysis of Composite Laminates*, Solid Mechanics and its Applications, Kluwer Academic Publishers, Dordrecht.

[85] Verijenko, V. E., Summers, E. B., Adali, S. & Reiss, T., 'Optimal Design of Laminated Shells for Minimum Deflection using Symbolic Computation', *Proceedings of 6th Kwazulu/Natal Mathematics Conference*, Durban, South Africa, May 1994, pp. 158–164.

[86] Verijenko, V. E., Summers, E. B., Adali, S. & Reiss, T., 'Optimal Design of Laminated Shells with Shear and Normal Deformation using Symbolic Computation', *Proceedings of 5th AIAA/USAF/NASA/ISSMO Symposium on Multidisciplinary Analysis and Optimisation*, Panama City , Florida, USA, September 1994, pp. 1066–1073.

[87] Walker, M., Adali, S., Verijenko, V. E. & Reiss, T., 'Optimal Design of Symmetric Angle–Ply Laminates subject to Nonuniform Buckling Loads and Inplane Restraints' to appear in *Thin–Walled Structures.*